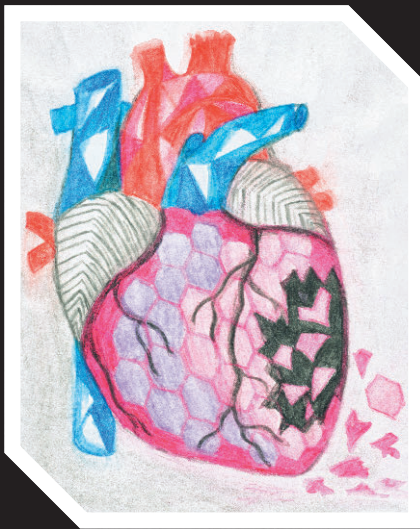**UNIVERSITY OF TURKU**

MOLECULAR IMAGING AND IMMUNOTHERAPY IN ATHEROSCLEROTIC CARDIOVASCULAR DISEASE

Mia Ståhle

UNIVERSITY OF TURKU

MOLECULAR IMAGING AND IMMUNOTHERAPY IN ATHEROSCLEROTIC CARDIOVASCULAR DISEASE

Mia Ståhle

University of Turku

Faculty of Medicine
Department of Clinical Physiology and Nuclear Medicine
Drug Research Doctoral Programme
Turku PET Centre

Supervised by

Professor Antti Saraste, MD, PhD
Heart Center and Turku PET Centre
University of Turku and
Turku University Hospital
Turku, Finland

Professor Anne Roivainen, PhD
Turku PET Centre and Turku Center for
Disease Modeling
University of Turku
Turku, Finland

Reviewed by

Adjunct Professor Päivi Lakkisto, MD, PhD
Unit of Cardiovascular Research
Minerva Foundation Institute for
Medical Research and Department of
Clinical Chemistry
University of Helsinki
Helsinki, Finland

Professor Dr. Christoph Rischpler, MD
Department of Nuclear Medicine
University Hospital Essen
Essen, Germany

Opponent

Professor Risto Kerkelä, MD, PhD
Research Unit of Biomedicine
Department of Pharmacology and Toxicology
University of Oulu
Oulu, Finland

To my family

*People rarely succeed unless
they have fun in what they are doing.*
- Dale Carnegie

UNIVERSITY OF TURKU
Faculty of Medicine
Department of Clinical Physiology and Nuclear Medicine
Turku PET Centre
MIA STÅHLE: Molecular Imaging and Immunotherapy in Atherosclerotic
Cardiovascular Disease
Doctoral Dissertation, 194 pp.
Drug Research Doctoral Programme
November 2020

ABSTRACT

Atherosclerotic cardiovascular disease (ASCVD) is a disorder that affects both heart and blood vessels. It is caused by atherosclerosis, a chronic, low-grade inflammatory disease, which is characterized by the accumulation of lipids in the arterial wall. Modified lipoproteins contain pro-inflammatory epitopes, such as phosphorylcholine (PC), that interact with inflammatory cells in the vascular wall, thereby accelerating the development of atherosclerotic lesions. The main cause of myocardial infarction (MI) arises from a rupture of an unstable, inflamed atherosclerotic lesion in the coronary artery. The MI induces an intense inflammatory response that is essential for myocardial repair and scar formation, but which is also implicated in the onset of heart failure over time. Molecular imaging techniques can be potentially used for identification of new molecular targets, such as glucagon-like peptide-1 receptor (GLP-1R), that are involved in inflammatory and repair processes.

The aim of this thesis was to investigate whether a novel immunotherapy targeting the PC epitope improves vascular function and attenuates atherosclerotic inflammation in mice. A positron emission tomography (PET) tracer ^{68}Ga-NODAGA-exendin-4 was evaluated for detection and imaging of GLP-1R expression after MI and in atherosclerosis in experimental models. *In vivo* PET imaging, ultrasound imaging, tissue autoradiography, immunohistological stainings, and cell assays were utilized as the main methods in the studies.

This thesis showed that treatment with the PC immunotherapy preserved coronary artery function and attenuated the uptake of an established inflammation tracer, glucose analog ^{18}F-FDG, in atherosclerotic lesions in mice. ^{68}Ga-NODAGA-exendin-4 PET detected up-regulated cardiac GLP-1R expression during the healing of MI in rats. The uptake of ^{68}Ga-NODAGA-exendin-4 was also increased in inflamed atherosclerotic lesions in mice. In conclusion, PC immunotherapy might represent a potential approach to inhibit the lipid-driven inflammation in atherosclerosis. ^{68}Ga-NODAGA-exendin-4 PET may have implications for studying pharmacological modification of GLP-1R signaling in ASCVD.

KEYWORDS: atherosclerosis, myocardial infarction, inflammation, phosphoryl-choline, glucagon-like peptide-1 receptor, positron emission tomography

TURUN YLIOPISTO
Lääketieteellinen tiedekunta
Kliininen fysiologia ja isotooppilääketiede
Valtakunnallinen PET-keskus
MIA STÅHLE: Molekyylikuvantaminen ja immunoterapia ateroskleroottisissa sydän- ja verisuonitaudeissa
Väitöskirja, 194 s.
Lääketutkimuksen tohtoriohjelma
Marraskuu 2020

TIIVISTELMÄ

Sydän- ja verisuonitautien yleisin syy on ateroskleroosi, mikä on krooninen matala-asteinen tulehduksellinen sairaus, jossa rasvaa kertyy valtimoiden seinämiin. Muokkautuneiden rasvapartikkelien pinnalta on tunnistettu tulehdusreaktiota edistäviä molekyylejä kuten fosforyylikoliini, jotka ovat osallisena valtimoplakkien muodostumiseen. Suurimman osan sydäninfarkteista aiheuttaa epävakaan tulehtuneen ateroskleroottisen plakin repeytyminen sepelvaltimossa. Sydäninfarkti saa aikaan tulehdusreaktion ja arpikudoksen muodostumisen sydänlihaksessa, mikä pitkittyneenä voi johtaa myös sydämen vajaatoimintaan. Molekyylikuvantamisen avulla voisi olla mahdollista tunnistaa ja tutkia uusia kohteita kuten glukagonin kaltainen peptidi-1 (GLP-1) -reseptori, jotka liittyvät sydäninfarktinjälkeiseen tulehdusreaktioon ja arven paranemiseen.

Tämän väitöskirjan tarkoituksena oli tutkia koe-eläinmalleissa, miten uusi fosforyylikoliini-molekyyliin kohdentuva immunoterapia vaikuttaa ateroskleroottisten suonten toimintaan ja tulehdukseen. Lisäksi tutkittiin GLP-1-reseptorin ilmentymistä sydäninfarktin jälkeen ja ateroskleroottisissa plakeissa ^{68}Ga-NODAGA-exendin-4 merkkiaineen ja positroniemissiotomografia (PET) -kuvantamisen avulla. Tutkimusmenetelminä käytettiin *in vivo* PET- ja ultraäänikuvantamista, autoradiografiaa, kudosvärjäyksiä ja solukokeita.

Väitöskirjassa havaittiin, että fosforyylikoliini-immunoterapian jälkeen hiirten sepelvaltimoiden toiminta oli parantunut ja plakkeihin kertyi vähemmän ^{18}F-FDG-merkkiainetta, mikä kertoo laantuneesta tulehduksesta. ^{68}Ga-NODAGA-exendin-4 PET-kuvantaminen osoitti, että GLP-1-reseptorin ilmentyminen oli lisääntynyt infarktinjälkeisen tulehdusreaktion aikana. ^{68}Ga-NODAGA-exendin-4-merkkiaine kertyi myös selvästi tulehtuneisiin ateroskleroottisiin plakkeihin. Yhteenvetona voidaan todeta, että fosforyylikoliini-immunoterapia saattaisi olla potentiaalinen uusi lääkehoito valtimoplakkien tulehdusreaktion hillitsemiseksi. ^{68}Ga-NODAGA-exendin-4 PET-kuvantamista voitaisiin hyödyntää GLP-1-reseptoriin kohdentuvien lääkehoitojen tutkimisessa ateroskleroottisissa sydän- ja verisuonitaudeissa.

AVAINSANAT: ateroskleroosi, sydäninfarkti, tulehdus, fosforyylikoliini, glukagonin kaltainen peptidi-1 -reseptori, positroniemissiotomografia

Table of Contents

8

Abbreviations

^{18}F-FDG	2-deoxy-2-[^{18}F]-fluoro-*D*-glucose
α-SMA	α-smooth muscle actin
ACE	Angiotensin-converting enzyme
ACEI	ACE inhibitor
ACS	Acute coronary syndrome
AMI	Acute myocardial infarction
Ang II	Angiotensin II
ANP	Atrial natriuretic peptide
ApoB100	Apolipoprotein B100
ARB	AT_1 receptor blocker
ARNI	Angiotensin receptor-neprilysin inhibitor (sacubitril/valsartan)
ASCVD	Atherosclerotic cardiovascular disease
AT_1	Ang II receptor type 1
BNP	Brain natriuretic peptide
CAD	Coronary artery disease
CCL2	C-C motif chemokine ligand 2
CCR2	C-C motif chemokine receptor type 2
CCS	Chronic coronary syndrome
CD	Cluster of differentiation (e.g., CD36, CD68)
CFR	Coronary flow reserve
CMD	Coronary microvascular dysfunction
CT	Computed tomography
CTA	Computed tomography angiography
cTn	Cardiac troponin
CXCR4	Chemokine receptor 4
DAMP	Danger-associated molecular pattern
DAPI	4',6-diamino-2-phenylindole
DPP-4	Dipeptidyl peptidase-4 enzyme
EC	Endothelial cell
ECM	Extracellular matrix
EDV	End-diastolic volume

EF	Ejection fraction
eNOS	Endothelial nitric oxide synthase
ET-A	Endothelin receptor A
FFR	Fractional flow reserve
FH	Familial hypercholesterolemia
GLP-1	Glucagon-like peptide-1
GLP-1R	Glucagon-like peptide-1 receptor
HAEC	Human aortic endothelial cell
HDL	High-density lipoprotein
HE	Hematoxylin and eosin
HF	Heart failure
HFpEF	HF with preserved EF
HFrEF	HF with reduced EF
HMG-CoA	3-hydroxy-3-methyl-glutaryl-coenzyme A
HPLC	High-performance liquid chromatography
hsCRP	High-sensitivity C-reactive protein
I/R	Ischemia-reperfusion
ICA	Invasive coronary angiography
ICAM-1	Intercellular adhesion molecule-1
IDL	Intermediate-density lipoprotein
IGF-II	Insulin-like growth factor II
IgG1	Immunoglobulin G1
IgM	Immunoglobulin M
IL	Interleukin
IMT	Intima-media thickness
K_i	Net influx rate
LAD	Left anterior descending coronary artery
LCA	Left coronary artery
LDL	Low-density lipoprotein
LDL-C	Low-density lipoprotein cholesterol
LDLR	LDL receptor
Lp(a)	Lipoprotein(a)
LV	Left ventricle
Ly6C	Lymphocyte antigen 6 complex
M1	Pro-inflammatory macrophage
M2	Anti-inflammatory macrophage
mAb	Monoclonal antibody
MBF	Myocardial blood flow
MCP-1	Monocyte chemoattractant protein-1 (also known as CCL2)
MDA	Malondialdehyde

MI	Myocardial infarction
MMP	Matrix metalloproteinase
MRA	Mineralocorticoid (aldosterone) receptor antagonist
MRI	Magnetic resonance imaging
NEP	Neprilysin
NF-κB	Nuclear factor κB
NLRP3	NOD-, LRR-, and pyrin domain-containing protein 3
NO	Nitric oxide
OxLDL	Oxidized LDL
OxPL	Oxidized phospholipid
PC	Phosphorylcholine
PCI	Percutaneous coronary intervention
PCSK9	Proprotein convertase subtilisin/kexin type 9
PET	Positron emission tomography
PSL/mm^2	Photostimulated luminescence per square millimeter
qPCR	Quantitative polymerase chain reaction
RAAS	Renin-angiotensin-aldosterone system
RGD	Arginine-glycine-aspartate motif
RNA	Ribonucleic acid
ROI	Region of interest
SMC	Smooth muscle cell
SNS	Sympathetic (adrenergic) nervous system
SPECT	Single-photon emission computed tomography
SR	Scavenger receptor
SSTR2	Somatostatin receptor type 2
STEMI	ST-segment elevation MI
SUV	Standardized uptake value
SV	Stroke volume
T2DM	Type 2 diabetes mellitus
TAC	Time-activity curve
TBR	Target-to-background ratio
TG	Triglycerides
TGF-β	Transforming growth factor-β
TLR	Toll-like receptor
TNF	Tumor necrosis factor
TSPO	Translocator protein
VAP-1	Vascular adhesion protein-1
VCAM-1	Vascular cell adhesion molecule-1
VEGF	Vascular endothelial growth factor
VLDL	Very low-density lipoprotein

List of Original Publications

This dissertation is based on the following original publications, which are referred to in the text by their Roman numerals:

I   Mia Ståhle, Johanna M. U. Silvola, Sanna Hellberg, Margreet de Vries, Paul H. A. Quax, Jeffrey Kroon, Petteri Rinne, Alwin de Jong, Heidi Liljenbäck, Nina Savisto, Anna Wickman, Erik S. G. Stroes, Seppo Ylä-Herttuala, Pekka Saukko, Tommy Abrahamsson, Knut Pettersson, Juhani Knuuti, Anne Roivainen, Antti Saraste. Therapeutic antibody against phosphorylcholine preserves coronary function and attenuates vascular ^{18}F-FDG uptake in atherosclerotic mice. *JACC: Basic to Translational Science* 2020;5(4):360–373.

II Mia Ståhle, Ville Kytö, Max Kiugel, Heidi Liljenbäck, Olli Metsälä, Meeri Käkelä, Xiang-Guo Li, Vesa Oikonen, Pekka Saukko, Pirjo Nuutila, Juhani Knuuti, Anne Roivainen, Antti Saraste. Glucagon-like peptide-1 receptor expression after myocardial infarction: Imaging study using ^{68}Ga-NODAGA-exendin-4 positron emission tomography. *Journal of Nuclear Cardiology*, Published online on December 13, 2018.

III Mia Ståhle, Sanna Hellberg, Jenni Virta, Heidi Liljenbäck, Olli Metsälä, Matti Jauhiainen, Pekka Saukko, Seppo Ylä-Herttuala, Pirjo Nuutila, Juhani Knuuti, Antti Saraste, Anne Roivainen. Evaluation of glucagon-like peptide-1 receptor expression in non-diabetic and diabetic atherosclerotic mice using PET tracer ^{68}Ga-NODAGA-exendin-4. *Manuscript submitted for publication*.

The original publications have been reproduced with the permission of the copyright holders.

1 Introduction

Despite significant diagnostic and therapeutic advances, atherosclerotic cardiovascular disease (ASCVD) and its clinical consequences, ischemic heart disease, and stroke remain leading causes of death and disability worldwide. Although cardiovascular mortality has markedly declined during the past decades, the increasing incidence of obesity and type 2 diabetes mellitus (T2DM), especially in the Western countries, contribute to the high prevalence rate of ASCVD. Other modifiable risk factors for ASCVD include high blood cholesterol levels, elevated blood pressure, cigarette smoking, and low physical activity. Genetic susceptibility such as familial hypercholesterolemia (FH) causes premature ASCVD due to lifelong increase in plasma low-density lipoprotein cholesterol (LDL-C). In clinical practice, the assessment of the total risk is recommended for the prevention of ASCVD. The higher the total risk, the more intense action, i.e., lifestyle modification and appropriate treatment, is required. (Pasterkamp et al., 2016; Mach et al., 2020)

The current concept recognizes atherosclerosis as a complex, lipid-driven inflammatory disease of arteries. Lipoproteins interact with inflammatory cells in the vessel wall accelerating the development of atherosclerotic lesions. The main cause of myocardial infarction (MI) arises from a rupture of atherosclerotic lesion and thrombus formation in the coronary artery. The MI triggers an intense inflammatory response that is essential for myocardial healing, but which is also implicated in the pathogenesis of heart failure. Thus, the inflammatory process has emerged as a potential target for development of new therapeutic strategies in ASCVD. (Libby & Hansson, 2019)

Molecular imaging modalities can reveal structural, cellular, and molecular alterations in ASCVD, and therefore, might be particularly promising for the identification of patients with adverse inflammatory response, and could potentially be utilized to predict disease outcome, monitor treatment response, and develop new therapies. (Werner et al., 2020) This thesis investigates phosphorylcholine (PC) as a target for novel immunotherapy, and glucagon-like peptide-1 receptor (GLP-1R) as a new imaging biomarker in experimental models.

2 Review of the Literature

2.1 Atherosclerotic cardiovascular disease

Atherosclerotic cardiovascular disease (ASCVD) is a disorder that affects both heart and blood vessels. ASCVD include coronary artery disease (CAD), stroke, and peripheral artery disease with atherosclerosis involved in the pathogenesis. CAD can further lead to complications including unstable angina pectoris defined as chest pain caused by restricted blood flow to the myocardium, and myocardial infarction (MI) where the blood flow to the myocardium is acutely obstructed. Furthermore, patients suffering MI remain at risk for developing heart failure (HF), which is a chronic clinical syndrome in which the heart is unable to pump enough blood to meet the needs of the body. HF can be a result of different etiologies, including CAD, hypertension or valve disease, which often occur simultaneously. (Pasterkamp et al., 2016)

2.1.1 Atherosclerosis and coronary artery disease

Atherosclerosis, a disease of large and middle-sized arteries, is characterized by low-grade, chronic inflammation of the arterial wall triggered by the subendothelial accumulation of lipoproteins from the blood circulation into the inner layer of the arterial wall, the intima (Bäck et al., 2019). CAD results from atherosclerotic lesions within the epicardial coronary arteries. When the lesion grows in size, it may narrow the coronary artery and restrict the blood flow to the myocardium and/or become unstable and ultimately rupture causing, a thrombus, a blood clot in the coronary artery. (Goldstein & Brown, 2015) CAD begins early in life and is a slowly progressing disease that typically has a long clinically silent phase. Hence, the acute MI is often the first manifestation of CAD. (Stary, 2000)

The pioneering work of pathologists Virchow and von Rokitansky in the mid-1800s described for the first time lipid accumulation, cell proliferation, "elements of inflammation", and incorporated thrombus as key pathogenic processes in atherosclerosis (Virchow 1858). The schema of lipid storage disease introduced by Anitschkow and co-workers was a dominating hypothesis until the 1970s (Anitschkow & Chalatow 1913). Thereafter, the initiating role of smooth muscle cell

(SMC) proliferation and endothelial cell (EC) dysfunction in lesion formation was acknowledged (Ross, 1993), followed by observations of innate and adaptive immune responses in atherogenesis (Libby, 2002). The current concept involves elements from each of the previous theories, recognizing atherosclerosis as a complex, lipid-driven inflammatory disease (Libby & Hansson, 2019).

2.1.1.1   Blood lipids and lipoproteins

Lipids derived from food intake and endogenous biosynthesis are essential for energy utilization, steroid hormone production and bile acid formation. Because lipids are insoluble in water, they are packaged into lipoproteins for transportation in blood. The hydrophobic core of a lipoprotein particle is rich in cholesterol esters and triglycerides (TG), and it is surrounded by a hydrophilic membrane consisting of phospholipids, unesterified cholesterol, and apolipoproteins. The major lipoproteins in bloodstream are chylomicrons, very low-, intermediate-, low-, and high-density lipoproteins (VLDL, IDL, LDL and HDL), and lipoprotein(a) [Lp(a)]. (Mach et al., 2020)

Chylomicrons are responsible for the transportation of dietary lipids from intestine to liver and peripheral tissues. LDL is derived from VLDL and IDL synthetized by the liver, and it is a principal carrier of cholesterol in plasma. VLDL, IDL, LDL, and Lp(a) particles contain an apolipoprotein B100 (ApoB100) molecule on their surface. Lp(a) is an LDL-like particle with an Apo(a) moiety covalently bound to its ApoB100 molecule. The function of ApoB100 is to maintain the structural integrity of particles and serve as a ligand for LDL receptor (LDLR) mediating hepatic clearance of lipoproteins. However, all ApoB100-containing lipoproteins <70 nanometer in diameter, including remnant particles, can cross the endothelium, thus provoking a pro-atherogenic process. In contrast, HDL is considered anti-atherogenic since it contains apolipoprotein A1 on the surface and has a crucial role in reverse cholesterol transport from peripheral tissues to the liver. (Boren et al., 2020)

Plasma LDL-C is a measure of the cholesterol mass carried by LDL particles, and it provides an estimate of the concentration of circulating LDL. It has been consistently proven in large studies that LDL-C is causally associated with the risk of ASCVD and that therapies lowering LDL-C levels reduce cardiovascular risk and mortality. (Mach et al., 2020) Although LDL is recognized as the principal driver of the initiation and progression of atherosclerosis, emerging evidence support an independent, causal role of Lp(a) in ASCVD (Nordestgaard & Langsted, 2016). Atherogenicity of Lp(a) is discussed further in Chapter 2.3.
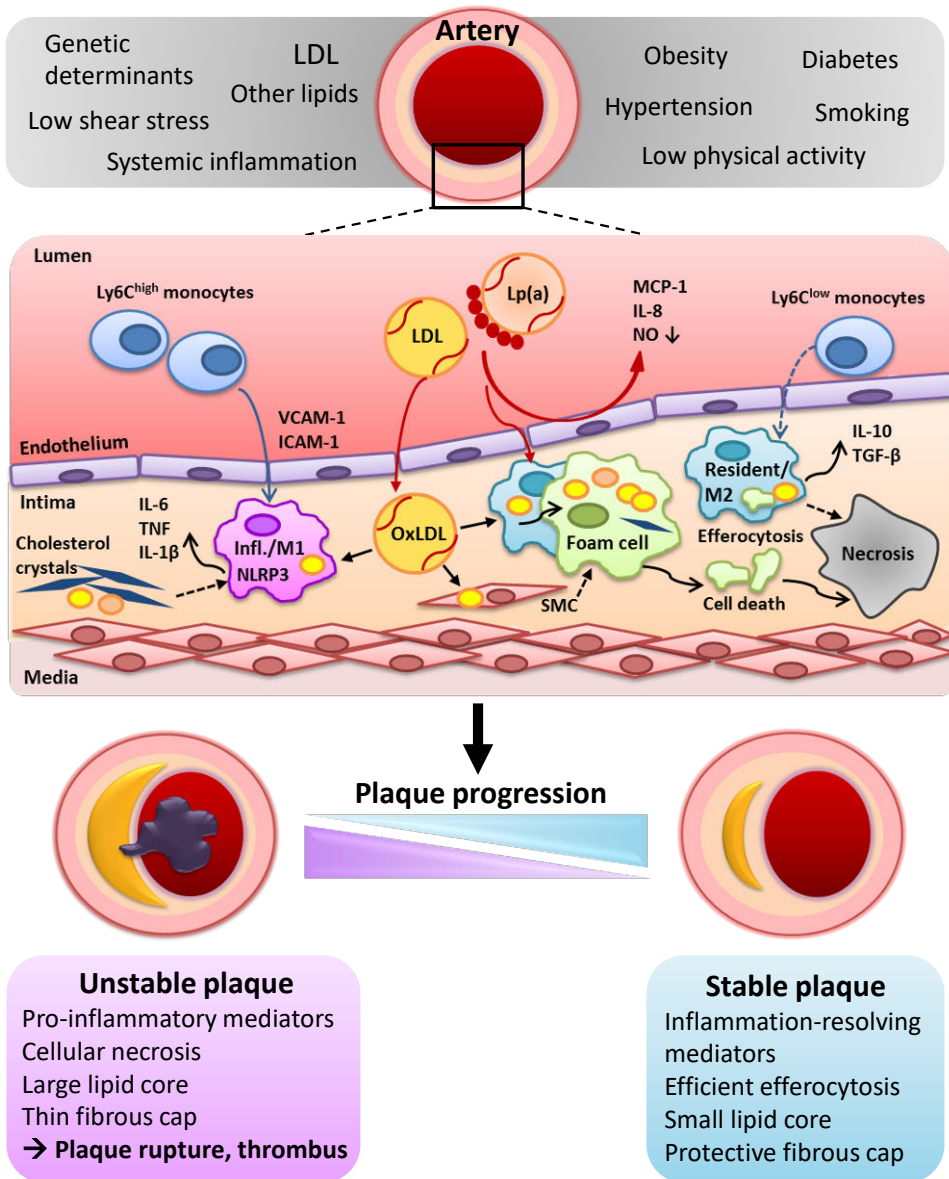
Figure 1. Pathogenesis of coronary artery disease. Summary of the main risk factors and mechanisms underlying the endothelial dysfunction, retention of LDL particles and formation of foam cells in the artery wall, and subsequent inflammatory responses. Inflammatory/M1 macrophages accelerate the pro-inflammatory status by producing such mediators as IL-1β, TNF, and IL-6 in response to inflammasome (NLRP3) activation. Resident/M2 macrophages secrete pro-resolving mediators, such as IL-10 and TGF-β to suppress inflammation and promote healing. The capacity of M2 macrophages to clean dying cells becomes overloaded during the progression of atherosclerosis, thereby resulting in the formation of necrotic core and worsening of inflammation. The final clinical outcome depends on the balance of pro-inflammatory and inflammation-resolving mediators. The rupture-prone unstable plaque is typically characterized by a pronounced inflammation, large lipid-rich necrotic core, low SMC density, and thin fibrous cap.

2.1.1.2 Endothelial dysfunction

The artery wall has three layers of which the innermost layer, tunica intima, consists of the endothelium and subendothelial connective tissue. ECs form a continuous monolayer that serves as a lining for all blood vessels to maintain vascular homeostasis in response to hemodynamic forces and chemical signals. The middle layer, tunica media, consists primarily of SMCs while the outermost layer, tunica adventitia, involves connective tissue. (Gimbrone & García-Cardeña, 2016)

Normally-functioning endothelium regulates vascular tone, supplies substances between blood and tissues, controls angiogenesis, i.e., the formation of new vessels and cell proliferation, modulates immune responses, and acts as a barrier to macromolecules, such as bacterial products (Félétou & Vanhoutte, 2006). Moreover, the normal endothelium exhibits anti-thrombotic properties by preventing the activation of coagulation cascade and adhesion of platelets and immune cells to the vascular wall. However, noxious stimuli such as hyperlipidemia, hyperglycemia, cigarette smoke, hypertension, or altered hemodynamic forces can trigger an endothelial dysfunction. (Gimbrone & García-Cardeña, 2016)

The loss of normal, protective function of endothelium was defined as endothelial dysfunction in the mid-1980s. The seminal observations of Furchgott and Zawadzki showed that the vasodilation response to acetylcholine was endothelium-dependent mediated by a humoral factor (Furchgott and Zawadzki 1980). This factor was first described as endothelium-derived relaxing factor and later identified as nitric oxide (NO) (Palmer 1987). The observations of impaired endothelium-mediated vasodilation in the context of hypercholesterolemia in rabbits (Verbeuren et al., 1986) and coronary arteries of atherosclerotic patients (Ludmer et al., 1986) suggested that a deficiency in endothelial NO production or its bioavailability precede the formation of atherosclerotic lesions.

Endothelial nitric oxide synthase (eNOS) is a key enzyme generating NO from L-arginine in ECs. The most important factor regulating eNOS expression and activity are hemodynamic forces, fluid shear stress in particular. Shear stress is defined as frictional force acting on the endothelial surface as a result of viscous fluid, the blood flow. (Malek & Alper, 1999) Atherosclerosis originates mainly at arterial bifurcations, branch points, and regions of high curvature. These sites are prone to disturbed flow patterns including low flow, flow separation, low shear stress, and turbulent flow. Low shear stress combined with other pro-inflammatory agents, such as modified lipoproteins, results in reduced NO production that is associated with impaired relaxation of SMCs and EC activation. (Hahn & Schwartz, 2008) Endothelial activation further leads to increased permeability, increased oxidative stress, cell surface expression of vascular cell adhesion molecule-1 (VCAM-1) and intercellular adhesion molecule-1 (ICAM-1), and secretion of pro-thrombotic mediators, pro-inflammatory cytokines [e.g.,

interleukin-8 (IL-8)] and chemokines [e.g., monocyte chemoattractant protein-1 (MCP-1), also known as C-C motif chemokine ligand 2 (CCL2)], thereby facilitating lipoprotein penetration, monocyte adhesion to and transmigration across the endothelial layer (Figure 1). (Gimbrone & García-Cardeña, 2016) It has been demonstrated in patients that low local endothelial shear stress at baseline is associated with subsequent lesion progression to a clinical event (Stone et al., 2012). Thus, if the ECs fail to maintain the normal quiescent phenotype, it can lead to a dysfunctional endothelium and inflammatory milieu that is susceptible for development of atherosclerosis.

2.1.1.3   Inflammation in atherosclerosis

The acute inflammatory response in the arterial wall is initiated by ApoB100-containing lipoproteins, selectively LDL, crossing the permeable endothelium by both passive filtration and active, receptor-mediated transcytosis. In the intima, ApoB100 moiety of LDL interacts with intimal extracellular proteoglycans and the LDL is trapped. This process is referred to as retention. The retained LDL is susceptible for modifications including oxidation and aggregation. Oxidation occurs by enzymes and oxidants leading to the generation of oxidized LDL (OxLDL) that contains several bioactive molecules on its surface, such as oxidized phospholipids (OxPL), which mediate pro-inflammatory effects. (Boren et al., 2020; Ylä-Herttuala et al., 1989) OxPLs are discussed in more detail in Chapter 2.3.

The predominant immune cells in both human and mouse atherosclerotic lesions are macrophages, which originate mainly from circulating monocytes, but also from local proliferation of tissue-resident macrophages and trans-differentiation of intimal SMCs into macrophage-like cells. Other inflammatory cells include lymphocytes, mast cells, dendritic cells, and neutrophils. In mice under physiological state, circulating non-classical Ly6C^{low} monocytes patrol the endothelium to maintain protective function, whereas in atherosclerosis, pro-inflammatory classical Ly6C^{high} monocytes predominate in the blood circulation (CD14^{+}CD16^{+} and CD14^{+}CD16^{-} monocytes in humans, respectively) and are recruited into the intima, where they differentiate into macrophages. Macrophages can use different combinations of scavenger receptors (SR), including CD36, SRA1 and 2, SRB1, CD68, and lectin-type oxidized LDL receptor 1 (LOX1), to recognize and ingest OxLDL followed by the generation of cytoplasmic cholesteryl ester droplets, which make the macrophages "foamy". (Moore et al., 2018) SMCs can also form foam cells (Allahverdian et al., 2014). Foam cell formation is a hallmark of early atherosclerotic lesions, so-called "fatty streaks" (Virmani et al., 2000). (Figure 1)

Formation of foam cells is a beneficial process in early lesions, since free cholesterol is stored in lipid droplets and effluxed to HDL for transportation to the

liver. However, with excessive free cholesterol uptake, lipid metabolism can become defective. It leads to the formation of cholesterol crystals that activate a multiprotein complex, NOD-, LRR-, and pyrin domain-containing protein 3 (NLRP3) inflammasome, resulting in secretion of pro-inflammatory cytokines, interleukin-1β (IL-1β) and interleukin-18 (IL-18) from macrophages (Duewell et al., 2010). IL-1β can downstream promote the tumor necrosis factor (TNF) and interleukin-6 (IL-6) pathway, leading to increased production of C-reactive protein (CRP) from the liver (Ridker & Lüscher, 2014). It is well established that elevated plasma levels of CRP [measured by high-sensitivity (hs) assay and termed as hsCRP], and IL-6 are associated with an increased risk of cardiovascular events, independent of cholesterol levels (Ridker et al., 2000). It is important to note that this acute-phase inflammatory reaction is protective when functioning properly and temporally like a defense against infections. However, if the resolution of inflammation fails, it can persist and lead to chronic inflammatory conditions.

The inflammation-resolution response is an active process orchestrated by various pro-resolving mediators, such as annexin A1, IL-10, and NO, as well as macrophages. In advanced lesions, dysfunctional foam cells die easily and release their content to extracellular space, leading to necrotic core formation. The cells that die via apoptosis are cleared by the surrounding counterpart macrophages; the process is called efferocytosis. (Tabas, 2010) Efficient efferocytosis in early atherogenesis reduces the development of atherosclerotic lesion and does not tend to trigger an inflammatory response (Hamada et al., 2014). However, foam cells can also die via pyroptosis and necroptosis, which leads to the release of pro-inflammatory mediators and inflammasome activation. Furthermore, the capacity of efferocytes to ingest apoptotic cells becomes impaired during the progression of atherosclerosis, thereby resulting in secondary necrosis and worsening of the inflammatory status. (Tait et al., 2014) (Figure 1)

The phenotype heterogeneity of intimal macrophages is wide, rather complex, and likely to change during the atherosclerosis progression in response to different microenvironmental conditions, such as growth factors, cytokines, hypoxia, and lipid accumulation. A novel atlas of the immune cell repertoire in atherosclerosis defined by single-cell ribonucleic acid (RNA) sequencing has revealed unique macrophage subsets with both pathogenic and protective functions. (Cochain et al., 2018; Winkels et al., 2018). The modern classification distributes macrophages into 5 different subsets: resident-like, inflammatory (CCR2$^+$), foamy Trem2, interferon-inducible cell (IFNIC), and cavity macrophages (Zernecke et al., 2020). The traditional classification divides macrophages into pro-inflammatory M1 and anti-inflammatory M2 macrophages. These groups represent the opposite ends of the whole spectrum, but it is still a useful classification in the context of inflammation resolution. M1 macrophages accelerate the pro-inflammatory status by producing

such mediators as IL-1β, IL-6, IL-12, TNF, MCP-1, and inducible nitric oxide synthase (iNOS), which further promote the recruitment of new monocytes, cell death and secretion of matrix metalloproteinases (MMPs) contributing to lesion vulnerability. In contrast, M2 macrophages secrete pro-resolving mediators to suppress inflammation and promote healing. For example, IL-10 enhances efferocytosis and transforming growth factor-β (TGF-β) induces collagen production by fibroblasts, thus promoting the formation of protective fibrous cap in the lesion. (Tabas & Bornfeldt, 2016)

As a result, the final clinical outcome depends on the balance of pro-inflammatory and pro-resolving mediators, combined with other risk factors. If the resolution of inflammation is successful, it ensures proper healing and formation of a stable plaque manifesting, clinically as a chronic coronary syndrome (CCS). However, stable coronary plaques may become stenotic and cause symptoms such as chest pain and myocardial ischemia, usually during exercise. In contrast, when the pro-inflammatory mediators dominate, it can lead to an unstable advanced plaque that is characterized by a large lipid-rich necrotic core, pronounced inflammation, low SMC density and thin fibrous cap, and is frequently non-stenotic. An unstable plaque is prone to the erosion of the endothelial lining or rupture of the surface fibrous cap via both biomechanical and hemodynamic factors. The exposure of lesion components to blood initiates a coagulation cascade and thrombus formation, resulting in obstructed blood flow, which may manifest clinically as an acute coronary syndrome (ACS) or a stroke. (Figure 1) (Falk et al., 2013; Virmani et al., 2000)

2.1.2 Myocardial infarction and heart failure

Clinically, common presentations of life-threatening ACS include unstable angina, arrhythmias, acute myocardial infarction (AMI), and sudden cardiac death. Rupture of an unstable plaque resulting in thrombosis accounts for up to 70% of all acute MI events. (Pasterkamp et al., 2016) Although short-time mortality following AMI has declined significantly during recent years, patients surviving AMI still remain at risk for developing HF in the long term, which is associated with a high mortality rate. Thus, in order to prevent the onset of HF in patients suffering AMI, the main strategy is to reduce the MI size and preserve the left ventricular (LV) function. In this regard, the endogenous myocardial inflammatory response and repair process following AMI have a crucial role in infarct healing and can either propagate or defend against HF. (Adamo et al., 2020; Braunwald, 2013)

2.1.2.1   Ischemia and acute myocardial infarction

Coronary circulation comprises the epicardial conductance arteries (diameter 1-6 mm) that feed downstream the microcirculation consisting of small arteries, arterioles, and capillaries (<300-400 µm), which mostly run within the ventricular wall. That is the site of the regulation of myocardial blood flow (MBF) and exchange of gas and metabolites with the myocardium, the contractile unit. (Levy et al., 2019) The heart is an aerobic organ that in normal conditions relies almost exclusively on the aerobic oxidation of substrates, largely fatty acids, in mitochondria for the generation of energy. (Braunwald, 1971) Hence, insufficient supply of blood (oxygen and nutrients) mainly due to CCS or ACS results in myocardial ischemia. At the myocyte level, prolonged ischemia leads to a metabolic switch towards anaerobic glycolysis, progressive membrane damage with cell swelling and death (oncosis), mitochondrial stress, and apoptosis, resulting in necrosis and loss of contractile function. (Buja & Vander Heide, 2016; Stanley et al., 2005) When the acute myocardial injury (necrosis), detected by a rise and/or fall in circulating cardiac biomarkers [preferably cardiac troponin (cTn) I or T] in the setting of acute myocardial ischemia, is evident, AMI should be used as a clinical definition. In addition to abnormal cTn values, one of the following diagnostic criteria for AMI should be present: ischemic symptoms, abnormal electrocardiographic (ECG) findings [e.g. ST-segment elevation MI (STEMI)], or imaging evidence of an intracoronary thrombus, new loss of viable myocardium, or new regional wall motion abnormality. (Thygesen et al., 2019)

Ischemia can be reversible if the blood flow is restored by an early and successful reperfusion. The seminal work by Reimer and co-workers showed that, in rabbits, irreversible injury begins at 20 min in the ischemic subendocardium and papillary muscle, extends into the mid-myocardium by 60-90 min, and forms a transmural infarction after 3-4 hours (Reimer et al., 1977; Reimer & Jennings, 1979). A similar time course appears in humans. Currently, patients with STEMI are referred to revascularization primarily by percutaneous coronary intervention (PCI) involving balloon dilatation and stenting, when feasible, to achieve maximum salvage of myocardium (Scholz et al., 2018). Paradoxically, the reperfusion process itself can cause additional myocardial damage, the so-called ischemia/reperfusion (I/R) injury, which is characterized by myocardial stunning (transient contractile impairment that recovers over time), reperfusion arrhythmias, coronary no-reflow phenomenon (inability to perfuse the myocardium at the level of microvasculature), and cardiomyocyte death (the lethal form of I/R injury). (Yellon & Housenloy, 2007) Thus, the I/R injury also contributes to the final MI size, and the approaches limiting the infarct size, i.e., cardioprotection, are crucial for preventing LV dysfunction.

2.1.2.2 Inflammatory response and myocardial repair

In general, MI shares many features with wounds resulting from trauma or surgery with the exception that MI is a sterile injury of the heart, inflicting one of the most lethal wounds. The healthy heart contains cardiomyocytes, fibroblasts, vascular cells, resident mast cells and macrophages, and small populations of other leukocytes, such as monocytes, neutrophils, and B and T cells. (Nahrendorf & Swirski, 2013) In the steady-state heart, macrophages have an important housekeeping role against infections, but it has been suggested that they also participate in normal electrical conductance (Hulsmans et al., 2017) and physiological cardiac remodeling that occurs during pregnancy or endurance training. The adult mammalian heart has little regenerative capacity therefore, a well-coordinated cascade of cellular events is required for healing and formation of a collagen-rich scar that does not compromise heart function. (Swirski & Nahrendorf, 2018)

Healing of the infarcted myocardium involves the pro-inflammatory phase (clearance of dead cells) and the reparative phase (resolution of inflammation), which results in maturation of a durable scar (Figure 2). Within minutes after the onset of ischemia, dying cardiomyocytes release various danger-associated molecular patterns (DAMP), including alarmins that provide the main stimulus for the activation of innate immune system. DAMPs are recognized by immune cells via toll-like receptors (TLR), such as TLR4, that downstream stimulate the nuclear factor κB (NF-κB) signaling and NLRP3 inflammasome leading to the activation of the complement system. (Timmers et al., 2012) Furthermore, the mast cells release their granules, the cardiomyocytes, resident macrophages and fibroblasts begin to produce pro-inflammatory cytokines, chemokines and growth factors, such as IL-1β, TNF, MCP-1, and vascular ECs express adhesion molecules, such as VCAM-1, thereby triggering a recruitment of inflammatory cells from the circulation into the myocardium. (Frangogiannis, 2014; Swirski & Nahrendorf, 2018)

Neutrophils are the first immune cells entering the infarcted myocardium and mediating clearance of necrotic cells and extracellular matrix (ECM) debris. Neutrophils may contribute to an acute I/R injury, but they are also involved in cardiac repair by polarizing macrophages towards a reparative phenotype. (Horckmans et al., 2016) Neutrophil infiltration is rapidly followed by the recruitment of pro-inflammatory Ly6C^{high} monocytes in response to the activation of the myocardial MCP-1 and its receptor CCR2. Leukocytes originate mainly from the bone marrow but also from the spleen, which, especially at later phases, serves as a large reservoir of immune cells that can be rapidly recruited to the heart. The number of neutrophils decreases after 3 days and they almost completely disappear after 7 days, whereas Ly6C^{high} monocytes continue to accumulate and differentiate into CCR[+] (M1-type) macrophages. The main function of Ly6C^{high} monocytes/M1

macrophages is to clear the infarct of debris by phagocytosis. They also secrete pro-inflammatory cytokines, MMPs, and proteases that further fuel inflammation. The peak of initial pro-inflammatory phase is seen 3 to 4 days after MI, followed by a second wave of immune cells promoting tissue repair. (Figure 2) (Bajpai et al., 2018; Epelman et al., 2014; Hilgendorf et al., 2014; Lavine et al., 2014; Nahrendorf et al., 2007; van der Laan et al., 2014)

Approximately 4 days after MI, the secretion of pro-inflammatory cytokines decreases and Ly6C^{low} monocytes begin to accumulate in the infarcted myocardium and differentiate into reparative CCR$^-$ (M2-type) macrophages mediating the resolution of inflammation (Epelman et al., 2014; Lavine et al., 2014; Nahrendorf et al., 2007). Alternatively, it has been proposed that local monocyte/macrophage turnover from Ly6C^{high}/M1 to Ly6C^{low}/M2 or direct differentiation from Ly6C^{high} monocytes may be the main source of M2 macrophages in the infarct (Bajpai et al., 2018; Hilgendorf et al., 2014). Ly6C^{low} monocytes/M2 macrophages outnumber their pro-inflammatory counterparts on day 7. Although first observed in mice, similar monocyte kinetics has been confirmed in patients with AMI (Tsujioka et al., 2009; van der Laan et al., 2014). As a result, Ly6C^{low} monocytes/M2 macrophages secrete IL-10 that enhances efferocytosis and dampens the IL-6, TNF and MMP-9 expression (Krishnamurthy et al., 2009), produce TGF-β to promote collagen and fibronectin production in fibroblasts (Dobaczewski et al., 2011), and secrete vascular endothelial growth factor (VEGF) to support angiogenesis (Nahrendorf et al., 2007). Thus, the necrotic area is replaced with newly forming tissue referred to as granulation tissue.

As pro-inflammatory signaling is repressed, the activation of the TGF-β signaling, in particular, promotes the expansion and proliferation of cardiac fibroblasts, and the transdifferentiation of fibroblasts into myofibroblasts, and stimulates a pro-fibrotic matrix-preserving program. (Dobaczewski et al., 2011) Myofibroblasts are cells that express contractile proteins, such as α-smooth muscle actin (α-SMA), and produce collagen that strengthens the emerging scar. It has been proposed that myofibroblasts can also originate from local ECs, SMCs and pericytes, but their specific functions in repair are largely unknown. (Travers et al., 2016; Willems et al., 1994) Furthermore, TGF-β interacts with other important pathways regulating fibrogenic responses such as renin-angiotensin-aldosterone system (RAAS). (Figure 2)

After the reparative phase, approximately on day 14 in mice, the ECM becomes cross-linked, myofibroblast density decreases, immune cell recruitment wanes, and reparative cells are inactivated and may undergo apoptosis, eventually resulting in a dense scar. The exact molecular stop-signals terminating the reparative phase remain unknown. (Prabhu & Frangogiannis, 2016) To maintain the integrity of the heart after MI, inflammatory and reparative functions have to be tightly in balance.

Otherwise, overactive early inflammatory response or impaired collagen deposition, for example, may lead to a thin and poorly healed infarct that is prone to rupture, thus causing a sudden cardiac death. The intense inflammatory response is essential for cardiac repair, but is also implicated in the pathogenesis of adverse LV remodeling and HF. (de Lemos et al., 2007; Frangogiannis, 2014; Tsujioka et al., 2009)
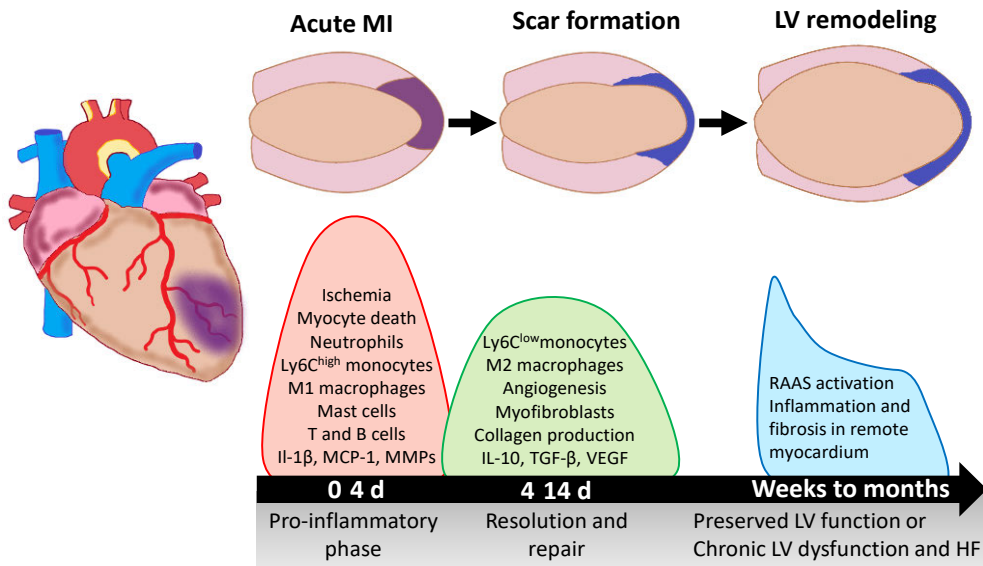
Acute MI **Scar formation** **LV remodeling**

Ischemia
Myocyte death
Neutrophils
Ly6C^{high} monocytes
M1 macrophages
Mast cells
T and B cells
Il-1β, MCP-1, MMPs

Ly6C^{low}monocytes
M2 macrophages
Angiogenesis
Myofibroblasts
Collagen production
IL-10, TGF-β, VEGF

RAAS activation
Inflammation and
fibrosis in remote
myocardium

0 4 d	4 14 d	Weeks to months
Pro-inflammatory phase	Resolution and repair	Preserved LV function or Chronic LV dysfunction and HF

Figure 2. Cardiac repair after myocardial infarction. Healing of the infarcted myocardium involves a pro-inflammatory phase (clearance of dead cells) and a reparative phase (resolution of inflammation), which results in the maturation of a durable scar and the possibly preserved LV function. Inflammatory and reparative functions are tightly and timely regulated in order to maintain the integrity of the heart after MI. Overactive inflammatory and neurohormonal responses affecting also the remote, non-infarcted myocardium are implicated in the pathogenesis of adverse LV remodeling and chronic HF.

2.1.2.3 Adverse left ventricular remodeling and heart failure

In addition to the infarcted myocardium, the remaining viable, remote myocardium undergoes molecular and structural alterations in response to the injury, termed a remodeling process, which may have significant consequences on cardiac function and the onset of HF over time (Braunwald, 2013). Large infarcts (Chareonthaitawee et al., 1995; McKay et al., 1986; Pfeffer et al., 1979) and the degree of neurohormonal (Cohn et al., 1984; Dzau et al., 1981) and inflammatory (Chen et al., 2012; de Lemos et al., 2007) activation are strong predictors of late LV remodeling and HF. (Figure 2) The cardiac architecture (size, shape and composition) is normally matched to function, wherefore, LV remodeling is considered first as an

adaptive, protective response that stabilizes contractile function and maintains stroke volume (SV, the volume of blood the LV pumps out during each contraction). The LV remodeling includes progressive LV dilatation, higher diastolic pressure, wall thinning, hypertrophy of the myocardium, fibrosis, and distortion of LV shape (sphericity). (Sutton & Sharpe, 2000) This process can take months and the clinical manifestation, HF with reduced ejection fraction (HFrEF, EF<40%), also called systolic HF, develops when the end diastolic volume (EDV) is high and the LV cannot eject normal SV. The typical clinical symptoms, although often non-specific, include breathlessness, ankle swelling, pulmonary crackles, and fatigue. (Katz & Rolett, 2015; Ponikowski et al., 2016)

The acute loss of myocardium due to MI results in alterations in circulatory hemodynamics and wall stresses that trigger a rapid compensatory activation of the sympathetic (adrenergic) nervous system (SNS) and RAAS. The neurohormonal response involves release of noradrenaline in the SNS and activation of $\beta1$-adrenoreceptors in the kidneys, which lead to up-regulation of renal RAAS components: renin, angiotensin II (Ang II), Ang II receptor type 1 (AT_1), angiotensin-converting enzyme (ACE), and aldosterone. The secretion of counter-regulatory hormones, atrial and brain natriuretic peptides (ANP and BNP), is initiated, but the peripheral resistance to ANP and BNP in HF keeps the RAAS activated. (Hartupee & Mann, 2016) ANP and BNP are well-established biomarkers of HF (Cowie et al., 1997). Although the neurohormonal activation maintains cardiovascular homeostasis and SV in the short term, a chronic stimulus will result in pressure and volume overload in the heart, cardiomyocyte hypertrophy and death, increased collagen production and ECM degradation (stiffness and thinning), $\beta1$-adrenoreceptor desensitization, dysregulation of intracellular Ca^{2+} (contraction), and defects in energetics and metabolism. (Braunwald, 2013; Hartupee & Mann, 2016)

The pharmacological blockade of the neurohormonal system improves outcomes in patients with HF (MERIT-HF, 1999; The SOLVD, 1991), but it does not fully explain the complex LV remodeling process. The remote myocardium recruits more leukocytes progressively from the spleen during remodeling (Ismahil et al., 2014), and resident macrophages survive and proliferate in remote areas, probably in response to the pro-inflammatory cytokine milieu and by exposure to LV stretch (Sager et al., 2016). Elevations in the systemic and local TNF, IL-1β, IL-6, MCP-1, and hsCRP levels are associated with chronic HF (Cesari et al., 2003; Damås et al., 2000; Torre-Amione et al., 1996), and human $CCR2^+$ macrophage abundance correlates with adverse remodeling (Bajpai et al., 2018). Furthermore, macrophages express ACE that provides a local source of Ang II, and myofibroblasts produce aldosterone, which promotes fibrosis in the remote myocardium (Silvestre et al., 1999; Y. Sun et al., 1994). Indeed, neurohormonal antagonists may have direct effects on macrophages and myofibroblasts by delaying adverse fibrosis and LV

remodeling (Yu et al., 2001). Although the sustained activation of inflammatory and fibrogenic pathways in the remote myocardium is associated with HF progression, the exact role of different macrophage subsets remains unclear in chronic HF, since no proper single-cell RNA sequencing of inflammatory cells in the remodeling myocardium has yet not been carried out. (Adamo et al., 2020)

2.1.3 Overview of standard pharmacological therapies

Lifestyle modifications and interventions targeting the known risk factors such as high cholesterol levels, high blood pressure, and hyperglycemia have a central role in the prevention and treatment of ASCVD. Key lifestyle interventions include cessation of smoking, healthy diet and weight, and physical activity. Plasma LDL-C lowering represents the primary target for reducing ASCVD risk and events, although the awareness of high Lp(a) and TG levels as independent risk factors has emerged recently (Tsimikas & Stroes, 2020).

Statins (e.g., atorvastatin, simvastatin) serve as a cornerstone in the treatment of dyslipidemia. Statins reduce cholesterol synthesis in the liver by competitively inhibiting the enzyme 3-hydroxy-3-methyl-glutaryl-coenzyme A (HMG-CoA) reductase that leads to increased LDLR expression and enhanced LDL uptake in hepatocytes. The degree of LDL-C lowering is dose-dependent (on average 30-50%) and varies inter-individually and between different statins. Other lipid-lowering drugs include cholesterol absorption inhibitors (ezetimibe), bile acid sequestrants, and fibrates. Recently, a new therapeutic class of agents, proprotein convertase subtilisin/kexin type 9 (PCSK9) inhibitors, has become available for statin-intolerant patients or patients at very high risk (Robinson et al., 2015a). Blockade of the PCSK9 protein with fully human antibody (alirocumab or evolocumab) results in lower concentration or function of PCSK9 and thus, increased expression of LDLRs. PCSK9 inhibitors, either alone or in combination with statins and/or other lipid-lowering therapies, have been shown to reduce LDL-C levels on average by 60%. (Mach et al., 2020)

In the context of CCS, statins are recommended for all patients. In symptomatic CCS patients, anti-ischemic drugs (e.g., nitrates, β-adrenoreceptor blockers) relieve angina symptoms, and an anti-platelet drug (preferably low-dose aspirin) is recommended for prevention of ischemic events in patients with previous MI or definite evidence of CAD. A second anti-thrombotic drug (e.g., anti-coagulant rivaroxaban) can be added to aspirin for high-risk patients. Moreover, if hypertension, LV dysfunction or diabetes coexist in CCS patients, ACE inhibitors (ACEI) or β-blockers are to be considered. Dual anti-platelet therapy [low-dose aspirin and oral $P2Y_{12}$ inhibitor (e.g., clopidogrel)] should be started for all patients

after MI and/or undergoing primary PCI to reduce the risk of thrombotic events (maintained 6-12 months). (Knuuti et al., 2020)

The standard care of patients with HF aims to improve their functional capacity and quality of life, prevent hospital admission and reduce mortality. Inhibition of RAAS activation with ACEIs (e.g., captopril, enalapril) or AT_1 receptor blockers (ARB, e.g., candesartan, valsartan) in combination with β-blockers (e.g., bisoprolol) form the backbone for the treatment of HF and are recommended for every patient with HFrEF. ARBs are typically recommended if ACEIs are contraindicated or not tolerated. Mineralocorticoid (aldosterone) receptor antagonists (MRA, spironolactone or eplerenone) can be added as a complementary treatment in selected symptomatic patients. Neurohormonal antagonists, ACEIs, ARBs, β-blockers, and MRAs have been shown to reduce the risk of HF hospitalization and mortality and morbidity in HFrEF patients. (Ponikowski et al., 2016) A new dual blocker drug combining the ARB (valsartan) and a neprilysin (NEP) inhibitor (sacubitril) in a single compound (ARNI) has become available as a replacement for ACEI for patients who remain symptomatic despite optimal therapy (McMurray et al., 2014). Inhibition of NEP decreases degradation of vasoactive peptides such as ANP and BNP. In symptomatic HFrEF patients, diuretics (to alleviate symptoms) and selected inotropic agents can be used in conjunction with the above-mentioned therapies. In asymptomatic patients with LV systolic dysfunction, ACEIs and β-blockers are recommended preventively to reduce the risk of HF development. (Ponikowski et al., 2016) The novel approaches for the management of ASCVD in diabetic patients are addressed in Chapter 2.4.

Despite the contemporary therapies, the so-called residual inflammatory risk still exists in some patients (Lawler et al., 2020). The CANTOS trial in 2017 showed that an antibody therapy targeting IL-1β (canakinumab) reduces recurrent cardiovascular events in patients with previous MI and high hsCRP levels (Ridker et al., 2017), thereby providing eventually a clinical proof that inflammation has a crucial role in atherogenesis. Furthermore, a pre-specified sub-analysis of the CANTOS trial suggested that canakinumab reduces HF-related hospitalization and mortality (Everett et al., 2019). Recently, an old drug, colchicine that is indicated for the treatment of gout and pericarditis, was shown to reduce the risk of ischemic cardiovascular events in patients with recent MI (Tardif et al., 2019) or CCS (Nidorf et al., 2020) Colchicine possibly inhibits neutrophil function, secretion of inflammatory chemokines, and inflammasome activation. To date, although some of the current therapies may exert pleiotropic anti-inflammatory properties, no therapy that specifically attenuates cardiovascular inflammation is approved for the treatment of ASCVD or HF. However, targeted anti-inflammatory therapies bear clinical potential, but precise identification of patients with a "cardio-inflammatory" phenotype would be required. (Adamo et al., 2020; Lawler et al., 2020)

2.2 Advances in non-invasive cardiovascular imaging

Both invasive and non-invasive cardiovascular imaging hold an essential role in the diagnosis of CAD and HF, provide prognostic information, and guide the treatment strategies. In general, cardiovascular imaging techniques include anatomical, functional, and molecular imaging approaches that are commonly used in combination for multimodal or hybrid imaging. Invasive coronary angiography (ICA) is considered the reference standard test for the evaluation of coronary artery anatomy and the severity of luminal obstruction caused by atherosclerotic lesion. ICA is based on the intracoronary injection of an iodinated contrast medium through a catheter under X-ray fluoroscopy. The spatial resolution of ICA is high. In the presence of an angiographically intermediate lesion, the functional severity of stenosis can be determined by the invasive measurement of myocardial fractional flow reserve (FFR) or instantenous wave-free ratio (iFR). The FFR is derived from the ratio of the mean distal coronary artery pressure to the mean aortic pressure during pharmacologically induced coronary vasodilatation, thus providing an estimate of stenosis-induced flow impairment. The iFR differs from the FFR in that the ratio is measured at a distinct time in cardiac diastole, termed the wave-free period, in non-vasodilated conditions. In addition to visual classification by ICA, the FFR and iFR provide valuable information for decision-making during catheterization as to whether or not coronary revascularization is needed. Other invasive approaches to assess stenosis severity include intravascular ultrasound imaging (IVUS) and optical coherence tomography (OCT). (Dewey et al., 2020; Jensen et al., 2020)

Angiography can also be conducted non-invasively by coronary computed tomography angiography (CTA), which involves an X-ray computed tomography (CT) scan combined with an intravenously injected contrast agent. Modern CT scanners provide submillimeter spatial resolution and excellent image quality. In addition to the assessment of luminal stenosis, the advantages of coronary CTA include the evaluation of lesion morphology. Coronary lesions are traditionally categorized according to the degree of calcified components detected by CT. In the context of non-calcified lesions, CTA allows the identification of high-risk plaque features including the napkin-ring sign (differentiation between high-attenuation fibrous area and low-attenuation necrotic core), positive remodeling (compensatory enlargement of the vessel wall with little luminal narrowing), low attenuation, and spotty calcification, which may provide incremental prognostic information. The assessment of FFR by a CT-derived methods is also possible. (Maurovich-Horvat et al., 2014) Although coronary CTA cannot directly distinguish a stable lesion from an acute plaque rupture, it is an accurate diagnostic tool to rule out obstructive CAD, thereby significantly reducing the number of unnecessary ICAs (Newby et al., 2018;

Shaw et al., 2012). The recent Guidelines recommend the use of either coronary CTA or non-invasive functional imaging of ischemia as the first-line diagnostic test for patients with low-to-intermediate clinical likelihood of CAD (Knuuti et al., 2020).

Ischemia can be detected through ECG changes (exercise ECG), wall motion abnormalities by stress echocardiography (ultrasound) or stress cardiac magnetic resonance imaging (MRI), or measurement of blood flow through the myocardium (perfusion) during stress testing. Perfusion imaging modalities include single-photon emission computed tomography (SPECT), positron emission tomography (PET), myocardial contrast echocardiography, and contrast cardiac MRI. (Knuuti et al., 2020). The most commonly used clinical application to assess myocardial perfusion is ^{99m}Tc-Sestamibi or ^{99m}Tc-Tetrofosmin SPECT due to its wide availability and low cost. The relative assessment of SPECT perfusion images is well established for the diagnosis of myocardial ischemia, and further, provides incremental prognostic value. PET perfusion imaging with ^{82}Rubidium, ^{15}O-water or ^{13}N-Ammonia is generally considered superior to SPECT due to accurate attenuate correction, higher spatial resolution, and possibility for an absolute measurement of myocardial blood flow (MBF, mL/g/min) at rest and during pharmacologic (vasodilator) stress. (Klein et al., 2020) PET perfusion imaging alone is an accurate method to confirm or exclude ischemia, it provides incremental prognostic value, and, in combination with coronary CTA, helps to distinguish whether ischemia is caused by coronary stenosis or rather by coronary microvascular dysfunction (CMD) (see Chapter 2.2.2). For revascularization decisions, information on both anatomy and ischemia is needed for most patients. In patients with HF, perfusion imaging plays a critical role in differentiating disease etiology, i.e., ischemic or non-ischemic origin, thereby providing guidance for optimal treatment. (Danad et al., 2017; Dewey et al., 2020)

Cardiac MRI and echocardiography are non-invasive approaches to evaluate cardiac structure and function without the need for ionizing radiation. MRI is based on the use of a strong magnetic field that excites hydrogen atoms found in water to change the direction of the rotational axis, thus allowing a precise soft tissue discrimination, whereas ultrasound utilizes high frequency sound waves and their echoes from the tissues with different reflection properties. For the assessment of myocardial ischemia, dobutamine stress MRI and exercise or dobutamine stress echocardiography can be used as alternative functional tests for perfusion imaging. Ischemia is detected by monitoring regional wall motion and thickening during infusion of increasing doses of dobutamine (or during exercise). The imaging protocol is identical between the MRI and echocardiography, but the MRI benefits from constantly good image quality. Perfusion imaging is also possible with MRI and echocardiography by using an intravenous contrast medium and vasodilator (commonly adenosine) stress. (Schwitter & Arai 2011; Pellikka at al., 2020) Furthermore, non-invasive angiography can be conducted with MRI, and high-risk

features of coronary and carotid artery lesions or thrombi can be characterized with multi-contrast MRI (T1/T2-weighted imaging) and/or gadolinium-based intravenous contrast medium. Despite the recent developments in cardiac MRI, coronary imaging is still challenging due to motion artifacts. Ultrasound, in turn, is typically used for an initial test to assess carotid or peripheral artery disease. Carotid intima-media thickness (IMT) can be measured with ultrasound, and the functional measurement of arterial blood flow with Doppler ultrasound allows the estimation of stenosis severity. (Tarkin et al., 2015)

In patients with suspected HF, echocardiography is the first-line diagnostic method of choice due to its high accuracy, availability (portability), safety, and low cost. Echocardiography allows measurements of cardiac structure (e.g., wall thickness), LV systolic function in which the EF is the most important parameter, diastolic function, and valvular defects (e.g., regurgitation). Microbubbles can be used as a contrast medium. Cardiac MRI is the gold standard for the measurements of the volumes, mass, and EF of both the left and right ventricles and is usually used in patients with a complex disease. Furthermore, myocardial fibrosis (MI scar), edema, and viability can be assessed using cardiac MRI with late gadolinium enhancement and T1/T2-mapping. (Dewey et al., 2020; Ponikowski et al., 2016)

Importantly, the selection of an appropriate clinical imaging test is guided by patient characteristics, local expertise, and the availability of such modalities. Furthermore, non-invasive molecular imaging capable of interrogating disease biology and molecular pathways beyond the anatomy and function provides novel opportunities for more accurate diagnostics and treatment.

2.2.1　Molecular imaging

Molecular imaging is defined as the "visualization, characterization, and measurement of biological processes at the molecular and cellular levels in humans and other living systems" (Mankoff, 2007). Nuclear imaging techniques, i.e., SPECT and PET, provide the main clinical molecular imaging modalities, with the latter being the leading approach. PET is based on the use of an intravenously injected radiotracer, i.e., a small-molecule, peptide or antibody agent labeled with a short-lived positron emitting radionuclide, such as ^{11}C, ^{68}Ga or ^{18}F, that binds to a molecular target of interest. When the radionuclide undergoes radioactive decay, it emits a positron that travels a short distance in the tissue before it encounters a nearby electron. This collision results in annihilation and creation of a pair of 511 kilo-electron volt (gamma) photons, which travel in opposite directions. Simultaneous detection of two opposite photons on the PET scanner ring-like detectors allows the localization of the tracer accumulation in the tissue, which can be further transferred and reconstructed to a 3D image. (Turkington 2001) The utilization of radiotracers

permits excellent target specificity and sensitivity, and spatial resolution of around 4 mm (1.5 mm in small-animal scanners). An important advantage is that the PET tracer uptake is quantifiable. However, disadvantages include limited spatial resolution and poor anatomic contrast, and therefore, PET is usually combined with a CT or MR scan. The combination of PET and CT also benefit from the quick attenuation correction. (Meester et al., 2019)

PET imaging has been widely and successfully used in non-cardiac conditions and indeed, most of the tracers have been adopted from the field of oncology to nuclear cardiology. The evolution of radionuclide imaging methods in nuclear cardiology has offered new possibilities where molecular-targeted PET imaging can be potentially utilized to predict the disease outcome at early stages, guide treatment selection and timing, monitor therapy response, and investigate the pathophysiology of the disease, thus facilitating the development of novel therapies. (Werner et al., 2020)

2.2.1.1   PET imaging of inflammation in atherosclerosis

Despite the possibility to evaluate adverse plaque characteristics by coronary CTA and MRI, anatomical imaging cannot directly assess the activity of the disease process. Inflammatory cells, macrophages in particular, are the most abundant cell type in high-risk atherosclerotic lesions, thereby representing an attractive target for the identification of active disease. (Dweck et al., 2016) In the past decade, several radiopharmaceuticals have been studied for the assessment of atherosclerosis in animal models, but only few of them have been successfully translated to clinical studies. The most relevant PET tracers characterized for the imaging of inflammation in atherosclerosis *in vivo* are presented in Table 1.

Glucose analog 2-deoxy-2-[^{18}F]-fluoro-*D*-glucose (^{18}F-FDG) is the most commonly used radiotracer in PET imaging. ^{18}F-FDG is taken up by metabolically active cells via glucose transporters (GLUT) 1 and 3, and is then phosphorylated into ^{18}F-FDG-6-phosphate by the hexokinase enzyme. Unlike its physiological counterpart, ^{18}F-FDG-6-phosphate cannot proceed the glycolytic pathway further and therefore, becomes trapped within the cells, reflecting the real-time metabolic activity of the tissue. (Hyafil & Vigne, 2019) The first observations of ^{18}F-FDG uptake in the aorta were described in oncologic patients (Yun et al., 2001), and, in 2002, Rudd and co-workers showed that ^{18}F-FDG accumulates in symptomatic carotid atherosclerotic lesions. *Ex vivo* autoradiography experiments in excised carotid plaques demonstrated that tritiated deoxyglucose co-localizes in macrophage-rich areas. (Rudd et al., 2002) Since then, several studies in different animal models (Hyafil et al., 2009; Ogawa et al., 2004; Zhang et al., 2006) and in patients (Liu et al., 2016; Tawakol et al., 2006) have confirmed that ^{18}F-FDG uptake

in plaques correlates with the histological degree of macrophages. Indeed, glucose turnover in macrophages and foam cells is increased in atherosclerotic lesions, but other cell types, such as activated SMCs, fibroblasts, and ECs, may also contribute to the uptake in response to inflammatory stimuli (Folco et al., 2011; Liu et al., 2016; Ogawa et al., 2012). Moreover, OxLDL (Lee et al., 2016) and hypoxia (Folco et al., 2011; Tawakol et al., 2015) have been implicated as important regulators of macrophage ^{18}F-FDG uptake. A recent elegant study on carotid plaque specimens highlights the role of cellular metabolism, glycolysis in particular, in fueling inflammation and a high-risk plaque phenotype (Tomas et al., 2018).

Table 1. PET tracers characterized for the imaging of inflammation in atherosclerosis.

Target	Tracer	Development stage	References
Inflammatory cells (macrophages)			
Glucose metabolism	^{18}F-FDG	Clinical and pre-clinical application	Rudd et al. 2002; 2009 Silvola et al. 2011; Tawakol et al. 2005
Somatostatin receptor type 2	^{68}Ga-DOTATATE	Clinical coronary, carotid Mouse	Tarkin et al. 2017 Li et al. 2013
	^{64}Cu-DOTATATE	Clinical carotid	Pedersen et al. 2015
	^{68}Ga-DOTANOC	Mouse	Rinne et al. 2015
Chemokine receptor 4	^{68}Ga-Pentixafor	Clinical coronary, aortic Rabbit	Derlin et al. 2018; Li et al. 2018 Hyafil et al. 2017
Phospholipid metabolism	^{18}F-FCH	Clinical carotid	Vöö et al. 2016
	^{18}F-FMC	Mouse	Hellberg et al. 2016
	^{11}C-Choline	Mouse	Laitinen et al. 2010
Translocator protein	^{11}C-PK11195	Clinical carotid	Gaemperli et al. 2012
	^{18}F-FEMPA	Mouse	Hellberg et al. 2017
	^{18}F-GE-180	Mouse	Hellberg et al. 2018
Mannose receptor	^{68}Ga-NOTA-MSA	Rabbit	Kim et al. 2016
	^{18}F-FDM	Rabbit	Tahara et al. 2014
Folate receptor β	^{18}F-FOL	Mouse, rabbit	Silvola et al. 2018
Cannabinoid recptor 2	^{11}C-RS-016	Mouse	Meletta et al. 2017
Scavenger receptor CD68	^{64}Cu-CD68-Fc	Mouse	Bigalke et al. 2014
Leukocyte proliferation	^{18}F-FLT	Mouse, rabbit, patients	Ye et al. 2015
Adhesion molecules			
VCAM-1	^{18}F-4V	Mouse	Nahrendorf et al. 2009
P-selectin	^{64}Cu-DOTA-anti-P-selectin mAb	Mouse	Nakamura et al. 2013
	^{68}Ga-Fucoidan	Mouse	Li et al. 2014
VAP-1	^{68}Ga-DOTA-Siglec-9	Mouse	Silvola et al. 2016
Integrins			
αvβ3	^{18}F-Fluciclatide	Clinical aortic	Jenkins et al. 2019
	^{18}F-Galacto-RGD	Clinical carotid Mouse	Beer et al. 2014 Laitinen et al. 2009
	^{18}F-Flotegatide	Mouse	Su et al. 2014
	^{68}Ga-NOTA-RGD	Mouse	Haukkala et al. 2009; Paeng et al. 2013
Matrix metalloproteinases			
MMP-2/9	^{68}Ga-DOTA-TCTP-1	Mouse	Kiugel et al. 2018

Although the exact mechanisms underlying lesional ^{18}F-FDG intake are still a matter of debate, ^{18}F-FDG PET/CT studies (performed in oncologic indications)

have demonstrated that high arterial ^{18}F-FDG uptake provides an independent predictor of future cardiovascular events (Figueroa et al., 2013; Paulmier et al., 2008; Rominger et al., 2009). Furthermore, vascular ^{18}F-FDG PET imaging is a highly reproducible and sensitive method and, interestingly, even individuals with atherogenic risk factors show a higher arterial ^{18}F-FDG uptake compared to healthy controls (van der Valk et al., 2016a). Statin therapies demonstrated a clear and consistent dose-dependent reduction in arterial ^{18}F-FDG uptake in patients with ASCVD or cardiovascular risk factors (Ishii et al., 2010; Tahara et al., 2006; Tawakol et al., 2013), and vascular ^{18}F-FDG PET imaging has been increasingly used as a surrogate marker to evaluate the effects of novel therapies on atherosclerotic inflammation. For example, two investigational drugs, namely, a cholesteryl ester transfer protein inhibitor, dalcetrapib (Fayad et al., 2011), and a lipoprotein-associated phospholipase A2 inhibitor, rilapladip (Tawakol et al., 2014), failed to demonstrate a reduction in vascular ^{18}F-FDG uptake. These proof-of-concept studies provide important guidance before proceeding to large clinical end-point trials. However, the main limitation of ^{18}F-FDG is that it is not specifically taken up by inflammatory cells only hence, the high physiological uptake in myocardium makes the coronary imaging challenging. (Hyafil & Vigne, 2019)

Recently, the somatostatin receptor type 2 (SSTR2) -targeting PET tracer ^{68}Ga-DOTATATE (Tarkin et al., 2017) and the chemokine receptor 4 (CXCR4) -targeting tracer ^{68}Ga-Pentixafor (Derlin et al., 2018) have demonstrated potential for the imaging of coronary artery plaques in patients. SSTR2 is expressed on the surface of activated macrophages (mainly M1 type) and ^{68}Ga-DOTATATE was shown to specifically bind to SSTR2 in macrophage-rich areas of the lesions. Interestingly, ^{68}Ga-DOTATATE was able to distinguish high-risk coronary and carotid artery lesions from low-risk lesions coupled with low myocardial uptake, thus being superior to ^{18}F-FDG. (Tarkin et al., 2017) CXCR4, in turn, is widely expressed in a variety of inflammatory cells as well as in ECs and SMCs, mediating immune cell recruitment at the site of inflammation. Focal uptake of ^{68}Ga-Pentixafor has been demonstrated in advanced coronary lesions, together with histologically confirmed CXCR4 expression in CD68^{+} macrophages. (Derlin et al., 2018) Furthermore, aortic ^{68}Ga-Pentixafor uptake correlated with cardiovascular risk factors (Li et al., 2018). Other promising targets for specific detection of macrophages in atherosclerotic lesions include phospholipid (choline) metabolism and translocator protein (TSPO) that interact with the PET tracers ^{18}F-Fluorocholine (Vöö et al., 2016) and ^{11}C-PK11195 (Gaemperli et al., 2012), respectively. Both tracers have allowed distinction between symptomatic and asymptomatic carotid artery plaques correlating with lesional CD68^{+} macrophage infiltration. PET imaging of $\alpha_v\beta_3$ integrin, which is expressed by macrophages and angiogenic ECs in plaques, has also been tested in clinical setting. The integrin $\alpha_v\beta_3$ -binding tracers, ^{18}F-Fluciclatide

(Jenkins et al., 2019) and ^{18}F-Galacto-RGD (Beer et al., 2014) showed moderate uptake in aortic and carotid lesions. Of note, an interesting target not directly reflecting the inflammation in plaques is microcalcification, which can be detected with ^{18}F-sodium fluoride (^{18}F-NaF). Although ^{18}F-NaF has demonstrated feasibility for imaging high-risk coronary lesions (Joshi et al., 2014), its value in predicting future cardiovascular events remains unclear. (Hyafil & Vigne, 2019)

Several PET tracers have been extensively validated in atherosclerotic animal models (Table 1). Potential targets on the surface of macrophages include mannose receptor (Kim et al., 2016; Tahara et al., 2014) and folate receptor β (Silvola et al., 2018) mainly expressed in M2 macrophages, cannabinoid receptor 2 (Meletta et al., 2017), and scavenger receptor CD68 (Bigalke et al., 2014). Imaging of macrophage proliferation in atherosclerotic lesions has been feasible as well (Ye et al., 2015). Other inflammation-related targets tested in murine models involve adhesion molecules such as VCAM-1 (Nahrendorf et al., 2009) and vascular adhesion protein-1 (VAP-1) (Silvola et al., 2016), and matrix metalloproteinases (Kiugel et al., 2018). Currently, ^{18}F-FDG is the only PET tracer with a clinical approval for imaging of inflammatory activities in atherosclerosis. However, recent studies have provided evidence that a more specific identification of high-risk lesions and active disease could be possible with alternative tracers, thus encouraging transformation towards image-guided personalized medicine. (Hyafil & Vigne, 2019)

2.2.1.2 PET imaging of myocardial inflammation and repair

In addition to myocardial perfusion imaging, PET molecular imaging is clinically utilized for the assessment of cardiomyocyte metabolism. Myocardial viability, defined as "ischemic, but alive myocardium" that has potential for functional recovery after revascularization, can be identified with ^{18}F-FDG PET. Reduced or absent ^{18}F-FDG uptake indicates scar formation, while preserved or increased uptake coupled with reduced myocardial perfusion identifies "hibernating", i.e., recoverable myocardium. However, the role of ^{18}F-FDG viability imaging in patient management is still controversial (Beanlands et al., 2007) and needs further investigation. (Bax et al., 2019) Other tracers for the evaluation of myocardial metabolism include ^{11}C-Acetate, which can be used for the measurement of myocardial oxygen consumption and efficiency (Knaapen et al., 2007), and fatty acid analogs, such as ^{18}F-FTHA reflecting myocardial fatty acid consumption (Tuunanen & Knuuti, 2011). Both of these tracers have provided added value in evaluating therapy response in HF. However, there is a need for specific PET tracers that can identify overactive inflammatory or fibrogenic signaling and potentially predict the functional outcome after MI. PET tracers characterized for the imaging of myocardial inflammation and repair post-MI *in vivo* are presented in Table 2.

Detection of inflammatory cells and their subtypes by PET may provide a unique insight into the MI healing process and help to develop new therapies. However, compared to atherosclerosis, the inflammatory process after MI is a demanding target as it is dynamic and rapidly evolving, involving a diverse repertoire of immune cell populations (Figure 2). In addition to viability studies, ^{18}F-FDG PET has been utilized for imaging myocardial inflammation. The peak ^{18}F-FDG signal in the MI area occurs 3 to 5 days after MI in both mice (Lee et al., 2012; Thackeray et al., 2015) and humans (Rischpler et al., 2016; Wollenweber et al., 2014), which is consistent with the time course of M1 monocyte/macrophage infiltration. Interestingly, the intensity of ^{18}F-FDG uptake correlated inversely with the functional outcome at 6 months after MI (Rischpler et al., 2016). Although the ^{18}F-FDG PET has shown to be feasible in detecting early inflammation, the suppression of background cardiomyocyte ^{18}F-FDG uptake is required. Different protocols, such as prolonged fasting and high-fat meals (anesthesia approaches in mice), have been applied, but the results vary among studies. (Thackeray & Bengel, 2018b)

Table 2. PET tracers evaluated for the imaging of myocardial inflammation and repair.

Target	Tracer	Development stage	References
Inflammatory cells (macrophages)			
Glucose metabolism	^{18}F-FDG	Clinical and pre-clinical application	Wollenweber 2014; Rischpler et al. 2016 Lee et al 2012
Chemokine receptor 4	^{68}Ga-Pentixafor	Clinical AMI Mouse MI, patients	Reiter et al. 2018; Lapa et al. 2015a Thackeray et al. 2015a; Hess et al. 2020
Somatostatin receptor type 2	^{68}Ga-DOTATOC ^{68}Ga-DOTATATE	Clinical AMI Mouse MI, patients	Lapa et al. 2015b Thackeray et al 2015b; Tarkin et al. 2019
Translocator protein	^{18}F-GE-180	Mouse MI, patients	Thackeray et al. 2018a
Amino acid metabolism	^{11}C-Methionine	Clinical AMI Mouse MI	Morooka et al. 2009 Thackeray et al. 2016
CCR2	^{68}Ga-DOTA-ECL1i	Mouse I/R	Heo et al. 2019
Angiogenesis			
αvβ3 integrin	^{18}F-Fluciclatide	Clinical AMI	Jenkins et al. 2017
	^{68}Ga-PRGD2	Clinical AMI	Sun et al. 2014
	^{18}F-Galacto-RGD	Clinical AMI Rat MI	Makowski et al. 2008 Higuchi et al. 2008; Sherif et al. 2012
	^{68}Ga-NOTA-RGD	Rat MI	Menichetti et al. 2013
	^{68}Ga-DOTA-RGD	Rat MI	Kiugel et al. 2014
	^{68}Ga-NODAGA-RGD	Rat, Pig MI	Laitinen at al. 2013; Grönman et al. 2017
VEGF receptor	^{64}Cu-DOTA-VEGF$_{121}$	Rat MI	Rodriguez-Porcel et al. 2008
Matrix remodeling and fibrosis			
Angiotensin II receptor 1	^{11}C-KR31173	Pig MI	Fukushima et al. 2012
Endothelin receptor A	^{18}F-FBzBMS	Rat MI	Higuchi et al. 2013
Plasma transglutinase	^{18}F-XIII factor	Mouse MI	Majmudar et al. 2013
MMP-2/9	^{68}Ga-DOTA-TCTP-1	Rat MI	Kiugel et al. 2018
Activated fibroblasts	^{68}Ga-FAPI-04	Mouse MI	Varasteh et al. 2019

In addition to imaging atherosclerotic plaques, the potential of targeting CXCR4, SSTR2, and TSPO in the post-MI inflammatory process has been investigated. ^{68}Ga-Pentixafor PET has shown focal CXCR4 up-regulation in the infarct area 3 days after

MI in mice, co-localizing with CD68^{+} macrophages in histology. Treatment with ACEI was able to attenuate ^{68}Ga-Pentixafor uptake. (Thackeray et al., 2015a) Moreover, early ^{68}Ga-Pentixafor signal predicted chronic LV dysfunction, and blockade of CXCR4 at the time of maximum imaging signal, but not off-peak, improved early and late cardiac outcome in mice (Hess et al., 2020). Patients with AMI have demonstrated high inter-individual variability in ^{68}Ga-Pentixafor uptake up to 14 days after AMI. (Lapa et al., 2015a; Reiter et al., 2018; Thackeray et al., 2015a, Hess et al., 2020)

Imaging of SSTR2 with ^{68}Ga-DOTATOC in patients has shown moderate uptake in the MI area 3 to 10 days after AMI (Lapa et al., 2015b), whereas ^{68}Ga-DOTATATE also detected residual inflammation in old infarcts (Tarkin et al., 2019). However, the histological validation is lacking and a mouse study suggests that ^{68}Ga-DOTATATE does not bind sufficiently to the SSTR2s in the inflamed MI region (Thackeray et al., 2015b). TSPO-targeting tracer ^{18}F-GE-180 has identified elevated TSPO expression 1 week after MI in both mice and patients, coupled with CD68^{+} macrophage infiltration in the infarct area. In mice, early ^{18}F-GE-180 uptake predicted subsequent LV remodeling at 8 weeks. The main limitation of ^{18}F-GE-180 is the myocardial background uptake due to the high mitochondrial content in cardiomyocytes. (Thackeray et al., 2018a) Elevated amino acid metabolism in damaged myocardium can be targeted with ^{11}C-Methionine, which has shown increased uptake early after MI in patients (Morooka et al., 2009). ^{11}C-Methionine was later shown to bind M1 macrophages with a peak signal seen in the infarct area 3 days after MI in mice (Thackeray et al., 2016). Recently, PET tracer ^{68}Ga-DOTA-ECL1i has shown potential to detect CCR2^{+} monocyte and macrophage infiltration in mouse I/R injury and human HF specimens (Heo et al., 2019).

Cardiac MRI can provide quantitative measures of myocardial fibrosis, but the PET imaging of ECM remodeling and activated myofibroblasts would offer the opportunity to assess the molecular mechanisms underlying reactive fibrosis, and eventually monitor the development of HF and response to antifibrosis therapies (Thackeray & Bengel, 2018b). The most extensively studied target in myocardial repair is $\alpha_v\beta_3$ integrin. It is expressed in vascular ECs, macrophages, and myofibroblasts during ECM remodeling. Several tracers targeting $\alpha_v\beta_3$ integrin have been tested in experimental MI models (Table 2), showing the highest uptake at 7 days to 3 weeks after MI, which reflects angiogenesis rather than active inflammation. ^{18}F-Galacto-RGD (Makowski et al., 2008), ^{68}Ga-PRGD2 (Sun et al., 2014), and ^{18}F-Fluciclatide (Jenkins et al., 2017) have also been studied in clinical setting. Interestingly, ^{18}F-Fluciclatide uptake was elevated at sites of acute infarction at 8 to 13 days after MI and associated with increase in probability of functional recovery (Jenkins et al., 2017). Another target mediating angiogenesis is a VEGF receptor that has shown feasibility for imaging MI repair in a rat model (Rodriguez-

Porcel et al., 2008). Other molecular targets associated with ECM remodeling and fibrosis, which have been tested in experimental models include AT_1 receptor, endothelin receptor A (ET-A), plasma transglutaminase FXIII (an enzyme involved in MI healing), and MMP-2/9 (Table 2). The uptake of AT_1 receptor-targeting tracer ^{11}C-KR31173 was observed in both infarct and remote myocardium in a pig MI model, and tracer uptake was blocked with an ACEI in healthy humans (Fukushima et al., 2012). Recently, a PET tracer ^{68}Ga-FAPI-04 demonstrated potential for *in vivo* imaging of activated fibroblasts after MI in mice (Varasteh et al., 2019).

Although the PET imaging of myocardial inflammation and healing process after MI is a relatively young field, recent studies indicate that the specific detection of the early inflammatory response after MI and the following repair mechanisms is possible, but the prognostic value of new tracers calls for further investigation in larger clinical trials. Importantly, coupling of an imaging biomarker with a therapeutic target holds genuine clinical potential to identify patients who will benefit from the treatment, optimize ideal timing of therapy, and provide a surrogate marker of therapeutic efficacy. (Thackeray & Bengel, 2018b)

2.2.2 Assessment of coronary vascular function with PET and ultrasound

Despite the absence of obstructive CAD or a successful PCI following stenotic lesions, ischemic symptoms frequently persist in those patients. It has become increasingly established that structural and functional alterations affecting the whole coronary circulation, including the microcirculation, serve as additional players beyond patient symptoms and CAD. (Camici et al., 2015)

The coronary circulation consists of functionally distinct vessel segments of decreasing size, with the pre-arterioles and arterioles involving most of the resistance circuit and having the responsibility of regulating and matching blood supply for myocardial oxygen consumption via the coronary capillaries. Under normal conditions, multiple autoregulation mechanisms at the arteriolar level maintain the coronary blood flow constant, e.g., increase or decrease in the arteriole diameter in response to flow changes affect the shear stress, which upstream induces endothelium-dependent vasodilatation of larger epicardial conductive vessels. However, these arterioles are susceptible to noxious stimuli, such as hyperlipidemia, hypertension, and diabetes, which may trigger CMD. The pathophysiology of CMD includes structural (e.g., vascular remodeling) and functional (e.g., endothelial dysfunction, vascular SMC dysfunction, and microvascular spasm) alterations, thereby comprising both impaired coronary microvascular dilatation and enhanced constriction. (Camici et al., 2015; Taqueti & Di Carli, 2018) It is well known that endothelial dysfunction in resistance arteries is an important contributor to CMD,

and the prevalence of CMD is also high in HF patients with preserved EF and without macrovascular CAD (Shah et al., 2018). Although the coronary microvasculature cannot be directly imaged *in vivo*, non-invasive functional imaging methods currently facilitate the assessment of parameters that are directly linked to CMD in both mice and humans.

Although ICA coupled with the measurement of FFR has been the historical gold-standard to evaluate the functional severity of stenosis, FFR primarily addresses hemodynamic consequences of focal epicardial lesions (Dewey et al., 2020). Coronary flow reserve (CFR), in turn, is an integrated measure of blood flow through both the epicardial coronary arteries and microvasculature. The characterization of microvascular function using CFR as a surrogate, requires induction of maximal vasodilatation and hyperemia that can be achieved by an intravenous administration of a pharmacological stressor, such as adenosine, regadenoson or dipyridamole. Accordingly, the coronary blood flow velocity measured in the epicardial artery or absolute MBF at rest and stress can be utilized to calculate CRF, which is the ratio of hyperemic to resting blood flow. (Camici et al., 2015) There is no clear threshold values for normal versus impaired CFR, but CFR >3 typically indicates a normal flow in healthy individuals. Depending on the population, i.e., the presence of risk factors only, established CAD or cardiomyopathy, CFR <1.8-2.5 has been reported as impaired. (Gould et al., 2013)

PET perfusion imaging is the most validated modality for the measurement of CFR. Post-processing, i.e., the kinetic modeling of dynamic rest and stress images, allows the quantification of regional and global MBF and calculation of CFR. The CFR can also be assessed with transthoracic ultrasound, where the mean or peak diastolic flow velocity is measured in the proximal left anterior descending coronary artery (LAD) at rest and stress by a pulsed-wave Doppler. Although the ultrasound method is relatively inexpensive and broadly available, it is a highly operator-dependent technique. (Mathew et al., 2019) Importantly, the assessment of CFR with Doppler ultrasound has been validated in mice (Gan et al., 2004; Saraste et al., 2008; Wikström et al., 2005), providing a translational technique to study coronary function non-invasively *in vivo* in rodents. Rodent studies also suggest that CFR might be modifiable with novel treatments (Adingupu et al., 2019; Grönros et al., 2011).

Several PET perfusion and ultrasound studies have demonstrated that impaired CFR is a strong predictor of adverse cardiovascular events and mortality in patients with suspected CAD (Gupta et al., 2017; Herzog et al., 2009; Murthy et al., 2011; Sicari et al., 2009; Ziadi et al., 2011) However, there are currently no therapies that specifically target CMD, although the conventional therapies such as statins or ACEIs may alleviate CMD. Furthermore, clinical studies using CFR as an end-point measure for monitoring therapy response are completely lacking or designed with a

small sample size (Marinescu et al., 2015). The multifactorial pathophysiology of CMD coupled with the prevalence across a variety of cardiovascular risk factors and diseases, makes it a complex target. Accordingly, the potential of imaged-guided treatment of CMD remains to be tested. (Taqueti & Di Carli, 2018) The interaction of CMD, CAD, and their adverse outcomes such as MI and HF, is likely to provide a future strategy for the development of new therapies and imaging biomarkers.

2.3   Phosphorylcholine as a therapeutic target

Oxidation reactions are vital parts of various biological processes. Reactive oxygen species (ROS) are generated as by-products of aerobic metabolism, which at low concentrations participate in physiological processes, such as cell metabolism and signal transduction. However, the impaired ROS elimination may lead to oxidative stress, which can cause damage to lipids, proteins and DNA. (Nathan & Cunningham-Bussel, 2013) Primary targets for oxidative damage are phospholipids, which are the building blocks of cells and lipoproteins. The newly generated oxidized phospholipids (OxPLs) can interfere with normal cellular functions and eventually trigger an inflammatory response. (Binder et al., 2016)

2.3.1   Oxidized phospholipids – Phosphorylcholine

Oxidatively modified molecules carry oxidation-specific epitopes such as OxPLs and malondialdehyde (MDA)-modified amino groups on their surface. Most of the research effort has focused on OxPLs. A specific moiety in the OxPL backbone is phosphorylcholine (PC) that is a polar head group of the membrane phospholipid phosphatidylcholine. The PC epitope is inactive and harmless when hidden inside the native LDL or viable cells, but becomes pro-inflammatory when exposed during peroxidation of phosphatidylcholine. (Watson et al., 1997) OxPL-PC has been found on the surface of ApoB100-containing particles, including OxLDL (Boullier et al., 2000), Lp(a) (Bergmark et al., 2008), and microvesicles (Tsiantoulas et al., 2015) as well as on apoptotic cells (Chang et al., 2004).

Oxidation-specific epitopes are DAMPs recognized by pattern recognition receptors, including several SRs of the innate immune system (Miller et al., 2011). OxPL-PC has been shown to be a high-affinity ligand of CD36 receptor mediating OxLDL uptake by macrophages (Boullier et al., 2000). Furthermore, toll-like receptors, such as TLR4, bind OxPL-PC (Imai et al., 2008), and CRP has been found to bind OxLDL and apoptotic cells via OxPL-PC (Chang et al., 2002), thus enhancing their complement-mediated clearance. Moreover, natural antibodies of the innate immune system can sense OxPL-PC (Shaw et al., 2000).

The recognition of oxidation-specific epitopes enables the immune system to mediate removal of damaged molecules and dying cells in order to maintain homeostasis. Evolutionarily, oxidation-specific epitopes play an important role in apoptotic cell removal during embryonic development. (Miller et al., 2011) Moreover, many oxidation-specific epitopes, such as PC, share molecular identity and/or mimicry with the PC moiety of microbial cell-wall polysaccharides that can be recognized by CRP (Volanakis & Kaplan, 1971). Upon tissue damage, the accumulation of oxidation-specific epitopes leads to a sterile inflammation that normally facilitates tissue repair. However, if unresolved, the sterile inflammation can trigger chronic inflammation. Oxidation-specific epitopes have been found in the diseased tissues of patients with infectious and sterile acute lung injury, atherosclerosis, multiple sclerosis, and Alzheimer's disease. (Binder et al., 2016)

2.3.2   Natural antibodies to phosphorylcholine

Natural antibodies (also called autoantibodies) are traditionally defined as antibodies that are found in healthy humans and other mammalian species in the absence of exogenous antigenic stimulation, providing a first line of host defense against pathogens. Natural antibodies are predominantly monoclonal immunoglobulin M (IgM) class antibodies produced by CD5-positive B1 cells. Natural IgM antibodies are the most-studied antibodies regulating atherosclerosis, since they contain a large repertoire for sensing oxidation-specific epitopes in both mice and humans. (Miller et al., 2011) The protective effects of natural IgM antibodies occur by neutralizing the pro-inflammatory effects of oxidation-specific epitopes, leading to activation of a complement cascade (Binder et al., 2016).

The prototypic natural IgM antibody, E06, was originally cloned from the spleens of hypercholesterolemic apolipoprotein E deficient (ApoE$^{-/-}$) mice. It was found to bind OxLDL and stain rabbit and human atherosclerotic lesions. (Palinski, 1996) It was later shown that IgM E06 specifically recognizes OxPL-PC epitope in OxLDL and blocks the binding and uptake of OxLD by macrophages *in vitro* (Boullier et al., 2000; Hörkkö et al., 1999). Furthermore, IgM E06 was demonstrated to bind to OxPL-PC on the surface of apoptotic cells, but not in normal cells, and to inhibit phagocytosis of apoptotic cells by macrophages similar to OxLDL (Chang et al., 1999; Chang et al., 2004). Interestingly, IgM E06 was found to be structurally and functionally identical to the classic germline-encoded natural antibody with the T15 idiotype (Shaw et al., 2000) that has been shown to provide an optimal protection against fatal infection caused by *S. pneumoniae* in mice (Briles et al., 1982). The T15/E06 IgM antibody against PC seems to represent a highly conserved natural antibody that is assumed to have gone through a natural selection during early immune development (Shaw et al., 2000). Other natural IgM antibodies to oxidation-

specific epitopes include E014, NA17, and LR04 binding to MDA epitope, and LR01 that binds to oxidized cardiolipin (Binder et al., 2016).

Associations of natural IgM antibodies with atherosclerosis-related diseases have been widely studied in clinical setting. An early work demonstrated that the plasma markers of OxLDL measured by murine E06 antibody showed significant temporal elevations following ACS (Tsimikas et al., 2003). It was later reported that low serum levels of IgM antibodies against OxPL-PC (anti-PC) in ACS were associated with increased risk of new cardiovascular events and all-cause mortality (Caidahl et al., 2012). In patients with CCS, low IgM anti-PC levels were associated with increased risk of fatal and non-fatal future coronary events (Imhof et al., 2015). Moreover, it has been suggested that the low serum levels of anti-PC IgM, IgA, and IgG1 (but not IgG2) could predict carotid IMT progression in patients with hypertension (Fiskesund et al., 2012). The IgM class antibodies, in particular, have been proposed to be independent protection markers for atherosclerosis progression (Fiskesund et al., 2012; Su et al., 2006). In line with that, low levels of IgM anti-PC have been associated with fast carotid IMT progression and cardiovascular risk in men at high cardiovascular risk (Gigante et al., 2014) Furthermore, IgM anti-PC serum levels may have potential to predict development of stroke (Fiskesund et al., 2010; Tsimikas et al., 2012), and have been shown to be a protection marker for atherosclerosis in systemic lupus erythematosus (Rahman et al., 2016).

In summary, low levels of natural IgM antibodies against PC are associated with an increased risk for cardiovascular events. The IgM anti-PC may have clinical value as a prognostic biomarker and can be useful in the development of PC-targeting immunotherapies.

2.3.3 Therapeutic concept in atherosclerosis

While the early work demonstrated that IgM T15/E06 inhibits the OxLDL uptake and phagocytosis of apoptotic cells by macrophages *in vitro* (Boullier et al., 2000; Chang et al., 1999; Hörkkö et al., 1999; Shaw et al., 2000), it has been extensively investigated whether the neutralization of PC epitopes on OxPLs by antibodies, i.e., immunotherapy, is atheroprotective and anti-inflammatory *in vivo*. The first proof was that the induction of PC antibody formation by immunization of LDL receptor deficient (LDLR$^{-/-}$) mice with *S. pneumoniae* decreased the extent of atherosclerosis. The splenic cells of immunized mice secreted IgM T15 antibody and the plasma derived from these mice successfully blocked the binding of OxLDL to macrophages. (Binder et al., 2003) The findings were replicated with PC-targeting immunization, showing that the aortic root lesion size was reduced in the PC-immunized ApoE$^{-/-}$ mice. This time, the serum from immunized mice was capable of reducing the macrophage foam cell formation in the presence of OxLDL *in vitro*.

(Caligiuri et al., 2007) Furthermore, direct infusion of a human oxidation-specific antibody has been shown to reduce the progression of atherosclerosis in LDLR$^{-/-}$ mice. The blockade of SR-mediated uptake of OxLDL in lesion macrophages has been proposed as the main atheroprotective mechanism. (Tsimikas et al., 2011) Similar findings have been reported also with antibodies targeting the MDA epitope (Schiopu et al., 2007).

Further mechanistic insights have been obtained by modifying the IgM expression in mouse models. In LDLR$^{-/-}$ mice deficient in serum IgM, atherosclerotic lesions are substantially larger on both low-fat and high-fat diet, with increased cholesterol crystal formation and SMC content in lesions (Lewis et al., 2009). A proof-of-concept study on anti-inflammatory effects demonstrates that hypercholesterolemic LDLR$^{-/-}$ mice expressing a single-chain variable fragment of E06 develop less atherosclerosis coupled with reduction in systemic inflammation and decrease in aortic valve calcification and liver steatosis. Macrophages derived from these mice favor an M2-like phenotype and express less TNF and IL-1β. (Que et al., 2018) Histological studies have further confirmed the presence of PC epitopes in the atherosclerotic lesions of mice and rabbits (Binder et al., 2003; Caligiuri et al., 2007; Lewis et al., 2009; Que et al., 2018; Shaw et al., 2000). In human atherosclerosis samples, PC epitopes are more prevalent in advanced lesions mainly associated with foamy macrophages, whereas MDA epitopes are more common in early lesions, such as early fibroatheromas (van Dijk et al., 2012).

In addition to macrophages, ECs have been proposed to be major sensors of OxPL-PC in atherosclerosis. However, little is known about the effects of OxPL-PC or PC antibodies on endothelial dysfunction. An early work indicated that "cell-modified" LDL causes an impairment of endothelium-dependent arterial relaxation *in vitro* (Kugiyama et al., 1990). It was further demonstrated that OxPL-PC inhibits endothelium-dependent arterial relaxation via an NO-mediated mechanism in aortic preparations (Rikitake et al., 2000; Yan et al., 2017). Moreover, OxPL-PC can induce gene expression of pro-inflammatory cytokines and adhesion molecules in ECs, and enhance monocyte binding to vascular ECs (Leitinger et al., 1999). The monocyte binding is partly mediated by the endothelial TLR4 receptor, leading to increased IL-8 synthesis (Walton et al., 2003). Interestingly, apoptotic cells carrying PC epitopes have been shown to activate ECs to induce monocyte adhesion mediated in part through IL-8, which can be blocked by the E06 antibody (Chang et al., 2004).

Recent findings indicate that the main carrier of OxPL-PC in human plasma is Lp(a) (Tsimikas et al., 2005; van der Valk et al., 2016b). Subjects with elevated Lp(a) have increased inflammatory activity in the arterial wall as measured by ^{18}F-FDG PET. Due to its OxPL-PC content, Lp(a) was found to have enhanced capacity to induce monocyte trafficking to the arterial wall and to mediate pro-inflammatory responses, because the E06 antibody was able to block these pro-inflammatory

effects of Lp(a) *ex vivo*. (van der Valk, et al., 2016b) Furthermore, a multimodal imaging study demonstrated that OxPL-PC bound to Lp(a) could promote valve calcification and disease progression in patients with aortic stenosis, since the E06 antibody was found to prevent the Lp(a)-mediated osteogenic differentiation of valvular interstitial cells *in vitro* (Zheng et al., 2019). Interestingly, a recent study showed that the Lp(a)-bound OxPL-PC activates the endothelium by enhancing glycolysis, thereby facilitating inflammation and monocyte migration (Schnitzler et al., 2020).

To date, one therapeutic antibody targeting OxPLs has entered the clinical trial phase (Lehrer-Graiwer et al., 2015). Treatment with a human recombinant IgG1 antibody against MDA epitopes on ApoB100-containing particles was found not to reduce arterial ^{18}F-FDG uptake in hypercholesterolemic minipigs (Poulsen et al., 2016) or in patients with stable inflammatory vascular lesions (Lehrer-Graiwer et al., 2015). Despite the negative findings with the MDA-targeting antibody, previous proof-of-concept studies in both animals and humans support the concept that OxPL-PC epitopes on ApoB100-containing particles and apoptotic cells elicit arterial wall inflammation and thus, novel therapies targeting and eliminating OxPL-PC may bear clinical potential in atherosclerosis.

2.4   Glucagon-like peptide-1 receptor (GLP-1R) as an imaging target

The first descriptions of a glucagon-like peptide-1 [GLP-1 (7-36) amide] (Drucker 1986) that was shown to stimulate insulin secretion and bind to a putative receptor in the pancreas were published in 1986-1988 (Drucker 2015). Subsequently, the 7-transmembrane G protein-coupled GLP-1R was cloned from rats in 1992 (Thorens, 1992) and humans in 1993 (Graziano et al., 1993). At the time, GLP-1-related peptide, exendin-4 [(1-39) amide] was isolated from the saliva of a poisonous lizard, *Heloderma suspectum.* It was found to mimic the physiological effects of GLP-1. (Eng et al., 1992) Exendin-4 shares structural homology of only 53% with mammalian GLP-1, but has 10-times higher binding affinity to GLP-1R and is resistant to degradation by the dipeptidyl peptidase-4 (DPP-4) enzyme (Goke et al., 1993). Discovery of GLP-1 and exendin-4 peptides provided a basis for a new class of antidiabetic drugs.

2.4.1   GLP-1R signaling in normal physiology

The incretin effect mediated by the peptide hormones GLP-1 and gastric inhibitory polypeptide (GIP) is responsible for up to 70% of insulin secretion after food intake in healthy individuals, whereas in patients with T2DM, the incretin effect is almost

abolished. GLP-1 is produced in and secreted from intestinal enteroendocrine L cells in response to nutrients. The effects of GLP-1 are mediated through the GLP-1R, which is physiologically expressed in the pancreas, gastrointestinal tract, brain, enteric and peripheral nervous system, heart, kidneys, lungs and adipose tissue. Overexpression of GLP-1R is detected in such pathologies as insulinomas. The sequence homology of the GLP-1R is over 90% across mammalian species, which underlines the physiological importance of the GLP-1 and its receptor. GLP-1 stimulates insulin secretion in pancreatic β-cells and inhibits glucagon secretion in α-cells in a glucose-dependent manner. The release of GLP-1 also leads to the inhibition of gastric emptying and small bowel motility. The activation of GLP-1Rs in the hypothalamus and brainstem promotes satiety, which may lead to reduced food intake and body weight loss. In the kidney, GLP-1 increases natriuresis by the inhibition of sodium reabsorption. (Andersen et al., 2018)

The short plasma half-life (1-2 minutes) of native GLP-1, due to its rapid degradation by the DPP4 enzyme, limits its therapeutic use. Several strategies have been utilized to extend the half-life, including alterations in the amino acid sequence, binding to plasma albumin or using the exendin-4 peptide as a GLP-1 analog. A distinct approach is to apply DPP-4 inhibitors, which prevent the degradation and inactivation of both native GLP-1 and GIP. The first GLP-1R agonist, exenatide, was approved for the treatment of T2DM in 2005. (Knudsen & Lau, 2019) Currently, different GLP-1R agonists that are based on the structure of GLP-1 or exendin-4, and DPP-4 inhibitors are used for the treatment of hyperglycemia in diabetic patients. Furthermore, the pharmacological activation of GLP-1R signaling has shown to exert pleiotropic actions in the cardiovascular system, but the exact mechanisms remain largely unknown (Nauck et al., 2017).

2.4.1.1   GLP-1R expression in the heart and vasculature

In the human and nonhuman primate heart, the expression of GLP-1R protein has been localized to myocytes in the sinoatrial node, but not in ventricular myocytes (Baggio et al., 2018; Pyke et al., 2014). However, GLP-1R messenger RNA transcripts have been detected in ventricular tissue. The GLP-1R is not expressed in cardiac fibroblast, coronary artery ECs, or vascular SMCs. (Baggio et al., 2018) In rodents, initial studies identified GLP-1R protein expression in the cardiomyocytes (Ban et al., 2008), but it was later shown that, like in humans, GLP-1R is not expressed in ventricular myocytes. Atrial expression of GLP-1R has been detected in rodents (Kim et al., 2013; Richards et al., 2014; Wohlfart et al., 2013).

Convincing evidence for the expression of GLP-1R within major blood vessels is lacking. The expression of GLP-1R protein has been detected in the mouse aorta as well as the arteries and arterioles of the heart, kidney, pancreas and intestine, co-

localizing with α-SMA. (Richards et al., 2014) In nonhuman primates, the GLP-1R expression can be detected in SMCs within the arteries of the kidney and lung (Pyke et al., 2014). Immunohistochemistry is the most often used and validated technique to study cellular expression of a certain protein, but it is commonly recognized that antibodies to G protein-coupled receptors, including GLP-1R lack sensitivity and specificity (Pyke & Knudsen, 2013). Thus, other specific techniques are needed in order to confirm the exact cellular localization of GLP-1R in the heart and vasculature.

2.4.2 Cardiovascular effects of GLP-1-based therapies

Cardiovascular outcome trials are required for all novel glucose-lowering therapeutics to establish their cardiovascular safety. These trials are double-blind, randomized placebo-controlled clinical trials including patients with T2DM at increased risk of cardiovascular events. All approved GLP-1R agonists have demonstrated cardiovascular safety as compared to a placebo. Interestingly, four of these drugs; Liraglutide (Marso, et al., 2016a), Semaglutide (Marso et al., 2016b), Albiglutide (Hernandez et al., 2018), and Dulaglutide (Gerstein et al., 2019) have also provided cardiovascular benefits. These benefits include decrease in non-fatal MI or stroke as well as reduction in cardiovascular death or all-cause mortality, i.e., reduction in the "hard end-points".

Cardiovascular effects of GLP-1R agonists have been studied in more detail in patients with STEMI and chronic HF. Administration of GLP-1R agonist or native GLP-1 at the time of PCI increases the myocardial salvage index and reduces the MI size (Chen et al., 2016; Lønborg et al., 2012; Woo et al., 2013), as well as improves the LV function (Chen et al., 2015; Nikolaidis et al., 2004; Woo et al., 2013) independent of diabetes. There are also contradictory findings, suggesting that GLP-1R agonists do not exhibit any beneficial effects on the MI size (Roos et al., 2016) or LV function (Lønborg et al., 2012) in acute STEMI. In patients with chronic HF, an initial pilot study indicated that infusion of GLP-1 improves the LV function (Sokos et al., 2006). However, larger studies now show that treatment with GLP-1R agonists do not improve the LV function, myocardial metabolism or blood flow, and do not affect the time to death or rehospitalization for HF in chronic HF patients with or without diabetes (Jorsal et al., 2017; Lepore et al., 2016; Margulies et al., 2016; Nielsen et al., 2017). All GLP-1R agonists slightly increase the heart rate, which may partly explain the neutral effect on HF outcome (Sun et al., 2015).

Clinical studies on the effects of treatments with GLP-1R agonists on atherosclerosis are limited. These therapies consistently modulate the lipid profile by lowering total cholesterol, LDL-C and TGs (Sun et al., 2015a), and reduce blood pressure (Sun et al., 2015b). Small trials in patients with T2DM suggest that

treatments with GLP-1R agonists reduce the levels of macrophage-derived sCD163 and TNF, IL-1β, and IL-6 (Hogan et al., 2014) as well as hsCRP (Wu et al., 2011). Pilot studies indicate that GLP-1R agonists may decrease carotid IMT (Rizzo et al., 2014) and favor a stable plaque phenotype characterized by a thickened fibrous cap and increased collagen content (Balestrieri et al., 2015). Furthermore, CMD has been assessed during the course of GLP-1R agonist therapies. The first study showed no benefit on CFR measured by Doppler ultrasound (Faber et al., 2015), while the second study demonstrated a slight improvement in CFR after the therapy (Wei et al., 2016). However, native GLP-1 and a GLP-1R agonist have been shown to improve brachial artery endothelial function evaluated by the flow mediated dilation technique (Irace et al., 2013; Nyström et al., 2004).

Thus, the beneficial cardiovascular effects of GLP-1R agonists have been recognized and the current guidelines advise to consider a GLP-1R agonist for T2DM patients with an established or high risk of ASCVD, except for HF patients (Davies et al., 2019; Seferović et al., 2020).

2.4.2.1 Mechanisms of cardiovascular action

Preclinical studies have yielded mechanistic insights regarding the protective effects of GLP-1R agonists on ischemic myocardial injury, atherosclerotic lesion progression, and endothelial dysfunction. In line with the clinical studies, it has been shown that infusion of native GLP-1 before or during an induction of I/R injury in the isolated or intact rodent heart protects against an ischemic myocardial injury. The protection appears to involve reduction in MI size and increase in myocardial glucose uptake, coronary flow, functional recovery, and cardiomyocyte viability. (Aravindhan et al., 2015; Ban et al., 2008; Bose et al., 2005, 2007; Zhao et al., 2006) Furthermore, GLP-1R agonists reduced the MI size in an acute setting (Ban et al., 2008; Wohlfart et al., 2013), and improved the cardiac function when administered long term after I/R injury in rats (Wohlfart et al., 2013). In porcine models of I/R injury, native GLP-1 and GLP-1R agonists reduced the MI size, augmented the cardiac output, and improved the LV function in some (Goodwill et al., 2014; Timmers et al., 2009), but not all studies (Kristensen et al., 2009). Mechanistically, the myocardial expression of active caspase-3 indicating apoptosis as well as the amount of apoptotic cells were decreased after the treatment (Timmers et al., 2009). In murine cardiomyocytes exposed to ischemia, GLP-1 and GLP-1R agonists have been shown to exert direct cytoprotective actions via inhibiting apoptosis through a pro-survival signaling pathway (Ban et al., 2010; Ravassa et al., 2011; Wohlfart et al., 2013).

Chronic administration (2 to 12 weeks) of GLP-1 or GLP-1R agonists in rodents with HF following permanent coronary occlusion improved the cardiac function, LV

remodeling and survival (Chen et al., 2017; DeNicola et al., 2014; Liu et al., 2010; Robinson et al., 2015b), which was associated with decrease in cardiomyocyte hypertrophy and apoptosis, as well as the attenuation of myocardial inflammatory response and fibrosis (Chen et al., 2017; DeNicola et al., 2014; Robinson et al., 2015). Contradictory findings on LV remodeling have been reported as well (Kyhl et al., 2017).

Protection against cardiac dysfunction and remodeling may occur secondary to modulation of inflammation, since GLP-1R agonists have been shown to inhibit myocardial macrophage infiltration and alter the expression of IL-10, IL-1β and IL-6 in macrophages in the absence of direct actions on cardiac fibroblasts (Robinson et al., 2015b; Tate et al., 2016). Furthermore, in mice overexpressing MCP-1 in cardiomyocytes, a GLP-1R agonist ameliorated LV dysfunction by reducing cardiac macrophage infiltration, fibrosis, and apoptosis (Younce et al., 2014). The beneficial effects on LV remodeling may also be related to the improved Ca^{2+} handling in myocytes (Chen et al., 2017; Younce et al., 2014) or the attenuation of Ang II-induced fibrosis (Zhang et al., 2015a). In obese swine with MI, treatment with GLP-1R agonist improved cardiac efficiency and function by decreasing β1-adrenoceptor expression similarly to β-blockade therapies (Sassoon et al., 2017). GLP-1R independent mechanisms may also contribute to the protective effects of GLP-1R agonists, since alterations in the gene expression profiles of remodeling and inflammation pathways comparable to the ACEI have been observed in heart samples in the absence of GLP-1R mRNA expression detection (Wohlfart et al., 2013). Furthermore, a GLP-1R agonist has been capable of inducing cardioprotection in experimental MI, despite ablation of cardiomyocyte GLP-1R activity in Glp1r$^{CM-/-}$ mice (Ussher et al., 2014).

In atherosclerotic mouse and rabbit models, treatments with GLP-1 and GLP-1R agonists have been shown to reduce systemic inflammation (Bruen et al., 2019; Rakipovski et al., 2018; Vinué et al., 2017) and attenuate the atherosclerotic lesion development and size (Arakawa et al., 2010; Bruen et al., 2017, 2019; Jojima et al., 2017; Nagashima et al., 2011; Rakipovski et al., 2018; Sudo et al., 2017; Vinué et al., 2017). The atheroprotective mechanisms involved increase in lesion collagen content (Burgmaier et al., 2013; Sudo et al., 2017; Vinué et al., 2017), inhibition of monocyte/macrophage infiltration in the vascular wall (Arakawa et al., 2010; Bruen et al., 2017; Nagashima et al., 2011; Sudo et al., 2017; Vinué et al., 2017), suppression of macrophage foam cell formation (Nagashima et al., 2011), and reprogramming of macrophages towards M2 phenotype (Bruen et al., 2017, 2019; Vinué et al., 2017). *In vitro*, GLP-1 and GLP-1R agonists have been shown to prevent the adhesion of human monocytes to ECs (Noyan-Ashraf et al., 2009), decrease the IL-1β, TNF, and MCP-1 secretion (Bruen et al., 2017, 2019), and induce M2 polarization in human macrophages (Bruen et al., 2017; Shiraishi et al., 2012).

GLP-1R expression has been found in macrophages in the atherosclerotic lesions of mice and in isolated mouse and human macrophages in some (Arakawa et al., 2010; Bruen et al., 2017; Nagashima et al., 2011), but not all studies (Panjwani et al., 2013).

Furthermore, GLP-1R agonists have been shown to improve endothelium-mediated vasodilation in atherosclerotic mice (Gaspari et al., 2011; Jojima et al., 2017). Studies on human aortic and coronary artery ECs suggested that GLP-1R agonists activate the signaling pathways leading to increased eNOS activity and NO production (Erdogdu et al., 2010; Gaspari et al., 2011; Nyström et al., 2004), and decrease the levels of inflammatory cytokines and adhesion molecules (Garczorz et al., 2018; Gaspari et al., 2011; Shiraki et al., 2012). Moreover, GLP-1R agonists may inhibit SMC proliferation (Jojima et al., 2017), and the osteoblastic differentiation and calcification of SMCs (Zhan et al., 2015b) *in vitro*.

In summary, multiple direct and indirect mechanisms linking the activation of GLP-1R signaling in cardiomyocytes or non-cardiac cell types have been suggested, but it remains currently unclear which cell types and cross-organ communications are necessary for the protective effects of GLP-1R agonists on the cardiovascular system.

2.4.3   Targeting GLP-1R with PET imaging

Imaging of GLP-1R expression with PET is of high interest, since it would enable the *in vivo* quantification of pancreatic β-cell mass in diabetic patients and localization of neuroendocrine tumors, such as insulinomas. Indeed, PET imaging agents targeting GLP-1R have demonstrated clinical value for the detection of insulinomas in patients (Antwi et al., 2015; Christ et al., 2013; Eriksson et al., 2014; Luo et al., 2016). It has been proposed that GLP-1R-targeting imaging can be utilized for the selection of treatment, prediction of drug efficacy, and monitoring of treatment response in diabetes and cancer (Velikyan & Eriksson, 2020).

GLP-1R-targeting radiopharmaceuticals are mainly based on exendin-4 peptide structure. Exendin-4 has favorable kinetics owing to its plasma half-life of 2.4 h, it binds to the same GLP-1R site as endogenous GLP-1, and it is internalized into the cells (Jodal et al., 2014; Wild et al., 2010). Exendin-4 can be labeled with different radionuclides such as ^{68}Ga, ^{18}F or ^{111}In. Since the expression levels and density of GLP-1R are relatively low in many tissues, a low peptide mass with high specific radioactivity should be injected. Other limitations include high kidney uptake, especially with metal radionuclide labeled tracers, and high physiological potency occuring even in the microdoses of the ligands. (Velikyan & Eriksson, 2020) For example, pigs have demonstrated tachycardia after intravenous injection of exendin-4 tracer (Nalin et al., 2014); however to date, clinical studies have not shown such adverse effects. Multiple promising exendin-4 PET tracers have been developed for

the imaging of pancreatic β-cells (Mikkola et al., 2013; Nalin et al., 2014; Selvaraju et al., 2013) and different GLP-1R-positive tumors (Jodal et al., 2014; Kiesewetter et al., 2012; Monazzam et al., 2018; Wild et al., 2010) in animals. Interestingly, one study revealed up-regulation of GLP-1R expression in the myocardium after I/R injury in rats by using ^{18}F-FBEM-Cys^{40}-exendin-4 PET imaging (Gao et al., 2012).

In summary, GLP-1R-targeting PET imaging can be potentially adopted from endocrinology to cardiovascular indications in order to elucidate the role of GLP-1R signaling in the cardiovascular system.

3   Aims

The purpose of this study was to investigate whether a novel PC immunotherapy affects vascular function and atherosclerotic inflammation in mice. Another aim was to evaluate the feasibility of a PET tracer ^{68}Ga-NODAGA-exendin-4 for the detection and imaging of GLP-1R expression after MI and in atherosclerosis in experimental models.

The specific aims of this study were:

1. To investigate the therapeutic effects of a novel monoclonal IgG1 antibody against PC on coronary artery function and atherosclerotic inflammation in hypercholesterolemic mice by utilizing established non-invasive imaging techniques, ultrasound-derived CFR and ^{18}F-FDG PET.

2. To evaluate ^{68}Ga-NODAGA-exendin-4 PET for the assessment of GLP-1R expression related to myocardial repair after MI in rats.

3. To assess GLP-1R expression in inflamed atherosclerotic lesions in non-diabetic and diabetic hypercholesterolemic mice with a PET tracer ^{68}Ga-NODAGA-exendin-4.

4 Materials and Methods

4.1 Experimental animals

All of the animal experiments were approved by the national Animal Experiment Board in Finland and the Regional State Administrative Agency for Southern Finland (License numbers ESAVI/2163/04.10.07/2015, ESAVI/4567/2018, and ESAVI/1545/04.10.07/2014). The studies were carried out in compliance with the European Union legislation relating to the conduct of animal experimentation. The animals were bred and housed in the Central Animal Laboratory, University of Turku under standard conditions with a 12-hour light-dark cycle and *ad libitum* access to water and food throughout the studies. Genetically modified atherosclerotic mouse models and a rat model with surgical coronary artery ligation were utilized.

4.1.1 Mouse models of atherosclerosis (I, III)

Two strains of hypercholesterolemic mice were used: low-density lipoprotein receptor deficient mice expressing only ApoB100 (n = 46 LDLR$^{-/-}$ApoB$^{100/100}$, strain #003000, The Jackson Laboratory, Bar Harbor, ME, USA) (Powell-Braxton et al., 1998) and their diabetic counterparts, LDLR$^{-/-}$ApoB$^{100/100}$ mice overexpressing insulin-like growth factor II in pancreatic β-cells (n = 12 IGF-II/LDLR$^{-/-}$ApoB$^{100/100}$, A. I. Virtanen Institute for Molecular Sciences, University of Eastern Finland, Kuopio, Finland) (Heinonen et al., 2007). Genetic modifications providing deficiency of LDLR combined with the expression of ApoB100 only (also called lack of ApoB48) result in impaired lipoprotein clearance, and eventually a lipid profile and lesion formation that closely resembles the type found in patients with FH (Véniant et al., 1998, Powell-Braxton et al., 1998). In addition to atherosclerosis, IGF-II/LDLR$^{-/-}$ApoB$^{100/100}$ mice represent the characteristics of T2DM, including impaired glucose tolerance and insulin resistance. They also develop a more pro-inflammatory phenotype characterized as more complex lesions with increased calcification and higher IL-6 expression. (Heinonen et al., 2007) To accelerate atherosclerosis development, the mice were fed with a high-fat diet (0.2% total cholesterol, TD 88137, Envigo, Indianapolis, IN, USA) for 12 to 16 weeks, starting

at the age of 8 weeks. Since both strains were originally crossbred onto a C57BL/6N background, healthy age-matched C57BL/6N mice (n = 12) fed with a regular chow diet (CRM [E], product code 801730, 9.1% calories from fat, Special Diet Services, Essex, UK) served as controls in the studies.

4.1.2   Rat model of myocardial infarction (II)

Male Sprague-Dawley rats (n = 80, age 7 to 8 weeks, weight 280 ± 29 g, Strain Code 400, Charles River Laboratories, Wilmington, MA, USA) were utilized. MI was induced by a permanent ligation of the left coronary artery (LCA). Buprenorphine (0.05 mg/kg; Temgesic; RB Pharmaceuticals Limited, Berkshire, UK) was administered subcutaneously (s.c.) prior to the operation for analgesia. Anesthesia was induced with inhaled 3% isoflurane (Baxter, Berkshire, UK) and maintained with an intraperitoneal (i.p.) injection combining xylazine (10 mg/kg; Rompun; Bayer Animal Health GmbH, Leverkusen, Germany) and ketamine (80 mg/kg; Ketaminol; Intervet International BV, Baxumeer, The Netherlands). Body temperature was maintained using a heating pad. The rats were intubated and connected to a rodent ventilator (TOPO dual mode ventilator; Kent Scientific, Torrington, CT, USA). The heart was exposed by a left lateral thoracotomy of the fourth intercostal space and the LCA was ligated near its origin. Ligation was confirmed visually by the pale appearance of the myocardium at risk, the muscle layer and skin were sutured, and the anesthesia was reversed with an s.c. injection of atipamezole (1 mg/kg; Antisedan; Orion Pharma, Espoo, Finland). Control animals underwent a sham-operation, which consisted of the same protocol except for the LCA ligation. Pain medication (0.05 mg/kg of buprenorphine twice a day) was continued three days following the operation. The operation mortality was approximately 30% and occurred during the first two days after LCA ligation. Thereafter, only two rats with MI died spontaneously during the follow-up. Six rats were excluded from the final study group, because there was no MI despite the ligation. The final study group consisted of 25 rats with MI and 18 sham-operated rats (Table 3).

4.2   Study design

The numbers of animals in each study and the imaging experiments performed for each group are presented in Table 3.

Table 3. The number of animals in each study and the corresponding imaging experiments.

Tracers and groups	Study	Number of animals (n)	US (n)	MRI (n)	PET/CT (n)	ARG (n)	BD (n)
^{18}F-FDG	I	34					
LDLR$^{-/-}$ApoB$^{100/100}$		34	20			32	32
^{68}Ga-NODAGA-exendin-4	II	43					
MI 3 d		6			3	6	
MI 1 wk		7			7	7	
Block		3			3	3	
MI 12 wk		9	8*	2	8	9	
Sham 1 wk		9			8	9	
Sham 12 wk		9	9*	2	6	9	
^{68}Ga-NODAGA-exendin-4	III	36					
LDLR$^{-/-}$ApoB$^{100/100}$		10			2	7	
Block		2				2	
IGF-II/LDLR$^{-/-}$ApoB$^{100/100}$		10			2	8	
Block		2				2	
C57BL/6N		12			4	10	

US; ultrasound, MRI; magnetic resonance imaging; ARG; ex vivo autoradiography,
BD; ex vivo biodistribution, MI; myocardial infarction,
Block; unlabeled exendin-4 peptide injected before ^{68}Ga-NODAGA-exendin-4.
*Repeated measurements at 1 and 12 weeks.

4.2.1   Interventional protocol (I)

In Study I, the effects of a novel therapeutic antibody (designated X19-mu) against PC on vascular function and atherosclerotic inflammation were investigated in established atherosclerosis in LDLR$^{-/-}$ApoB$^{100/100}$ mice. To induce atherosclerosis, the mice were first fed with a high-fat diet for 12 weeks, starting at the age of 8 weeks, and then switched to a regular chow diet and randomized to receive i.p. injections containing either 10 mg/kg X19-mu (n = 17) or 0.9% saline solution as a vehicle (n = 17), once a week, for 6 weeks. The groups were gender and sibling matched. The selection of X19-mu antibody dose was based on the previous studies (Ewing et al., 2013) and a pilot study performed in LDLR$^{-/-}$ApoB$^{100/100}$ mice. Vascular function was assessed by measuring CFR in response to adenosine using Doppler ultrasound, repeatedly before and after 6 week treatments in a randomly selected, pre-specified subgroup of mice (n = 10/treatment). Inflammation in aortic atherosclerotic lesions was determined by the uptake of ^{18}F-FDG and histological stainings of several inflammatory markers. The study design is shown in Figure 3.

The X19-mu antibody (Athera Biotechnologies AB, Stockholm, Sweden) is a monoclonal mouse-human chimeric IgG1 antibody binding to PC epitope on OxPLs. The X19-mu antibody has been developed in parallel with a fully human

monoclonal IgG1 antibody against PC (PC-mAb, clone X19-A05, Athera Biotechnologies AB). This therapeutic PC-mAb has displayed similar properties to the IgM E06 antibody, including the inhibition of OxLDL uptake in macrophages, binding to apoptotic cells, blocking of OxLDL-induced release of MCP-1 from monocytes, and binding to inflammatory cells in human aortic atherosclerotic lesions (Ewing et al., 2013). The antigen-binding sequences and binding affinity to PC are identical between the fully human PC-mAb and X19-mu antibody, but X19-mu has a murine Fc fraction to lower the risk of an immune reaction to the treatment in mice. In Study I, the human PC-mAb was utilized to study the endothelial mechanism *in vitro* in human aortic endothelial cells (HAECs) stimulated with Lp(a).
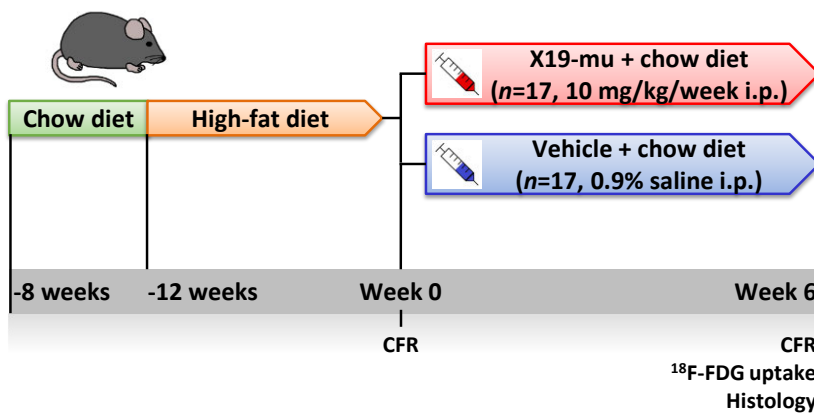
Figure 3. Study design for X19-mu intervention in LDLR$^{-/-}$ApoB$^{100/100}$ mice.

4.2.2 Imaging studies (II, III)

In Study II, the myocardial uptake of a GLP-1R-targeting tracer, ^{68}Ga-NODAGA-exendin-4, was studied 3 days, 1 week, and 12 weeks after MI as well as 1 and 12 weeks after the sham-operation (Table 3). In Study III, the ^{68}Ga-NODAGA-exendin-4 accumulation into the aorta was studied in hypercholesterolemic LDLR$^{-/-}$ApoB$^{100/100}$ and IGF-II/LDLR$^{-/-}$ApoB$^{100/100}$ mice, and healthy C57BL/6N mice (Table 3). In general, the animals were intravenously (i.v.) injected with ^{68}Ga-NODAGA-exendin-4 via the tail vein, and the tracer uptake in the heart and aorta was assessed by *in vivo* PET/CT imaging and *ex vivo* tissue autoradiography, followed by a histological analysis. Histological stainings included various markers, such as collagen, macrophages, and GLP-1R (Table 4). The specificity of tracer uptake in the MI and atherosclerotic lesions was confirmed by injecting unlabeled exendin-4 peptide before ^{68}Ga-NODAGA-exendin-4 in a subset of animals.

4.3 Ultrasound imaging

In Study I, the coronary artery function was examined by Doppler ultrasound before and after the treatment. A dedicated small animal ultrasound device (Vevo 2100, VisualSonics Inc., Toronto, ON, Canada) with a linear 22–55 MHz (MS550D) transducer was used to assess CFR, as described previously (Saraste et al., 2008). The mice were anesthetized with an i.p. injection of midazolam (8 mg/kg; Hameln Pharmaceuticals GmbH, Hameln, Germany) and ketamine (60 mg/kg; Intervet International BV, Boxmeer, The Netherlands). A tail vein was cannulated, and body temperature was maintained with a heating pad. Blood flow in the middle LCA was localized under color Doppler mapping using modified long-axis views, and the flow velocity spectrum was recorded by pulsed-wave Doppler, both at rest and under stress induced by infusion (maximum of 2 minutes) of adenosine (140 µg/kg/min; Life Medical Sweden AB, Stocksund, Sweden). Anesthesia was reversed with an s.c. injection of flumazenil (0.5 mg/kg; Hameln Pharmaceuticals GmbH, Hameln, Germany). The CFR was calculated as the ratio of the mean diastolic flow velocity during maximal adenosine-induced hyperemia to the flow at rest.

In Study II, to characterize the function and size of the LV, echocardiography was repeatedly conducted at 1 and 12 weeks after the coronary ligation or sham-operation (Table 3). Echocardiography was performed using the small animal ultrasound device with a linear 13-24 MHz (MS250) transducer. The rats were anesthetized with isoflurane and body temperature was maintained using a heating pad. Parasternal long-axis views in M-mode were acquired and the LV end-diastolic diameter, end-systolic diameter, and thickness of the interventricular septum and posterior wall were measured. Fractional shortening and LV mass were calculated. A subset of rats (2 MI and 2 sham) were also imaged with cardiac MRI after 12 weeks to visualize the LV shape and function. The MRI data was acquired using clinical Philips Achieva 3T device (Philips Medical Systems, Koninklijke, The Netherlands) combined with a rodent-dedicated heart coil.

4.4 Radiochemistry

The PET tracers were synthetized at the Radiopharmaceutical Chemistry Laboratory of Turku PET Centre. The ^{18}F-FDG was obtained from batches synthetized with a standard protocol and allocated for clinical use. The structure of [Nle^{14}Lys^{40}(Ahx-NODAGA)NH$_2$]-exendin-4 peptide is shown in Figure 4. ^{68}Ga was obtained from a ^{68}Ge/^{68}Ga generator (Eckert & Ziegler, Berlin, Germany) by elution with 0.1 M hydrochloric acid (HCl). The ^{68}Ga-GaCl$_3$ eluate (0.5 ml, 184 ± 19 MBq) was mixed with sodium acetate (18 mg, Merck, Kenilworth, NJ, US) and pH was adjusted to approximately 3.5 with 2 M HCl. Then, 24 µg of NODAGA-exendin-4 (5 nmol in deionized water) was added, and the reaction mixture was incubated at 95 ˚C for 15

min. The radiochemical purity was determined by a radio-high-performance liquid chromatography (radio-HPLC) (Jupiter C_{18}, 300 Å, 150×4.6 mm, 5µm column, Phenomenex, Torrance, CA, USA). The HPLC conditions were as follows: flow rate = 1 ml/min, λ = 215 nm, A = 0.1% trifluoroacetic acid (TFA) in water, B = 0.1% TFA in acetonitrile. Linear gradient was from 18% to 60% B/A over 9 min. The radiochemical purity exceeded 95% in every batch. The molar activities of ^{68}Ga-NODAGA-exendin-4 were 35 ± 7.0 MBq/nmol (Study II) and 58 ± 20 MBq/nmol (Study III) at the end of synthesis.
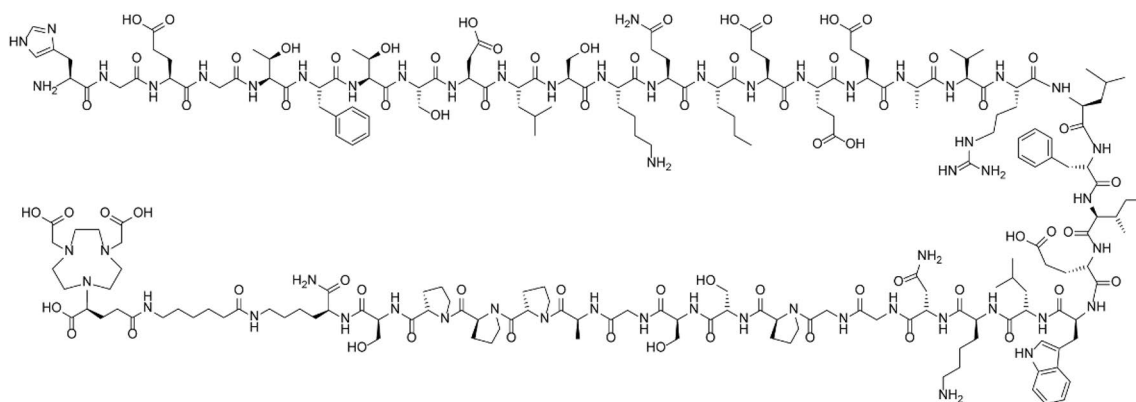
Figure 4. Structure of [Nle[14],Lys[40](Ahx-NODAGA)NH$_2$]-exendin-4 peptide. The chemical formula is $C_{212}H_{331}N_{56}O_{69}$ and molecular weight 4765.4 g/mol. NODAGA = 1,4,7-triazacyclononane-1-glutamic acid-4,7-diacetic acid.4 (Adopted from the original publication II supplementary data with a permission DOI: 10.1007/s12350-018-01547-1.)

4.4.1   *In vivo* tracer stability

In vivo stability and radiometabolism of ^{68}Ga-NODAGA-exendin-4 in plasma was studied by radio-HPLC at 12 weeks after the sham-operation (n = 3). Blood samples were obtained at 5, 15, 30, 60, and 80 min after tracer injection from the tail vein. Plasma was separated by centrifugation, and the samples were mixed with acetonitrile (1:1, v/v) for protein precipitation, centrifuged, and the supernatant was analyzed with radio-HPLC (Jupiter C_{18}, 300 Å, 10×250 mm, 5µm column, Phenomenex, Torrance, CA, USA).

4.5   PET/CT imaging

In all studies, the animals were fasted for 4 hours before tracer injection. The animals were anesthetized with isoflurane (4-5% for induction and 1.5-2% for maintenance), body temperature was maintained using a heating pad, and blood glucose levels were measured with a glucometer (Bayer Contour, Bayer AG, Leverkusen, Germany)

from blood samples withdrawn from the saphenous vein. A tail vein catheter was put in place and the following radioactivity doses were injected: 11 ± 0.38 MBq of ^{18}F-FDG in Study I, 52 ± 5.5 MBq and 20 ± 2.0 MBq of ^{68}Ga-NODAGA-exendin-4 in Studies II and III, respectively. The selection of radiotracer doses was based on the previous studies (Silvola et al., 2011; Mikkola et al., 2013; Kiugel et al., 2014) and the ^{68}Ga-NODAGA-exendin-4 dose was adjusted between the rats and mice (body weight).

In studies II and III, a subset of animals (Table 3) were imaged using a small-animal PET/CT scanner (Inveon Multimodality, Siemens Medical Solutions, Knoxville, TN, USA) for 60 minutes starting from the time of the ^{68}Ga-NODAGA-exendin-4 injection. Immediately after the PET, an iodinated contrast agent (eXIATM160XL, Binitio Biomedical Inc., Ottawa, ON, Canada) was injected (250 µl for rats and 100 µl for mice) and a high resolution contrast-enhanced CT was acquired in order to visualize the endocardial border (localization of myocardium) and large blood vessels. The PET images were reconstructed with a 3D ordered-subset expectation maximization algorithm (OSEM3D). Quantitative PET analyses were performed using the in-house Carimas v. 2.8 or 2.9 software (Turku PET Centre, Turku, Finland).

The PET and CT images were automatically superimposed and the co-localization was confirmed visually based on anatomical landmarks. According to the high-resolution CT, regions of interest (ROIs) were drawn in the infarcted region and remote myocardium (II), aorta (III), blood pool in the LV cavity, chest wound (II), lungs, liver, kidneys, muscle, and urinary bladder (III). The MI ROI was defined as corresponding to the infarcted region in the myocardium supplied by the LCA and the remote ROI was placed in the non-infarcted myocardium in the inferior septum. In sham-operated rats, ROIs were drawn in the anterolateral wall corresponding to the LCA territory and septum. The ROIs in the aorta were defined in the aortic arch and aortic root in both atherosclerotic and control mice.

Optimal contrast between ^{68}Ga-NODAGA-exendin-4 uptake in the infarcted area/atherosclerotic aorta and blood pool was observed 50-60 minutes after injection, and therefore the regional mean radioactivity concentrations (Bq/ml) were used to calculate the standardized uptake values (SUV_{mean} 50-60 min). The SUV is determined as the regional Bq/ml value divided by the injected radioactivity dose per animal weight. Uptake in the aorta was normalized by calculating the target-to-background ratio (TBR): $SUV_{max, aorta}/SUV_{mean, blood}$.

4.5.1 Kinetic modeling

In Study II, the dynamic ^{68}Ga-NODAGA-exendin-4 data was further analyzed by the graphical Patlak model (Patlak et al., 1983) to estimate the irreversible tracer uptake

as net influx rate (K_i). Metabolite-corrected plasma time-activity curves (TAC) were used as input function in the Patlak plot analysis. Image-derived blood curves were converted into metabolite-corrected plasma curves using the group median plasma-to-blood ratio and percentage of intact ^{68}Ga-NODAGA-exendin-4 measured in the metabolite analysis. K_i was calculated as the slope of the plot after the linear phase was reached 20 minutes after tracer injection. Reported K_i values are based on the analysis of regional TACs, whereas representative parametric K_i images were obtained by using Patlak plots.

4.6   Autoradiography of tissue sections

High-resolution digital autoradiography *ex vivo* was used to quantify the tracer uptake in tissue sections in more detail. At 90 minutes (I), 80 minutes (II) or 60 minutes (III) post-injection, blood was collected by cardiac puncture and the animals were sacrificed by cervical dislocation under deep anesthesia.

The thoracic aorta from the sinotubular junction to the level of the diaphragm (I, III), LV (II) or pancreas (III) were excised, rinsed with saline to remove blood, frozen in cooled isopentane, and cut into sequential longitudinal or transverse (LV) cryosections of 20 and 8 μm, thus providing sections throughout the region on a single slide (n = 6–8 intervals/specimen). The cryosections were air-dried and placed under a radiation-sensitive imaging plate (Fuji Imaging Plate BAS-TR2025, Fuji Photo Film Co., Ltd., Tokyo, Japan) for a specific time depending on the radionuclide decay, and then scanned with a Fuji Analyser BAS-5000 (internal resolution of 25 μm, Fuji, Tokyo, Japan). Thereafter, the 20 μm sections were stained with hematoxylin and eosin (HE) and the parallel 8 μm sections were immunohistochemically stained with Mac-3 (I, III) or CD68 (II) antibodies to detect macrophages, α-SMA (II) to detect myofibroblasts or insulin (III) to localize pancreatic β-cells (Table 4). The sections were scanned with a slide scanner (Pannoramic 250 Flash, 3DHistech Ltd., Budapest, Hungary) and co-registered with autoradiographs. Tracer accumulation was measured as photostimulated luminescence per square millimeter (PSL/mm^2), using Tina 2.1 software (Raytest Isotopenmessgeräte, GmbH, Straubenhardt, Germany). Background radiation was subtracted from the image data, and the results for each animal were decay corrected to injection time and exposure time and normalized for injected radioactivity dose per animal weight in order to compare absolute PSL/mm^2 values between animals. Alternatively, the TBR was calculated.

In Study I, ROIs were placed on the atherosclerotic lesions (n = 22/mouse) and vessel walls without lesions (n = 16/mouse), and the TBR (lesion-to-wall ratio) was calculated for each mouse. The lesion-to-wall ratios were compared between the mice treated with X19-mu or a vehicle. To assess the effects of treatment on [18]F-

FDG uptake in lesions containing different macrophage densities, the percentage of Mac-3$^+$ staining within the lesions was measured with ImageJ software (Fiji, NIH, Bethesda, MD, USA) and compared with the ^{18}F-FDG uptake (lesion-to-wall ratio) in the same lesions in the 8 μm sections (n = 7 randomly chosen mice/treatment; 8 lesions/mouse). In Study II, the average ^{68}Ga-NODAGA-exendin-4 uptake was measured as PSL/mm^2 in 4-5 sections per heart in the infarcted area, the border zone myocardium consisting of 3-5 myocyte layers adjacent to the infarct, and the remote myocardium in the septum. Furthermore, the ^{68}Ga-NODAGA-exendin-4 uptake was correlated with the percentage of CD68$^+$ macrophages and α-SMA$^+$ myofibroblasts in infarcted or remote regions in parallel 8 μm sections. In Study III, the ROIs were defined in the atherosclerotic lesions (n = 24/mouse), vessel walls without lesions (n = 16/mouse), and adventitia (n = 9/mouse). The results were expressed as PSL/mm^2 and lesion-to-wall ratios. In a subset of mice (n = 4 non-diabetic, n = 5 diabetic, and n = 4 control mice) the pancreatic uptake of ^{68}Ga-NODAGA-exendin-4 was measured in 6 sections per mouse in ROIs placed on the islets of Langerhans (n = 28/mouse) and exocrine pancreas (n = 28/mouse). Islet-to-exocrine pancreas ratio was calculated for each mouse.

4.7 Specificity of tracer binding

To assess the specificity of ^{68}Ga-NODAGA-exendin-4 accumulation, 12 mg/kg for rats and 14 mg/kg for mice of unlabeled exendin-4 peptide (ChinaPeptides Co. Ltd., Shanghai, China) was injected 10 minutes before ^{68}Ga-NODAGA-exendin-4 injection in order to block specific binding sites (Table 3). The dose of the blocking peptide was calculated to be an approximately 200-fold amount compared to the injected ^{68}Ga-NODAGA-exendin-4. The PET/CT imaging and/or autoradiography studies were performed as described above.

4.8 *Ex vivo* biodistribution

In Study I, no PET/CT imaging was performed, but the radioactivity concentrations of ^{18}F-FDG in certain tissues were assessed by *ex vivo* biodistribution analysis. After 90 minutes of tracer accumulation, in parallel to autoradiography study, the selected tissues including the brain, heart, liver, lungs, and spleen were excised, weighed, and measured for total radioactivity using a gamma counter (Triathler 3", Hidex Oy, Turku, Finland). Radioactivity values were normalized for injected radioactivity dose per animal weight, decay, and the weight of the tissue sample. The results were expressed as SUV values.

4.9　Histology, immunohistochemistry, and immunofluorescence

The general histology and relevant inflammatory and cardiac repair markers were investigated in all studies. In addition to aortic cryosections, the aortic root (I, III) was fixed overnight with 10% formalin, embedded in paraffin, and cut into serial 5 µm cross-sections at the level of the coronary ostium. In Study II, additional samples of the LV (n = 2 MI at 1 week and 2 MI and 2 sham at 12 weeks) were embedded in paraffin. Aortic root sections were stained with Movat's pentachrome for the measurement of atherosclerotic lesion area (I, III), and with Masson's trichrome (Sigma-Aldrich, St. Louis, MO, USA) for the quantification of lesion collagen content (I). Masson's trichrome staining was also used to determine the MI size and to measure collagen density in the LV cryosections. Antibodies used for immunohistochemistry and immunofluorescence are listed in Table 4.

In general, the staining protocol included heat-mediated antigen retrieval usually in citrate buffer, a blocking reagent such as 1% bovin serum albumin in PBS/Tween, incubation with primary antibody for 60 minutes or overnight, and appropriate secondary antibodies. In immunohistochemistry, detection was performed with Vectastain ABC-HRP kit (Vector Laboratories, Burlingame, CA, USA), coupled with chromogen (DAB, Dako K3468), and counterstained with Mayer's hematoxylin. Fluorescent Alexa secondary antibodies (Invitrogen, Carlsbad, CA, USA) were used for detection in immunofluorescence stainings and the sections were mounted in ProLong TM Gold Antifade Reagent including 4',6-diamino-2-phenylindole (DAPI) that stains nuclei (P36935, Invitrogen, Carlsbad, CA, USA). All staining protocols were optimized by using positive and negative tissue samples, as well as control non-immune IgG antibodies.

In Study I, macrophages in aortic root sections were detected by double immunofluorescence using Mac-3 antibody and either CCR2 or CD206 antibody detecting M1 or M2 macrophages, respectively. Macrophage apoptosis was studied by using Mac-3 and cleaved caspase-3 antibodies. Furthermore, VCAM-1, ICAM-1, IL-1β, and MCP-1 were detected by immunofluorescence. The presence of PC epitopes in atherosclerotic lesions was detected by immunofluorescence using the fully human PC-mAb directly labeled with Cy5 and co-stained with Mac-3 antibody and CD31 antibody detecting ECs. In Study II, in addition to the CD68 and α-SMA anyibody stainings performed for LV cryosections, serial 4 µm paraffin cross-sections were double immunofluorescence stained with GLP-1R and either a CD68 or α-SMA antibody in order to study the co-localization of GLP-1R with macrophages and α-SMA expressing myofibroblasts. In Study III, aortic root sections were co-stained for immunofluorescence using GLP-1R antibody and either Mac-3, iNOS detecting M1 macrophages, or CD206 antibody. Additional paraffin-embedded pancreatic sections were co-stained with GLP-1R and insulin antibody.

The sections were scanned with digital slide scanners (Pannoramic 250 Flash for histology or Pannoramic MIDI for immunofluorescence; 3DHistech Ltd., Budapest, Hungary) or appropriate fluorescence microscopes (Nikon Ti-2E, objective 20x/0.75; Nikon, Amsterdam, The Netherlands, and Zeiss LSM700, objective 40x/1.4 Oil DIC; Zeiss GmbH, Oberkochen, Germany). For each staining, 1-3 aortic root sections per mouse were analyzed using the ImageJ software. The intima and media were outlined and the lesion size was calculated as absolute intimal area (mm^2) (I) or intima-to-media ratio (III). The percentage of intimal area positive for macrophages, IL-1β, and MCP-1 staining was measured using specific color threshold values for each staining. Lesion endothelial lining positive for VCAM-1 and ICAM-1 was graded visually as 1 (<30%), 2 (30-60%) or 3 (>60%). Apoptotic macrophages were measured as the number of Mac-3 macrophages positive for caspase-3 per intimal area (mm^2) (I). The MI size was measured as the average percentage of LV circumference in Masson's trichrome stainings. Percentages of myocardium positive for CD68, α-SMA or collagen within the MI region or remote myocardium were measured in 4 sections per heart using specific color threshold values (II). In addition to myofibroblasts, the α-SMA antibody stains vascular SMC, and therefore, the most obvious vessels were carefully excluded from the MI and remote ROIs. The small capillaries could not be totally avoided.

Table 4.   Antibodies used in immunohistochemical and immunofluorescence stainings.

Antibody	Cat#	Company	Working dilution IHC	IF	Study
α-SMA	A522	Sigma-Aldrich	1:20 000	1:2000	II
Caspase-3	9661-s	Cell Signaling Technology		1:400	I
CCR2	ab21667	Abcam		1:400	I
CD206	ab64693	Abcam		1:200	I, III
CD31	sc-1506-R	SantaCruz		1:100	I
CD68	MCA341R	AbD Serotec	1:10 000	1:500	II
GLP-1R	ab39072	Abcam		1:500	II
GLP-1R	7F38	DSHB by Knudsen		1:100	III
ICAM-1	sc-1511-R	SantaCruz		1:300	I
IL-1β	ab9722	Abcam		1:100	I
iNOS	ab15323	Abcam		1:200	III
Insulin	ab63820	Abcam	1:1000	1:5000	III
Mac-3	550292	BD Pharmingen	1:5000	1:100	I, III
MCP-1	NBP1-42280	Novus Biologicals		1:300	I
PC	Non-commercial	Athera Biotechnologies		1:10	I
VCAM-1	ab134047	Abcam		1:100	I

IF; immunofluorescence, IHC; immunohistochemistry.

4.10   Glucose tolerance test

In Study III, to assess the glucose metabolism of the mice, an i.p. glucose tolerance test (GTT) was performed one week prior to the imaging study. The mice were fasted for 4 hours, and blood samples were withdrawn from the tail vein prior to and 20, 40, 60 and 90 min after i.p. glucose injection (1 g/kg glucose). Glucose values were measured from the whole venous blood using a glucometer.

4.11   Measurement of plasma lipids and biomarkers

Plasma concentrations of total cholesterol, LDL, HDL, and TGs were measured from terminal blood samples collected by heart puncture, using a Konelab 20i chemistry analyzer (Thermo Fisher Scientific, MA, USA) (I) or with appropriate lipid kits (Roche Diagnostics, Basel, Switzerland) (III). In Study III, the plasma levels of C-peptide, glucagon, insulin, and leptin were measured, from saphenous vein blood samples taken before the tracer injection, using a Luminex assay according to the manufacturer's instructions (MILLIPLEX MAP Mouse Metabolic Hormone Magnetic Bead Panel, Merck Millipore, Billerica, MA, USA). In Study I, X19-mu antibody levels were measured from the terminal blood samples with a modified CVDefine ELISA kit (Athera Biotechnologies AB, Stockholm, Sweden), where the original secondary antibody (detecting human IgM) was replaced with anti-IgG (AffiniPure goat anti-mouse IgG [H+L] and goat anti-human IgG [H+L], respectively; Jackson Immuno Research Laboratories, Baltimore, MD, USA).

4.12   Human aortic endothelial cell experiments

In Study I, primary HAECs (Lonza, Baltimore, MD, USA) were seeded on fibronectin-coated tissue culture-treated wells and maintained in EGM-2 medium (Lonza) at 37 °C and 5% CO_2. Cells between passage 4 to 7 were used for HAEC experiments. Lipoprotein fractions were obtained from plasma of three different male and female normolipidemic volunteers and Lp(a) was isolated (Schnitzler et al., 2017). HAECs were stimulated with 1 mg/ml of Lp(a) for 24 h in the presence of fully human PC-mAb or a non-specific IgG. Thereafter, cells were processed for gene expression measurements of *VCAM1*, *ICAM1*, *IL6*, and *IL8* (primers from Sigma Aldrich, Zwijndrecht, The Netherlands) by means of a quantitative polymerase chain reaction (qPCR) (SYBR Green Fast on a ViiA™ 7 PCR machine, Applied Biosystems, Bleiswijk, The Netherlands) as well as cytokine (protein) measurements of IL-6 and IL-8 (ELISA kit, Thermo Fisher Scientific, Carlsbad, CA, USA). Intracellular nitrate reflecting NO production was measured using a commercially available Nitric Oxide Assay Kit (fluorometric) according to the

manufacturer's instructions (ab65327, Abcam, Cambridge, UK). The experiments were repeated three times.

4.13   Statistical analysis

The results are presented as mean ± standard deviation (SD), unless otherwise indicated. The statistical analyses were conducted with SPSS Statistics software v. 22 (IBM, Armonk, New York, USA), and the graphs were created using GraphPad Prism 6 (GraphPad Software Inc., La Jolla, CA, USA). Normality was examined by the Shapiro-Wilk test, and equality of variances was tested with Levene's test. Student's *t*-test for unpaired data was used to compare differences between two independent groups. Multiple comparisons were made by one-way analysis of variance (ANOVA) followed by a Tukey-Kramer post-hoc test (II). Different measurements from the same animals (e.g., MI vs. remote) were analyzed using paired Student's *t*-test. Spearman's correlation was used to analyze correlation between two continuous variables (II). Analysis of covariance was conducted to compare repeated CFR and echocardiography measurements (I, II). Non-parametric tests, namely Fisher's exact test and Mann-Whitney U test were applied to analyze histological scores and *in vitro* data, respectively (I).

In study I, the ^{18}F-FDG uptake was higher in female than in male mice and thus, sex and treatment group were included as fixed factors in the statistical model (no interaction between sex and group was observed). There were no differences between females and males in other experiments. Two-way ANOVA was used to compare ^{18}F-FDG uptake in lesions divided into tertiles according to macrophage density. Macrophage density and treatment were included as fixed factors in the model (no interaction was observed). Assuming an average CFR of 2.5 ± 0.3 (Saraste et al., 2006) and ^{18}F-FDG uptake of 1.8 ± 0.25 (Rinne et al., 2014), sample sizes of 10 and 14 were calculated to be sufficient to detect a difference of 15% with 80% power and a type I error of 0.05, respectively. A p-value of <0.05 was considered statistically significant in all studies.

5 Results

5.1 Effects of a therapeutic PC antibody on vascular function and atherosclerotic inflammation

The 6-week treatment with X19-mu was well tolerated. The antibody remained present in the blood circulation until the end of the intervention, with the average plasma X19-mu concentration being 14 ± 9.8 mg/ml 5 to 7 days after the last injection. The final study group consisted of 16 mice in the vehicle group and 16 mice in the X19-mu group, since one mouse had to be excluded due to a failure in the dosing of X19-mu (no detectable levels of X19-mu in plasma), and one mouse due to failure in the dosing of ^{18}F-FDG. Following the treatment, the groups treated with either vehicle or X19-mu were similar in terms of body weight (30 ± 6.0 vs. 30 ± 7.7 g, $p = 0.89$), fasting blood glucose levels (10 ± 2.6 vs. 10 ± 2.3 mmol/l, $p = 0.77$), and total plasma cholesterol (8.8 ± 1.6 vs. 9.0 ± 1.8 mmol/l, $p = 0.76$) as well as LDL (6.8 ± 1.3 vs. 7.0 ± 1.6 mmol/l, $p = 0.66$) levels.

5.1.1 Lesion histology

All LDLR$^{-/-}$ApoB$^{100/100}$ mice demonstrated macrophage-rich atherosclerotic lesions in the aorta (Figures 5 and 7). PC-positive staining was detected in atherosclerotic lesions, co-localizing with Mac-3-positive macrophages and CD31-positive endothelial cells covering the lesions (Figure 5). The quantification of the results of the histological and immunofluorescence stainings of the aortic root sections is shown in Table 5. The absolute lesion area in the aortic root and intimal area positive for Mac-3 macrophage staining was similar between the vehicle- and X19-mu-treated mice. The Mac-3-positive area of the intima contained similar amounts of M1 (CCR2) and M2 (CD206) macrophages in both groups. However, the IL-1β expression was significantly reduced after X19-mu treatment as compared with vehicle-treated mice (p = 0.044). The extent of lesion endothelium positive for VCAM-1 or ICAM-1 did not differ between the groups. The expression of MCP-1, number of macrophages positive for cleaved caspase-3, and the lesion collagen content were also comparable between the vehicle- and X19-mu-treated mice.
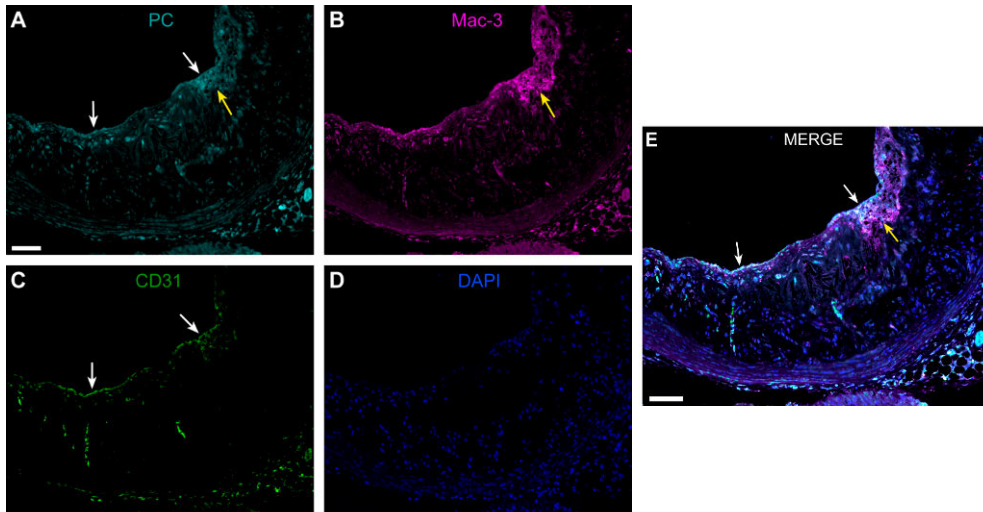
Figure 5. Phosphorylcholine (PC) epitopes are present in macrophages (yellow arrows) and endothelial cells (white arrows) in atherosclerotic lesions. Aortic root section stained with **(A)** PC antibody (PC-mAb), **(B)** Mac-3 antibody (macrophages), **(C)** CD31 antibody (endothelial cells), and **(D)** DAPI. **(E)** PC-positive staining co-localized with endothelial cells covering the lesion and macrophages (white color in merge). Scale bar = 75 µm. (Adopted from the original publication I with a permission. DOI: 10.1016/j.jacbts.2020.01.008)

Table 5. The effect of X19-mu treatment on lesion histology and inflammatory markers.

	Vehicle	X19-mu	*p-value*
Lesion area (mm^2)	0.68 ± 0.28	0.62 ± 0.28	0.57
Mac-3 (%)	19 ± 8.7	19 ± 10	0.93
CCR2 (% of Mac-3 area)	44 ± 13	43 ± 13	0.87
CD206 (% of Mac-3 area)	48 ± 26	60 ± 24	0.23
VCAM-1 (score*)	2.5 [2.0 and 3.0]	2.0 [2.0 and 3.0]	0.65
ICAM-1 (score*)	2.5 [2.0 and 3.0]	2.0 [1.0 and 2.0]	0.32
IL-1β (%)	24 ± 1.0	21 ± 0.83	0.044
MCP-1 (%)	10 ± 1.0	10 ± 0.60	0.82
Mac-3+Caspase-3 (cells/mm^2)	220 ± 65	230 ± 72	0.61
Collagen (%)	39 ± 5.6	40 ± 7.9	0.68

Values are mean ± SD with the exception of *median [25% and 75% percentiles].

Student's *t*-test for unpaired measurements and Fisher's exact test for scores.

n = 10-16/staining/group.

5.1.2   Coronary flow reserve

The CFR was measured as the ratio of coronary flow velocity in the middle LCA during adenosine stress and at rest by Doppler ultrasound before and after treatment (Figure 6). Compared with vehicle, the analysis of covariance for repeated measurements showed that the CFR preserved during the 6-week treatment with X19-mu ($p = 0.047$) (Figure 6B). Compared with week 0, CFR was $24 \pm 20\%$ lower after 6 weeks in vehicle-treated mice (1.9 ± 0.29 vs. 1.4 ± 0.23, $p < 0.01$), whereas there was a trend toward a higher ($9.0 \pm 23\%$) CFR after treatment with X19-mu (1.6 ± 0.24 vs. 1.7 ± 0.24, $p = 0.32$).
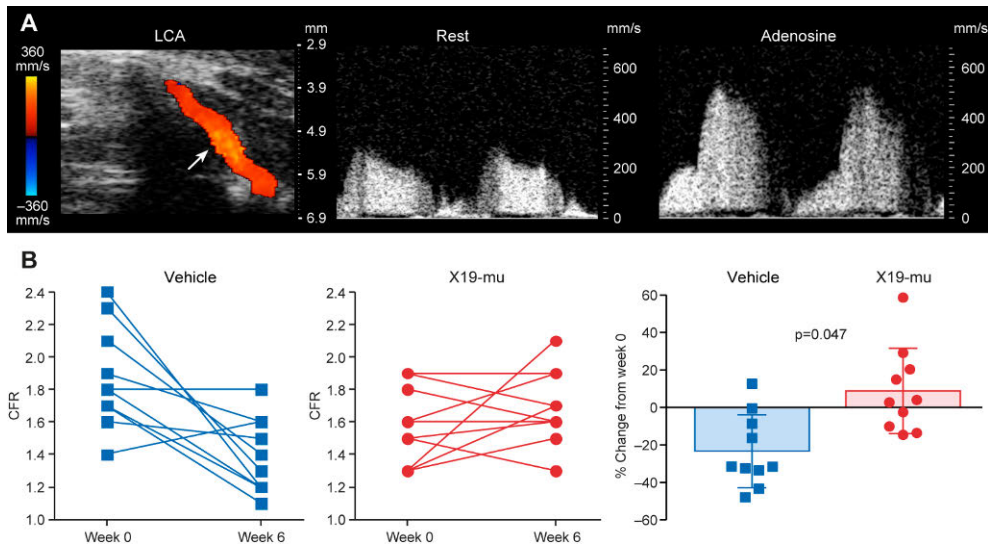
Figure 6.   Treatment with X19-mu preserves coronary flow reserve (CFR). **(A)** Blood flow in the left coronary artery (LCA) localized under color Doppler mapping (arrow) and the blood flow velocity profiles recorded by pulsed-wave Doppler at rest and during adenosine infusion. **(B)** Compared with vehicle, the CFR preserved in relation to the week 0 measurement was preserved after a 6-week treatment with X19-mu. (Mean ± SD in the histogram; analysis of covariance for repeated measurements; n = 10/group.) (Adopted from the original publication I with a permission. DOI: 10.1016/j.jacbts.2020.01.008)

5.1.3   Nitric oxide production and endothelium

To investigate the mechanism underlying the improved vascular function, NO production was measured in Lp(a)-stimulated HAECs in the presence of either PC-mAb or non-specific control IgG. The intracellular nitrate concentration, which reflects endothelial NO production, was reduced after a 24-h stimulation with Lp(a) and a nonspecific IgG (median [25% and 75% percentiles]: 144 [143 and 150] pmol/ ×106 cells vs. 118 [117 and 123] pmol/ ×106 cells, $p = 0.049$), but

preserved in the presence of PC-mAb (135 [133 and 172] pmol/ ×106 cells, p = 0.049 vs. nonspecific IgG). Furthermore, the gene expressions (fold change, median [25% and 75% percentiles]) of *VCAM1* (0.70 [0.63 and 7.2] vs. 2.2 [1.5 and 8.9], p = 0.28), *ICAM1* (0.73 [0.91 and 2.1] vs. 1.5 [1.2 and 3.9], p = 0.51), and *IL8* (0.75 [1.1 and 2.3] vs. 3.0 [1.8 and 3.8], p = 0.83) in HAECs tended to be lower in the presence of PC-mAb as compared with nonspecific IgG, although the differences were not statistically significant. The gene expression of *IL6* as well as the cytokine (protein) IL-6 and IL-8 levels were similar in the presence of PC-mAb and nonspecific IgG antibodies.

5.1.4 ^{18}F-FDG uptake

Focal uptake of ^{18}F-FDG was detected in macrophage-rich atherosclerotic lesions within the aorta by autoradiography (Figure 7A to 7C). The average uptake of ^{18}F-FDG in atherosclerotic lesions, expressed as lesion-to-wall ratio and adjusted by sex, was significantly lower after the 6-week treatment with X19-mu as compared with vehicle-treated mice (1.5 ± 0.17 vs. 1.7 ± 0.24, p = 0.002, Figure 7D). In a sub-analysis, ^{18}F-FDG uptake was compared in lesions with a low (on average 22%), intermediate (29%), or high (35%) density of macrophages. The higher the density of macrophages in the lesion, the higher the ^{18}F-FDG uptake (p = 0.039) in both the vehicle- and X19-mu-treated mice. However, X19-mu treatment reduced ^{18}F-FDG uptake in lesions with low (1.2 ± 0.32 vs. 1.4 ± 0.33), intermediate (1.2 ± 0.19 vs. 1.6 ± 0.33), and high (1.4 ± 0.19 vs. 1.9 ± 0.29) density of macrophages as compared with vehicle (p < 0.001). (Figure 7E) The *ex vivo* biodistribution showed that ^{18}F-FDG uptake was lower in the brain after X19-mu treatment compared with vehicle (SUV 1.3 ± 0.31 vs 1.6 ± 0.33, p = 0.036). There were no differences in other tissues.
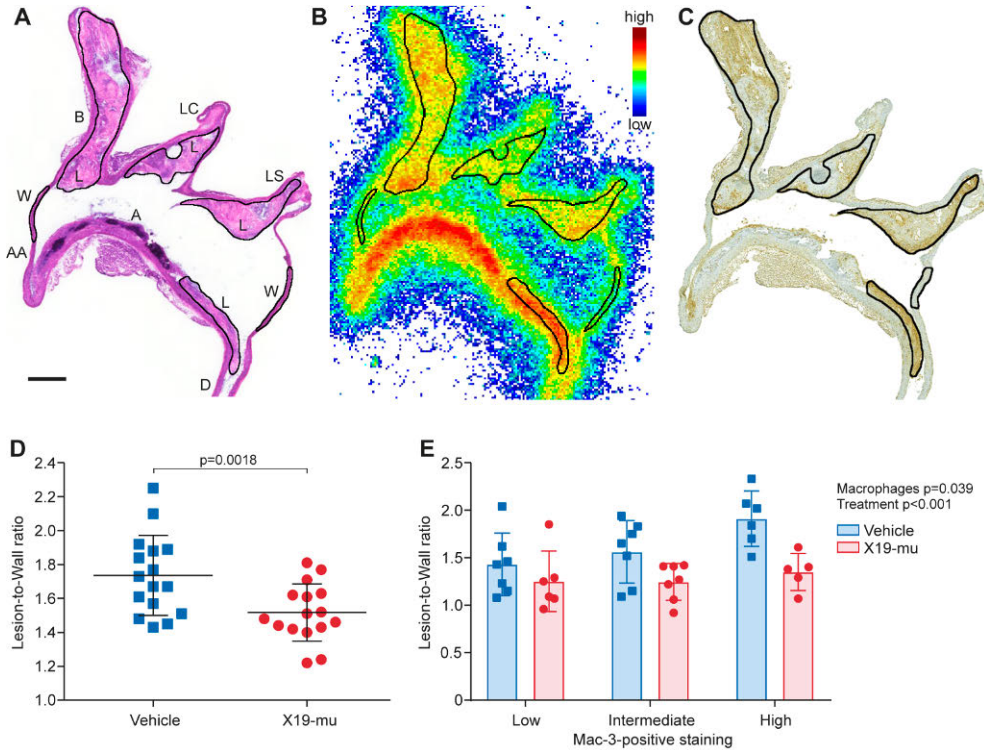
Figure 7. X19-mu treatment reduces ^{18}F-FDG uptake in atherosclerotic lesions. **(A)** A hematoxylin and eosin-stained longitudinal aortic cryosection, **(B)** corresponding autoradiograph, and **(C)** macrophage (Mac-3) staining. The regions of interest are defined in the atherosclerotic lesions and lesion-free vessel walls (black lines). **(D)** The average ^{18}F-FDG uptake in atherosclerotic lesions (expressed as lesion-to-wall ratio) was lower after a 6-week treatment with X19-mu than with vehicle. (n = 16 mice/group; mean ± SD; sex-adjusted model). **(E)** The sub-analysis showed that X19-mu treatment reduced ^{18}F-FDG uptake in lesions with low, intermediate, and high density of macrophages as compared with vehicle. (n = 5-7 mice/group in each sub-category; mean ± SD; two-way ANOVA for the main effects of macrophage density and treatment). Scale bar = 0.5 mm. A = arch; AA = ascending aorta; B = brachiocephalic artery; D = descending thoracic aorta; L = lesion; LC = left common carotid artery; LS = left subclavian artery; W = wall. (Adopted from the original publication I with a permission. DOI: 10.1016/j.jacbts.2020.01.008.)

5.2 Imaging of GLP-1R expression with ^{68}Ga-NODAGA-exendin-4

In Study II, none of the sham-operated rats showed myocardial injury, whereas in the rats that underwent LCA ligation, the average MI size was medium-to-large and it was comparable between the measurement time-points at day 3 (48 ± 7.4%, p = 0.54 vs. week 1 and p = 0.066 vs. week 12), week 1 (42 ± 6.7%, p = 0.40 vs. week 12), and week 12 (35 ± 14%). Echocardiography and cardiac MRI visualized significant LV enlargement and dysfunction at 12 weeks after MI (Figure 8). The fractional shortening was lower in the rats with MI at 1 and 12 weeks than in the sham-operated

rats ($17 \pm 5.0\%$ vs. $48 \pm 5.1\%$, $p < 0.0001$ and $13 \pm 5.1\%$ vs. $42 \pm 5.6\%$, $p < 0.0001$, respectively). Compared with the sham-operated rats, the absolute LV diastolic and systolic diameters increased in the rats with MI from 1 to 12 weeks (change 0.57 ± 0.70 mm vs. 2.7 ± 1.4 mm, $p < 0.0001$, Figure 8, and 0.83 ± 0.61 vs. 2.7 ± 1.2 mm, $p = 0.046$, respectively), thus indicating significant post-MI LV remodeling.

In Study III, plasma levels of total cholesterol were similar between non-diabetic (LDLR$^{-/-}$ApoB$^{100/100}$) and diabetic (IGF-II/LDLR$^{-/-}$ApoB$^{100/100}$) mice (46 ± 7.8 mmol/l vs. 50 ± 6.6 mmol/l, $p = 0.24$), but significantly higher in all hypercholesterolemic mice than in healthy (C57BL/6N) mice (2.0 ± 0.41, $p < 0.01$). The leptin levels were also higher in both non-diabetic (6300 ± 1800 pg/ml) and diabetic (6500 ± 2800 pg/ml) hypercholesterolemic mice as compared with healthy mice (2700 ± 2600 pg/ml, $p < 0.05$). The diabetic mice demonstrated impaired glucose tolerance (peak GTT value at 20 min 29 ± 4.6 mmol/l) as compared with non-diabetic (14 ± 2.6 mmol/l, $p \leq 0.001$) and healthy mice (13 ± 1.6 mmol/l, $p \leq 0.001$). Furthermore, compared with the non-diabetic hypercholesterolemic mice, the fasting plasma levels of insulin (1300 ± 1200 pg/ml vs. 2700 ± 1600 pg/ml, $p = 0.11$) and C-peptide (1000 ± 670 pg/ml vs. 1700 ± 1100 pg/ml, $p = 0.17$) tended to be higher and glucagon levels (120 ± 130 pg/ml vs. 87 ± 47 pg/ml vs, $p = 0.51$) lower in the diabetic mice.
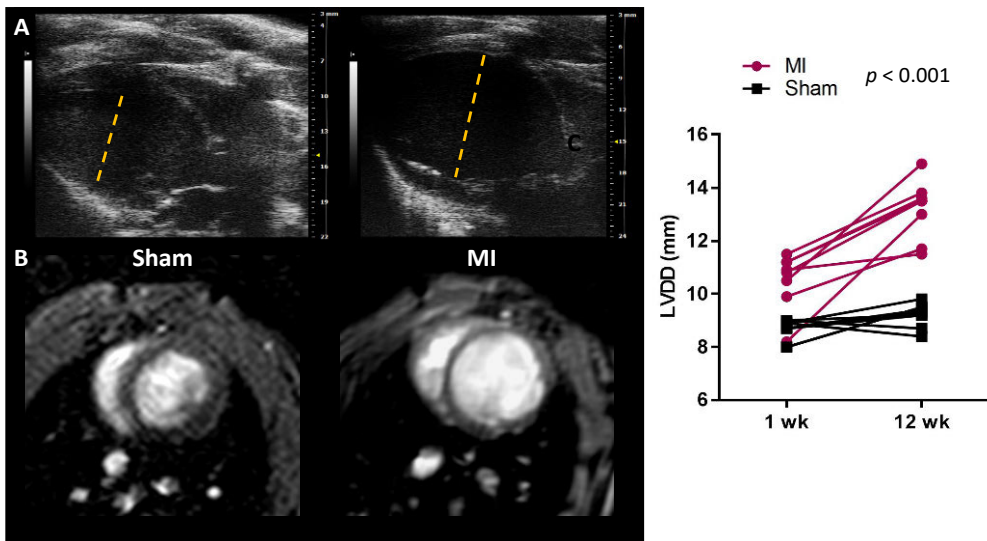
Figure 8. Echocardiography and cardiac magnetic resonance imaging (MRI) show significant left ventricle (LV) enlargement 12 weeks after myocardial infarction (MI). **(A)** Parasternal long-axis echocardiography images and **(B)** corresponding short-axis MR images (white color, left and right ventricle cavities) in a healthy sham-operated rat and in a rat with MI. The LV diastolic diameter (LVDD, yellow dotted lines) assessed by echocardiography increased in rats with MI from 1 to 12 weeks compared with sham-operated rats. (n = 8 MI and 9 Sham; analysis of covariance for repeated measurements)

5.2.1   Histology and immunostainings

In Study III, the Masson's trichrome stainings demonstrated that a dense collagenous scar developed in the infarcted region in time (areal percentage $16 \pm 5.9\%$ at day 3, $50 \pm 3.4\%$ at week 1, and $59 \pm 2.5\%$ at week 12). The area of interstitial fibrosis was small in the healthy myocardium of sham-operated rats ($3.9 \pm 1.6\%$ at week 1 and $4.3 \pm 1.2\%$ at week 12), but was increased in the remote myocardium after MI as compared with the sham-operated rats ($8.7 \pm 1.4\%$ at week 1, $p < 0.001$ and $11 \pm 2.0\%$ at 12 weeks, $p < 0.001$). The CD68-positive macrophages were most abundant in the infarcted area 3 days after MI (areal percentage $15 \pm 3.9\%$) and decreased gradually from day 3 to week 1 ($9.5 \pm 2.6\%$, $p = 0.0072$) and week 12 ($4.3 \pm 1.2\%$, $p = 0.0048$). There were very few CD68-positive macrophages (<1%) in the myocardium of sham-operated rats and the remote myocardium of rats with MI. In the infarcted region, the amount of α-SMA-positive myofibroblasts was high and remained stable from 1 week (areal percentage $22 \pm 7.0\%$) to week 12 ($22 \pm 7.4\%$, $p = 0.99$). Compared with the myocardium of sham-operated rats, the area of α-SMA staining was also increased in the remote myocardium at 1 week ($1.2 \pm 0.23\%$ vs. $1.9 \pm 0.73\%$, $p = 0.0087$) and at 12 weeks ($0.96 \pm 0.18\%$ vs. $1.8 \pm 0.70\%$, $p = 0.030$) after MI. In Study III, the area of atherosclerotic lesions in the aortic root was similar in non-diabetic and diabetic hypercholesterolemic mice (intima-to-media ratio 1.7 ± 0.47 vs. 1.7 ± 0.37, $p = 0.98$), as was the intimal area positive for Mac-3 macrophages ($14 \pm 4.1\%$ vs. $13 \pm 4.1\%$, $p = 0.67$).

In Study II, the expression of GLP-1R (protein) in the infarcted heart and atherosclerotic lesions was studied by immunofluorescence stainings. There was no GLP-1R-positive staining in the myocardium of sham-operated rats or in the healthy vessel wall of C57BL/6N mice. However, GLP-1R-positive staining was detected in the infarcted region, co-localizing with CD68-positive macrophages, whereas no co-localization with α-SMA-positive myofibroblasts was observed (Figure 9). In Study III, in the aortic root sections of hypercholesterolemic mice, GLP-1R-positive staining was present mainly in the superficial macrophage-rich areas detected with immunofluorescence stainings with Mac-3, iNOS, and CD206 macrophage markers. The co-localization was most prominent with M2 (CD206) macrophages in the atherosclerotic lesions.
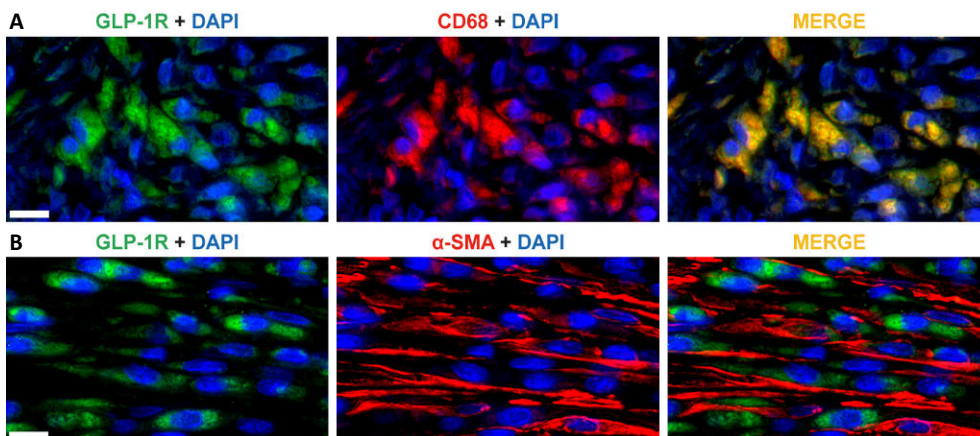
Figure 9. Glucagon-like peptide-1 receptor (GLP-1R) expression is detected in macrophages 1 week after myocardial infarction. Left ventricle sections stained with **(A)** GLP-1R antibody (green) and CD68 antibody (macrophages, red), and **(B)** GLP-1R antibody (green) and α-SMA antibody (myofibroblasts, red). GLP-1R-positive staining co-localized with macrophages in the infarcted area (**A**: merge, yellow), whereas no co-localization with myofibroblasts was detected (**B**: merge). Scale bar = 10 µm. (α-SMA, alpha-smooth muscle actin) (Adopted from the original publication II with a permission. DOI: 10.1007/s12350-018-01547-1)

5.2.2 PET/CT imaging

Representative PET/CT images of ^{68}Ga-NODAGA-exendin-4 uptake in the infarcted heart and atherosclerotic aorta are shown in Figure 10, and quantitative results are presented in Table 6. In Study II, PET/CT imaging showed increased ^{68}Ga-NODAGA-exendin-4 uptake (SUV_{mean} 50-60 min) in the infarcted anterior wall of the LV at 3 days and 1 week after MI as compared with the remote myocardium or the myocardium of sham-operated rats. Pre-injection of unlabeled exendin-4 peptide decreased the ^{68}Ga-NODAGA-exendin-4 signal in the infarcted region to the same level as detected in the sham-operated rats. There was no visible uptake of ^{68}Ga-NODAGA-exendin-4 in the myocardium of sham-operated rats or in the remote myocardium of rats with MI in PET/CT images. Furthermore, parametric K_i-images (Figure 10) and kinetic modeling confirmed ^{68}Ga-NODAGA-exendin-4 uptake in the infarcted area, whereas the uptake was low in the remote myocardium or the myocardium of sham-operated rats. According to the radio-HPLC analysis, 63% of plasma radioactivity originated from the intact tracer and two radio-metabolites of ^{68}Ga-NODAGA-exendin-4 were detected in sham-operated rats. Metabolite-correction was applied in the kinetic modeling. The net influx rate (K_i) of ^{68}Ga-NODAGA-exendin-4 was higher in the infarct region of the LV than remote myocardium at 3 days, 1 week and 12 weeks after MI. There was a good correlation between the SUV_{mean} and K_i values (r = 0.53, p = 0.0034).

In Study III, PET/CT imaging demonstrated elevated ^{68}Ga-NODAGA-exendin-4 uptake in the aortas of atherosclerotic mice at 50-60 min post-injection compared with the healthy aortas of control mice (Figure 10 and Table 6). The TBR ($SUV_{max, aorta}/SUV_{mean\ blood}$) was higher in atherosclerotic mice than in control mice (1.3 ± 0.15 vs. 1.1 ± 0.13, $p = 0.040$). The uptake in the organs adjacent to the heart (lungs and liver) was relatively low in both studies, whereas high radioactivity concentrations were found in kidneys and urine.
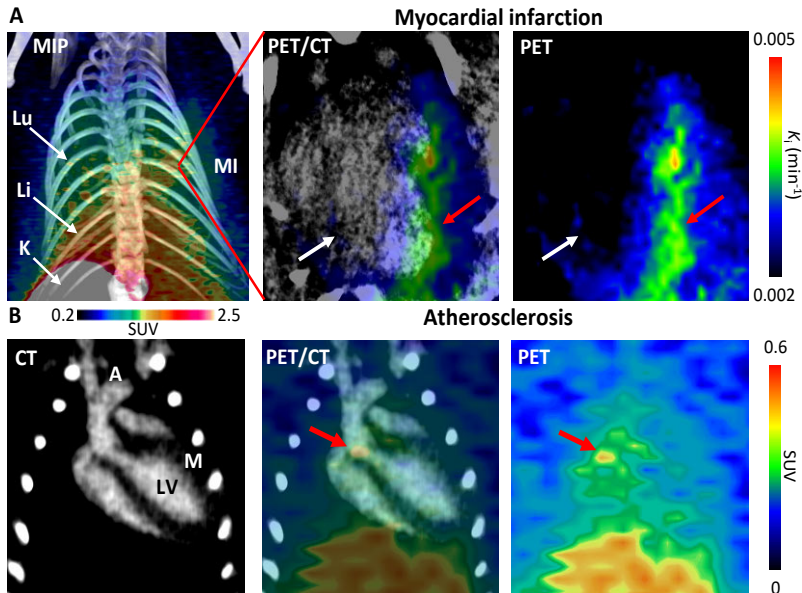
Figure 10. Positron emission tomography (PET) and contrast-enhanced computed tomgraphy (CT) imaging 50-60 minutes post-injection visualizes increased ^{68}Ga-NODAGA-exendin-4 uptake in the infarcted region and atherosclerotic aorta. **(A)** A maximum-intensity-projection (MIP) PET/CT image of the whole thorax and corresponding K_i-generated PET/CT images showed focally increased ^{68}Ga-NODAGA-exendin-4 uptake in the anterior wall of the left ventricle (LV) (red arrows) 1 week after myocardial infarction (MI) compared with remote myocardium (white arrows). **(B)** ^{68}Ga-NODAGA-exendin-4 uptake was focally increased in the aorta (red arrows) of an atherosclerotic IGF-II/LDLR$^{-/-}$ApoB$^{100/100}$ mouse. A = aorta, K = kidney, Li = liver, Lu = lungs. (Modified from the original publication II [DOI: 10.1007/s12350-018-01547-1] and III [*submitted*] with a permission.)

Table 6. Quantification of *in vivo* ^{68}Ga-NODAGA-exendin-4 uptake.

Rats	3 days	1 week	12 weeks
MI (SUV$_{mean}$)	0.67 ± 0.068*	0.59 ± 0.081	0.48 ± 0.092
p vs. Remote	0.026	<0.001	0.082
p vs. MI block		<0.01	
p vs. Sham		<0.01	0.14
MI (K_i ×10^{-3})	4.3 ± 0.48†	2.4 ± 0.41*	1.7 ± 0.42
p vs. Remote	<0.01	<0.001	0.037
p vs. MI block		0.066	
p vs. Sham		0.025	0.80
MI block (SUV$_{mean}$)		0.39 ± 0.081	
MI block (K_i ×10^{-3})		1.8 ± 0.45	
Remote (SUV$_{mean}$)	0.42 ± 0.034	0.43 ± 0.067	0.47 ± 0.098
Remote (K_i ×10^{-3})	1.4 ± 0.45	1.4 ± 0.26	1.1 ± 0.33
Sham (SUV$_{mean}$)		0.42 ± 0.12	0.41 ± 0.049
Sham (K_i ×10^{-3})		1.9 ± 0.33	1.8 ± 0.47
Mice	**Atherosclerotic**	**Control**	*p*-value
Aorta (SUV$_{max}$)	0.26 ± 0.039	0.17 ± 0.048	0.029
p vs. Blood	0.028	0.53	
Blood (SUV$_{mean}$)	0.20 ± 0.011	0.17 ± 0.040	0.140

Results are expressed as standardized uptake values
(SUV$_{mean/max}$ 50-60 min ± SD) or net influx rate (K_i).
MI; infarcted region or corresponding anterolateral wall in Sham,
Remote; septum. Student's *t*-test for unpaired and paired data.
*p <0.05 vs. 12 weeks, †p <0.001 vs.1 and 12 weeks (ANOVA).
Atherosclerotic mice; pooled results from 2 non-diabetic and 2 diabetic mice.

5.2.3   Autoradiography

After *in vivo* imaging, the ^{68}Ga-NODAGA-exendin-4 accumulation in different myocardial regions was studied in more detail by *ex vivo* tissue autoradiography (Figure 11). In Study II, tracer uptake was very low in the myocardium of sham-operated rats, whereas there was focally increased ^{68}Ga-NODAGA-exendin-4 uptake in the infarct scar in all rats with MI. The peak in ^{68}Ga-NODAGA-exendin-4 signal was seen at 3 days after coronary ligation. Compared with the myocardium of sham-operated rats, tracer uptake was 9-fold higher at 1 week and 5-fold higher at 12 weeks after MI. Furthermore, ^{68}Ga-NODAGA-exendin-4 uptake was 2- to 3-fold higher in the remote, non-infarcted myocardium and the MI border zone at 1 week and 12 weeks as compared with the myocardium of sham-operated rats. (Figure 11)
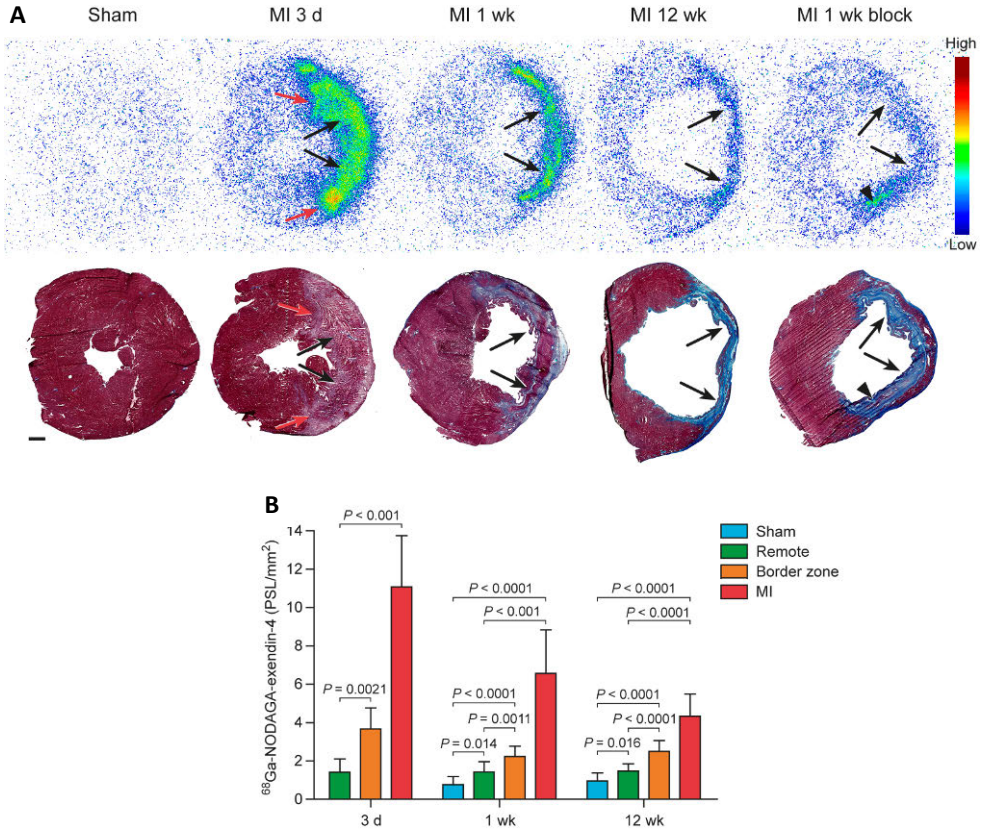
Figure 11. Autoradiography shows increased ^{68}Ga-NODAGA-exendin-4 accumulation in the infarcted area. **(A)** Autoradiographs and corresponding Masson's trichrome stainings of the left ventricle cross-sections showed focally increased ^{68}Ga-NODAGA-exendin-4 uptake in the infarcted area (black arrows) at 3 days, 1 week and 12 weeks after myocardial infarction (MI), whereas uptake was low in sham-operated rats and after pre-injection of unlabeled exendin-4 (MI 1 wk block). Red arrows indicate border zone and the arrowhead indicates non-specific residual activity in the area of necrotic myocyte debris. (Scale bar = 1 mm) **(B)** Quantification of ^{68}Ga- NODAGA-exendin-4 uptake, expressed as photo-stimulated luminescence per square millimeter (PSL/mm^2) in the infarcted area, border zone, remote myocardium, and myocardium of sham-operated rats. (n = 6-9/group; mean ± SD; Student's *t*-test for unpaired and paired [MI vs. remote] data) (Adopted from the original publication II with a permission DOI: 10.1007/s12350-018-01547-1.)

In Study III, autoradiography demonstrated increased accumulation of ^{68}Ga-NODAGA-exendin-4 into the macrophage-rich atherosclerotic lesions in both non-diabetic and diabetic hypercholesterolemic mice. Tracer uptake was similar in the normal vessel wall between non-diabetic, diabetic, and control mice. Quantitative analysis showed that ^{68}Ga-NODAGA-exendin-4 uptake was higher in atherosclerotic lesions than in normal vessel walls (lesion-to-wall ratio) in both non-diabetic (1.6 ± 0.10, *p*<0.0001) and diabetic (1.6 ± 0.078, *p*<0.0001) mice. The

lesion-to-wall ratio was reduced after the pre-injection of unlabeled exendin-4 peptide (block 1.4 ± 0.10, $p = 0.0018$ vs. non-diabetic and $p = 0.0025$ vs. diabetic mice). Since the diabetic strain was utilized in the study, the pancreatic uptake of ^{68}Ga-NODAGA-exendin-4 was also evaluated. There was focally increased tracer uptake in the islets of Langerhans in all groups. The islet-to-exocrine pancreas ratio was similar between non-diabetic and diabetic mice (9.0 ± 3.3 vs. 7.8 ± 2.5, $p=0.56$) and as compared with control mice (11 ± 1.7, $p = 0.42$ vs. non-diabetic and $p = 0.14$ vs. diabetic mice).

5.2.4 Histological correlations of ^{68}Ga-NODAGA-exendin-4 uptake

In Study II, the association of ^{68}Ga-NODAGA-exendin-4 uptake with histological findings was evaluated. The results were pooled for the time-points of 3 days, 1 week and 12 weeks. The degree of CD68 staining in the infarcted area correlated with the corresponding ^{68}Ga-NODAGA-exendin-4 SUV_{mean} ($r = 0.56$, $p = 0.018$) and K_i ($r = 0.74$, $p < 0.01$) values. In autoradiography, there was a good correlation between ^{68}Ga-NODAGA-exendin-4 uptake and CD68-positive macrophages in the infarcted area ($r = 0.71$, $p < 0.001$). The correlation between ^{68}Ga-NODAGA-exendin-4 uptake and the degree of α-SMA staining was negative in the infarcted area ($r = -0.49$, $p = 0.021$), whereas the tracer uptake correlated with α-SMA-positivity in the remote myocardium from 1 week to 12 weeks ($r = 0.52$, $p = 0.040$, pooled 1 week and 12 weeks). No correlation between tracer uptake and fibrosis was found.

6 Discussion

6.1 Phosphorylcholine immunotherapy in atherosclerosis

A crucial step in the initiation and progression of atherosclerosis is the retention and oxidation of LDL in the subendothelial space of arteries. OxLDL as well as Lp(a) display several oxidation-specific epitopes on their surface, including OxPL-PC. Phosphorylcholine (PC) is a pro-inflammatory epitope on OxPLs that mediates pro-atherogenic effects, such as endothelial dysfunction, the accumulation of inflammatory cells into the intima, and uptake of OxLDL by macrophages. Natural IgM antibodies of the innate immune system have capacity to recognize OxPL-PC and neutralize the pro-inflammatory effects. However, low plasma levels of natural IgM antibodies against PC are associated with an increased risk for cardiovascular events. Thus, immunotherapies targeting OxPL-PC may be beneficial in attenuating atherosclerosis. (Binder et al., 2016)

In Study I, treatment with an exogenous, therapeutic monoclonal IgG1 antibody targeting PC epitopes on OxPLs affected NO production in ECs, preserved coronary vascular function, and attenuated atherosclerotic inflammation as measured by the uptake of ^{18}F-FDG in atherosclerotic mice.

6.1.1 Vascular function

Endothelial dysfunction precedes the formation of an atherosclerotic lesion and thereby represents the earliest detectable marker of atherosclerosis. It is also an important contributor to CMD. Treatment of endothelial dysfunction is mainly based on the improvement of known risk factors for ASCVD and symptoms, rather than selective therapies targeting endothelial-based mechanisms. (Gimbrone & García-Cardeña, 2016)

Previous *ex vivo* studies suggest that OxPLs contribute to endothelial dysfunction by inhibiting NO-mediated vasodilatation (Kugiyama et al., 1990; Rikitake et al., 2000; Yan et al., 2017). Furthermore, the levels of the PC epitopes in OxLDL particles have been shown to be associated with the severity of endothelial dysfunction in CCS patients after lipid lowering therapy (Penny et al., 2001). In

young individuals, plasma levels of autoantibodies against OxLDL have been found to inversely correlate with the coronary vasodilatory response evaluated by PET-derived CFR (Raitakari et al., 1997). The present study provided the first evidence that the blockade of OxPL-PC with a therapeutic antibody preserved CFR *in vivo* in response to adenosine in hypercholesterolemic LDLR$^{-/-}$ApoB$^{100/100}$ mice, indicating that it prevented the progression of coronary vascular dysfunction. In LDLR$^{-/-}$ApoB$^{100/100}$ mice that develop obstructive CAD later in life, impaired CFR may reflect the early stages of atherosclerosis (Saraste et al., 2008). The adenosine-induced CFR mainly reflects the vascular SMC relaxation, i.e., an endothelium-independent effect, but it is also indirectly linked to endothelium-mediated vasodilatory function (Mathew et al., 2019). Hence, the endothelial mechanisms underlying the improved vascular function were further studied in Lp(a)-stimulated HAECs in the presence of human PC-mAb. Lp(a) was chosen instead of OxLDL, since it is the main carrier of OxPL-PC in the human plasma. The cell experiments revealed that PC-mAb has a capacity to preserve the endothelial NO production as compared with a nonspecific IgG.

Alternatively, the improved vasodilatory response may be a result of an anti-inflammatory effect of the antibody. In ECs, OxPL-PC has been found to induce the gene expression of pro-inflammatory cytokines and adhesion molecules, and enhance monocyte adhesion to ECs via the TLR4/IL-8 pathway, which can be blocked with the E06 antibody (Leitinger at al., 1999; Walton et al., 2003; Chang et al., 2004). In Lp(a)-stimulated HAECs, the gene-expression of IL-8*,* VCAM-1 and ICAM-1 tended to be lower in the presence of PC-mAb than nonspecific IgG, although the difference was not statistically significant. In line with the preserved CFR and *in vitro* findings, immunofluorescence stainings demonstrated PC-positive staining in the aortic root atherosclerotic lesions, co-localizing with ECs and macrophages.

6.1.2   Atherosclerotic inflammation

The vascular ^{18}F-FDG signal provides an independent predictor of future cardiovascular events and can be used as a surrogate marker of arterial wall inflammation indicating the efficacy of therapy. Several studies have shown that ^{18}F-FDG uptake in atherosclerotic lesions correlates with the quantity of macrophages with high glycolytic activity. (Hyafil & Vigne, 2019) Indeed, increased glycolysis has been recognized as an important marker of high-risk plaque phenotype (Tomas et al., 2018). Furthermore, OxLDL (Lee et al., 2016) and hypoxia (Tawakol et al., 2015) may stimulate macrophage ^{18}F-FDG uptake, and ^{18}F-FDG uptake is particularly high in the early phase of foam cell formation (Ogawa et al., 2012). Recently, increased arterial ^{18}F-FDG uptake was found in subjects with elevated

Lp(a) (van der Valk et al., 2016b). *Ex vivo* experiments demonstrated that the arterial inflammation was due to the OxPL-PC bound to Lp(a) (van der Valk et al., 2016b) that activates the endothelium by enhancing glycolysis, thereby facilitating inflammation and monocyte migration to the artery wall (Schnitzler et al., 2020). The E06 antibody prevented the pro-inflammatory effects of Lp(a).

The present study extended the previous findings by demonstrating that the therapeutic X19-mu antibody against OxPL-PC reduced ^{18}F-FDG uptake in atherosclerotic lesions with different macrophage densities in LDLR$^{-/-}$ApoB$^{100/100}$ mice. The 13% reduction in ^{18}F-FDG uptake as compared with vehicle-treated mice is in line with the degree of reduction in arterial ^{18}F-FDG uptake observed in patients treated with atorvastatin (5% to 15%) (Dweck et al., 2016; van der Valk et al., 2016a). To date, one therapeutic antibody against OxPLs has been studied in a clinical trial, in which the human recombinant IgG1 antibody against an MDA epitope on ApoB100-containing particles did not reduce arterial ^{18}F-FDG uptake in patients with stable inflammatory vascular lesions (Lehrer-Graiwer et al., 2015). This discrepancy may be explained by differences between the PC (phospholipid) and MDA (protein) epitopes, with the former being specifically associated with OxPLs, which are more prevalent in advanced, inflamed lesions (van Dijk et al., 2012).

Despite the attenuation of ^{18}F-FDG uptake, no reduction in the overall lesion macrophage quantity or apoptotic cells, the proportions of M1 and M2 macrophages, the expression of MCP-1 or VCAM-1, the lesion collagen content, or the atherosclerosis burden was found. Based on a previous ^{18}F-FDG validation study in LDLR$^{-/-}$ApoB$^{100/100}$ mice (Silvola et al., 2011), mice with established atherosclerosis were studied, and therefore, it was unlikely for any major plaque regression or changes in plaque cellular composition to occur during a short-term treatment. A different study design with, e.g., a longer follow-up time and younger mice with rapidly growing lesions, as used in previous studies (Caligiuri et al., 2007; Binder et al., 2003; Tsimikas et al., 2011; Que et al. 2018) would be needed for the evaluation of the effects of X19-mu antibody on the natural progression of atherosclerosis. It has been suggested that a metabolic marker such as ^{18}F-FDG uptake is sensitive to changes caused by short-term interventions, regardless of changes in plaque burden (Dweck et al., 2016). Despite the unchanged amount of macrophages, the IL-1β content in the lesions was significantly reduced after X19-mu treatment. This is in line with a previous study that showed reduced IL-1β expression in macrophages isolated from LDLR$^{-/-}$ mice expressing a single-chain variable fragment of the E06 antibody (Que et al., 2018). Furthermore, the lesion ICAM-1 content tended to be lower after X19-mu treatment, which has also recently been implicated in Lp(a)-stimulated HAECs in the presence of E06 (Schnitzler et al., 2020).

The results of the present study suggest that X19-mu immunotherapy may mitigate specific pro-inflammatory responses in inflammatory cells and possibly reduce metabolic activity in atherosclerotic lesions.

6.2 Imaging of GLP-1R expression with ^{68}Ga-NODAGA-exendin-4 in ASCVD

Treatments with GLP-1R agonists reduce cardiovascular events in T2DM patients, and protect from ischemic myocardial injury and progression of atherosclerosis as shown in both preclinical and clinical studies. The beneficial cardiovascular effects are potentially mediated through the attenuation of inflammatory responses, thereby making GLP-1R an attractive target also for cardiovascular imaging. Nevertheless, it remains uncertain whether the protective effects are a direct result of GLP-1R activation in the heart and vasculature. (Nauck et al., 2017)

In Study II, ^{68}Ga-NODAGA-exendin-4 PET imaging detected an increase in the myocardial GLP-1R expression after MI in rats, correlating with the presence of CD68-positive macrophages during the MI healing phase. The Study III showed elevated ^{68}Ga-NODAGA-exendin-4 uptake in macrophage-rich atherosclerotic lesions in both non-diabetic and diabetic hypercholesterolemic mice.

6.2.1 Myocardial infarction

Previous studies suggest that GLP-1R agonists attenuate myocardial inflammation and fibrosis after ischemic injury, resulting in reduced MI size and improved cardiac function (DeNicola et al., 2014; Robinson et al., 2015b; Liu et al., 2010; Wohlfart et al, 2013; Timmers et al., 2009; Woo et al., 2013). However, the beneficial effects of GLP-1R agonists on LV remodeling and HF outcome have been contradictory among the previous preclinical (DeNicola et al., 2014; Robinson et al., 2015b) and clinical studies (Jorsal et al., 2017; Margulies et al., 2016). A recent study demonstrated that, although, GLP-1R messenger RNA transcripts were detected in ventricular tissue, GLP-1R protein was not expressed in ventricular myocytes, cardiac fibroblasts, coronary artery ECs or vascular SMCs of human heart specimens (Baggio et al., 2018).

In the context of myocardial injury, one study has shown up-regulation of GLP-1R expression in the myocardium during the first days (8 hours to 3 days) after I/R injury in rats by using ^{18}F-FBEM-Cys^{40}-exendin-4 PET imaging (Gao et al., 2012). In line with that, the present study demonstrated a peak in the ^{68}Ga-NODAGA-exendin-4 signal 3 days after the permanent coronary artery ligation in rats, and extended the previous findings by showing that the ^{68}Ga-NODAGA-exendin-4 uptake was detectable by PET/CT in the infarcted region 1 week after MI. At the

same time-point, tissue autoradiography also showed a 9-fold higher uptake in the infarcted region than in the myocardium of sham-operated rats. Furthermore, the autoradiography analysis demonstrated elevated ^{68}Ga-NODAGA-exendin-4 accumulation in the infarct scar and in the remote, non-infarcted myocardium until 12 weeks after MI.

Previous *in vitro* studies with related NODAGA-exendin-4 radiotracers have suggested that 20-35% of the tracer is internalized into the cells (Jodal et al., 2014), which indicates irreversible tracer uptake. Therefore, a graphical Patlak model was applied to the *in vivo* ^{68}Ga-NODAGA-exendin-4 data. The kinetic modeling revealed that ^{68}Ga-NODAGA-exendin-4 uptake was higher in the infarcted region than in the remote myocardium at 3 days, 1 week, and 12 weeks after MI, thus supporting irreversible ^{68}Ga-NODAGA-exendin-4 uptake in the infarcted area. The observed irreversible compartment can be due to irreversible receptor binding and/or internalization, given that the Patlak analysis calculates the net influx rate of irreversible tracer uptake (Patlak et al., 1983). Importantly, pre-injection of unlabeled exendin-4 peptide significantly reduced tracer uptake in the infarcted area indicating specific receptor-mediated uptake.

The cellular substrate of ^{68}Ga-NODAGA-exendin-4 uptake in the infarcted and remote areas of the myocardium was investigated by coupling the tracer uptake with the histological markers of myocardial repair. Activation of GLP-1R has been shown to induce differentiation of human macrophages to the reparative M2 phenotype with elevated IL-10 secretion (Shiraishi et al., 2012), increase the amount of M2 macrophages after MI (Gross et al., 2016), and inhibit myocardial macrophage infiltration after MI (Robinson et al., 2015b, Tate et al., 2016) Expression of GLP-1R has been detected in macrophages in atherosclerotic lesions and in isolated mouse and human macrophages (Arakawa et al., 2010; Bruen et al., 2017; Nagashima et al., 2011), but there are also contradictory findings (Panjwani et al., 2013). The major problem is that the detection of immunoreactive GLP-1R is challenging due to the suboptimal sensitivity and specificity of the available antibodies (Pyke & Knudsen, 2013). In a previous imaging study, no co-localization of GLP-1R with CD11b neutrophils was observed after MI (Gao et al., 2012). However, the present study showed a positive correlation between the amount of CD68-positive macrophages and ^{68}Ga-NODAGA-exendin-4 uptake in the infarcted region both by PET *in vivo* and autoradiography *ex vivo*. Furthermore, immunofluorescence stainings demonstrated co-localization of GLP-1R with CD68-positive macrophages in the infarcted area.

The ^{68}Ga-NODAGA-exendin-4 uptake was moderately increased also in the remote myocardium 1 week and 12 weeks after MI, correlating with the presence of α-SMA-positive myofibroblasts. In contrast, there was a negative correlation between ^{68}Ga-NODAGA-exendin-4 uptake and α-SMA-positive staining in the

infarcted area. No co-localization between GLP-1R and α-SMA-positive myofibroblasts was detected in the infarct scar or remote areas. The low content of macrophages in the remote myocardium did not allow correlation analysis. However, this does not mean that the number of macrophages is not increased in the remote region after MI, since conventional histology is less sensitive to very small changes. Thus, the substrate of ^{68}Ga-NODAGA-exendin-4 uptake in the remote myocardium remained unexplained. It would require an *in vitro* cell experiment, where macrophages and/or myofibroblasts are incubated with ^{68}Ga-NODAGA-exendin-4. However, previous studies suggest that GLP-1 may attenuate ECM remodeling in the absence of direct actions on cardiac fibroblasts via macrophage-dependent mechanisms (Robinson et al., 2015b, Tate et al., 2016), angiotensin production (Zhang et al., 2015), or decreasing β1-adrenoceptor expression (Sassoon et al., 2017).

The present study indicates that the up-regulation of myocardial GLP-1R expression is potentially associated with the activation of repair mechanisms after ischemic injury, which may be evaluated using ^{68}Ga-NODAGA-exendin-4 PET imaging.

6.2.2   Atherosclerosis

The inflammatory hypothesis was further investigated in Study III in atherosclerotic mouse models. Previous small-scale clinical trials and preclinical studies propose that GLP-1R activation reduces systemic inflammation (Hogan et al., 2014; Rakipovski et al., 2018), attenuates atherosclerotic lesion development by modifying plaque composition (Rizzo et al., 2014; Balestrieri et al. 2015; Bruen et al., 2017; Nagashima et al., 2011), and inhibits macrophage infiltration into the vessel wall (Arakawa et al., 2010; Vinue et al., 2017). In ApoE$^{-/-}$ mice, lesional macrophages have been shown to express GLP-1R (Arakawa et al., 2010) and GLP-1R agonists to induce polarization of macrophages toward M2 phenotype (Bruen et al., 2017, 2019; Vinue et al., 2017). The present study represents the first vascular imaging study utilizing an exendin-4 radiotracer for the detection and imaging of GLP-1R expression in atherosclerotic lesions.

The present study demonstrated increased ^{68}Ga-NODAGA-exendin-4 uptake in macrophage-rich atherosclerotic lesions as compared with corresponding lesion-free vessel wall in both non-diabetic (LDLR$^{-/-}$ApoB$^{100/100}$) and diabetic (IGF-II/LDLR$^{-/-}$ ApoB$^{100/100}$) hypercholesterolemic mice, as assessed by the autoradiography analysis. The uptake in atherosclerotic lesions was significantly reduced after pre-injection of a blocking unlabeled exendin-4 peptide, indicating specific GLP-1R binding of the tracer. Furthermore, PET/CT imaging visualized ^{68}Ga-NODAGA-exendin-4 accumulation in the atherosclerotic aorta *in vivo*. The average TBR was

significantly higher in the atherosclerotic mice than in the control mice, although it was relatively low overall in both groups. As a result of the low *in vivo* uptake, no kinetic modeling was conducted in Study III. The present study extended the previous findings by demonstrating that the immunofluorescence stainings showed co-localization of GLP-1R with both M1 (iNOS) and M2 (CD206) macrophages in the aortic root atherosclerotic lesions. The co-localization was particularly prominent for M2 macrophages. In line with that, a recent study has suggested that a GLP-1R agonist treatment is capable of inducing CD206 gene expression in human macrophages (Bruen et al., 2019).

Previous clinical and preclinical studies have been conducted mainly in the presence of T2DM in subjects at increased risk of cardiovascular events (Heuvelman et al., 2020). The present study sought to investigate whether T2DM has an incremental effect on vascular ^{68}Ga-NODAGA-exendin-4 uptake in hypercholesterolemic mouse models. Previous studies have shown that IGF-II/LDLR$^{-/-}$ApoB$^{100/100}$ mice represent a more pro-inflammatory phenotype, including more complex lesions with increased calcification and higher IL-6 expression (Heinonen et al., 2007; Hellberg et al., 2016). Despite the similarity between the strains in terms of the lipid profile and number of macrophages, the IGF-II/LDLR$^{-/-}$ApoB$^{100/100}$ mice demonstrated hyperglycemia and impaired glucose tolerance when compared with the LDLR$^{-/-}$ApoB$^{100/100}$ counterparts. The pancreatic uptake of ^{68}Ga-NODAGA-exendin-4 (islet-to-exocrine pancreas ratio) tended to be lower in diabetic than non-diabetic hypercholesterolemic mice, although the difference was not significant. This may be due to the reduced β-cell mass and impaired β-cell function that occur in T2DM (Velikyan & Eriksson, 2020). However, the ^{68}Ga-NODAGA-exendin-4 uptake was similar in atherosclerotic lesions in both strains irrespective of T2DM. The observation may be important, since there are studies currently underway that aim to investigate whether other patients with cardiovascular disease, apart from subjects with T2DM and high cardiovascular risk, display a similar cardiovascular benefit of GLP-1R agonists (Heuvelman et al., 2020).

The present study provided evidence that the specific GLP-1R-targeting radioligand, ^{68}Ga-NODAGA-exendin-4, enables the detection and imaging of GLP-1R expression in atherosclerotic lesions associated with macrophages. On top of atherosclerosis, T2DM did not have any incremental effect on vascular ^{68}Ga-NODAGA-exendin-4 uptake.

6.3   Limitations

General limitations of the present research are related to animal models and methodology. Genetically modified mouse models have provided important insights

into the mechanisms of atherosclerosis, and the majority of contemporary studies are performed in mice. In the present study, the LDLR$^{-/-}$ApoB$^{100/100}$ mouse model was chosen instead of the widely used ApoE$^{-/-}$ or LDLR$^{-/-}$ mouse models, since cholesterol is mostly transported by LDL particles in LDLR$^{-/-}$ApoB$^{100/100}$ mice and their lipid profile closely resembles human FH (Veniant et al., 1998, Powell-Braxton et al., 1998). It was a prerequisite for studying the effects of PC immunotherapy. Although the pathobiology and development of atherosclerotic lesions is similar to that in humans, the primary sites of lesions in mice are the aortic root, aortic arch, and carotid arteries, not the coronary arteries. Moreover, lesion ruptures occur rarely in mice. However, the mice, including LDLR$^{-/-}$ApoB$^{100/100}$ model, do not have Lp(a), wherefore the protective effects of PC immunotherapy in mice were rather related to the inhibition of OxLDL. (von Scheidt et al., 2017) The IGF-II/LDLR$^{-/-}$ApoB$^{100/100}$ mouse model is a relevant model of human diseases, since T2DM is associated with increased risk of ASCVD. The IGF-II/LDLR$^{-/-}$ApoB$^{100/100}$ mice represent a more pro-inflammatory phenotype (Heinonen et al., 2007), but the model has not been widely used and thoroughly characterized yet.

Induction of MI by a permanent ligation of the LCA is a commonly used small animal model of LV remodeling and HF following MI, which was initially established in 1979 in rats (Pfeffer et al., 1979). The model has been utilized in several studies for studying the pathobiology of MI and development of new therapies and imaging techniques. In contrast to humans, the rat survives from an MI size >50% and seldom displays human-like HF symptoms even during a follow-up of 12 weeks, as in the present study. Furthermore, the LCA occlusion is typically induced in young rodents, which is contradictory to common patient population seen in the clinics. The I/R model would represent better the human phenotype, since it mimics the clinical situation where revascularization is performed after an acute MI. However, the I/R model exhibits a lower degree of tissue damage, and Study II aimed to investigate the chronic myocardial healing process in addition to the acute inflammatory response. (Riehle & Bauersachs 2019)

The obvious limitation of small animal cardiac PET imaging is the small size of the heart and aorta, coupled with the constant movement of the heart. The resolution of most small animal PET scanners is 1.5 mm, while the largest murine plaques have a diameter of ~1 mm. It was not possible to perform the ECG-gating in the present studies, but the co-localization of the PET signal to the vasculature and heart was facilitated with a contrast-enhanced CT. However, the partial volume effects (the target is smaller than the voxel size) and spillover from the blood or adjacent tissues may have impaired the quantification, resulting in an under- or overestimate of the measured radioactivity. For example, the infarct-to-remote myocardium ratios of ^{68}Ga-NODAGA-exendin uptake were lower *in vivo* than those observed in autoradiography analyses. Due to these challenges, the demonstration of specific

binding by means of the co-administration of a blocking compound, as performed in the present study, is currently requisite for a tracer characterization. Kinetic modeling, if applicable, would also provide more reliable estimates of tracer uptake kinetics than the SUV values. In Study I, ^{18}F-FDG uptake in the atherosclerotic lesions was not measured *in vivo* due to partial volume effects, but also because the high radiation exposure related to repeated high-resolution angiography might have influenced the health of mice. However, the high-resolution (25 μm) autoradiography technique allows the precise localization and characterization of the tracer uptake, coupled with different histological markers, thus providing useful information for possible clinical translation. Nevertheless, *ex vivo* autoradiography can underestimate the signal in very thin structures, including vessel wall, since radiation originating from ^{68}Ga-labeled tracers, in particular, scatters from its origin to the surrounds. (Meester et al., 2019)

Immunostaining for cell-specific antigens is the primary method in imaging studies for the purpose of assessing the cellular compositions of atherosclerotic lesions or an infarcted heart. Reliable quantification requires specific and validated antibodies, appropriate sample size (number of animals per group and sections analyzed per animal), sections from the same location (e.g., at the level of aortic sinus) cut with a similar thickness, ROIs that are defined in a similar pre-specified manner, and normalization of the measurements (e.g., percentage of total lesion/infarcted area). The antibodies used in the studies for this thesis were selected on the basis of literature and a specific research question. The selection of M1 and M2 macrophage markers is challenging due to the complex nature of current macrophage classification. Thus, the most commonly recognized markers, including CCR2/MCP-1, IL-1β, and CD206, were chosen. The conventional immunohistochemical protocols typically produce some background staining that impairs the quantification, and therefore, immunofluorescence stainings were primarily preferred. Moreover, co-stainings can be easily done by immunofluorescence, which provides more reliable and specific information on the target antigens. However, the quantification of immunostainings is not a sensitive method for the detection of very small differences, wherefore it is usually coupled with the mRNA measurements or flow cytometry analyses of different cell populations. These measurements would, however, have required additional study groups, while the main interest in this thesis was to compare the radioactive signal with a biological source, which, after autoradiography, can be done by analyzing corresponding tissue immunostainings. (Daugherty et al., 2017)

There are also some specific limitations regarding the present study. Aortic root is the most common and validated region for atherosclerosis quantification, but it is also the site of the most advanced lesions (Daugherty et al., 2017). This fact may

explain why differences in the lesion cellular composition, such as the number of macrophages or change in their phenotype, were not observed after PC immunotherapy. Importantly, ^{18}F-FDG uptake was measured throughout the thoracic aorta in different regions and multiple lesions. The Doppler ultrasound is a validated method for measuring CFR in mice (Gan et al., 2004; Saraste et al., 2008), although a highly operator-dependent technique. Because of the high variation in CFR values observed in mice in general (from 1.2 to >2.2) (Saraste et al., 2008; Wikström et al., 2008) and in individual mice in the present study, larger studies are needed to confirm the magnitude of the treatment effect on coronary vascular function. Saline was used as a vehicle treatment instead of an isotype IgG1 control, since the production of a corresponding mouse-human chimeric isotype IgG1 not binding to PC is challenging. The role of natural IgG antibodies in atherosclerosis is still a matter of debate, and thus, the risk of interference of a non-specific IgG with the naturally occurring antibody responses was avoided by using saline as a control (Centa et al., 2019).

A question that remained open in Studies II and III is whether the increased uptake of ^{68}Ga-NODAGA-exendin-4 after MI or in atherosclerotic lesions indicates pro-inflammatory or protective mechanisms. Recent studies have shown that GLP-1 secretion is increased in response to CAD (Piotrowski et al., 2013) and STEMI (Diebold et al., 2018). Moreover, elevated levels of GLP-1 are shown to predict cardiovascular events and death in patients with acute MI similarly to hsCRP or natriuretic peptides (Kahles et al., 2019). It has been hypothesized that increased plasma levels of GLP-1 might be in line with natriuretic peptides, which are up-regulated following inflammatory stimuli and predict adverse clinical outcomes in patients with MI, but still remain organoprotective as endogenous counter-regulatory factors (Kahles et al., 2019). Thus, it needs to be studied prospectively whether the observed up-regulation of the myocardial GLP-1R expression soon after MI is related to clinical outcome, i.e., whether ^{68}Ga-NODAGA-exendin-4 PET can predict cardiac function and LV remodeling. Furthermore, it would be of high interest to modify the ^{68}Ga-NODAGA-exendin-4 signal with a GLP-1R agonist treatment or anti-inflammatory therapy and measure the GLP-1R expression levels after treatment. In comparison to MI, the ^{68}Ga-NODAGA-exendin-4 uptake was quite low and diffuse in atherosclerotic lesions, which may indicate a relatively low receptor density that impairs the *in vivo* imaging. However, the background uptake in the myocardium and lungs was low, which is advantageous for the visualization of ^{68}Ga-NODAGA-exendin-4 signal adjacent to these organs. Thus, ^{68}Ga-NODAGA-exendin-4 may have implications for studies of pharmacological modification of GLP-1R signaling in atherosclerosis.

6.4   Strengths and future directions

The ultimate strength of this thesis is the possibility for clinical translation in future studies. The imaging approaches used, PET and ultrasound, allow prompt performance of the same experiments in mice, larger animals, and humans, thus facilitating direct comparison and unification of basic and clinical research. The true value of novel therapies and imaging biomarkers in humans cannot be accomplished without the development of multi-disciplinary strategies for translation. The Study I was designed on the basis of the non-invasive imaging techniques, CFR and ^{18}F-FDG PET, which may be used as possible surrogate markers for the efficacy of PC immunotherapy also in clinical studies. In addition to the mouse model, the effects of human PC antibody were studied *in vitro* in response to Lp(a) isolated from different subjects, thereby mimicking the clinical situation. The starting point for Studies II and III was different, since GLP-1R agonist treatments have already demonstrated cardiovascular benefits in clinical studies. However, the role of GLP-1R signaling in the cardiovascular system has proven challenging to investigate. PET imaging is not only used for diagnostic purposes, but also for the assessment of the pathobiology underlying the disease. Thus, the validated GLP-1R-targeting radioligand, ^{68}Ga-NODAGA-exendin-4, may provide an advantageous tool for studying cardiac GLP-1R signaling in humans in future studies.

6.4.1   Promises and challenges of targeting cardiovascular inflammation

Virchow and von Rokitansky stated already in the mid-1800s that atherosclerosis is a chronic inflammatory disease induced by cholesterol, but it took time to prove that an anti-inflammatory therapy has capacity to reduce cardiovascular events and mortality in ASCVD patients (Ridker et al., 2017). Although the guideline-recommended LDL-C levels can be achieved with contemporary therapies, the residual risk of ASCVD events still persists in some but not all individuals. In addition to inflammation, the residual risk includes such components as residual cholesterol, Lp(a), triglyceride, thrombosis, and diabetes risk, without forgetting the CMD. Recent randomized clinical trials have provided evidence that, on top of statin therapy, it is worthwhile to target these risks with specific treatments, such as PCSK9 inhibitors and GLP-1R agonists. It is obvious that residual risks overlap and are linked; for example, PC immunotherapy may inhibit atherogenicity of Lp(a) and OxLDL, which downstream improves endothelial function and reduces vascular inflammation. Although the multiple inflammatory pathways and mechanisms in ASCVD are well-known, the clinical translation of anti-inflammatory therapies has proven challenging. The extent of inflammation varies during atheroprogression, and increasingly rapid changes in immune cell infiltration can be seen after MI, coupled

with inter-individual variability in inflammatory response. To date, several clinical trials targeting the early inflammatory response after MI have been neutral or conducted in small patient populations. Although, the treatment with low-dose colchicine demonstrated a reduction in ischemic cardiovascular events among patients with recent MI, the long-term safety and efficacy of colchicine need to be confirmed in larger trials. In the future, the prevention of ASCVD events will likely call for individualized therapies, and for that purpose, patient populations with a targetable "cardio-inflammatory" phenotype need to be identified. In this regard, blood-based biomarkers, such as hsCRP, or novel imaging biomarkers may offer a promise to target the right patient, with the right therapy, at the right time. (Adamo et al., 2020; Lawler et al., 2020)

6.4.2 Integration of molecular imaging and therapeutic target

The imaging-guided therapy concept has been successfully employed in the field of oncology and neurology, and is now emerging in the cardiovascular context. Imaging of myocardial perfusion, function, and viability is currently used for therapeutic guidance in ASCVD, but novel therapies would require more sophisticated applications. Molecular imaging bears potential for the characterization of individual disease biology and the identification of a molecular target, which can be directly modified by a specific drug, binding via the identical mechanism. The GLP-1R, ^{68}Ga-NODAGA-exendin-4, and GLP-1R agonist therapy represent a potential combination. Thus, the characteristics desired of a clinically valuable PET tracer include high specificity for the target that is "druggable" and potential to predict the disease outcome at early stages, guide treatment selection and timing, and monitor therapy response. None of the current tracers in nuclear cardiology meet all of these "criteria" yet, but, e.g., CXCR4 targeting PET tracer ^{68}Ga-Pentixafor has demonstrated these characteristics in mice (Hess et al., 2020) and thus, is a very promising candidate. (Hess et al., 2019; Werner et al., 2020)

Another open question related to inflammation imaging is whether the identification of macrophage subpopulations provides additional value. A recent *in vitro* study demonstrated that clinically relevant inflammation tracers can specifically recognize different immune cell populations, e.g., the TSPO-targeting tracer ^{18}F-GE-180 binds primarily to M1 macrophages, whereas ^{68}Ga-Pentixafor binds to a broad range of immune cells (Borchert et al., 2019). Specific targeting of M1 and M2 macrophages by means of molecular imaging may have potential to identify adverse immune responses, especially after MI, and contribute to the development of targeted immunotherapies to achieve optimal myocardial healing or stabilize atherosclerotic lesions. It is also recognized that the cardiovascular system

does not operate independently in response to damage. The ischemic myocardial injury is associated with increased activity in hematopoietic organs, such as spleen (Thackeray et al., 2015a), and with neuroinflammation (Thackeray et al., 2018a), which further fuel ASCVD and increase the risk of complications. The cross-organ communications would be particularly important to investigate in the context of GLP-1R signaling, since the receptor is expressed all over the body and the cardioprotective effects can be mediated also via indirect effects. The advantage of PET imaging is that it allows simultaneous imaging of the heart and other organs. Altogether, the emerging knowledge of disease pathobiology, new translational technologies, and therapeutic opportunities pave the way for the new era of precision cardiology. (Hess et al., 2019; Werner et al., 2020)

7   Conclusions

This thesis investigated the effects of a novel PC immunotherapy on vascular function and atherosclerotic inflammation, and evaluated ^{68}Ga-NODAGA-exendin-4 PET for the assessment of GLP-1R expression after MI and in atherosclerotic lesions by utilizing experimental models. The main conclusions were as follows:

1. Six weeks of treatment with a monoclonal antibody against PC on OxPLs preserved coronary artery function, enhanced NO production in ECs, and attenuated ^{18}F-FDG uptake in atherosclerotic lesions in hypercholesterolemic LDLR$^{-/-}$ApoB$^{100/100}$ mice. Non-invasive imaging techniques, CFR and ^{18}F-FDG PET, represent translational tools for assessing the effects of PC-targeting immunotherapy on vascular function and atherosclerosis.

2. ^{68}Ga-NODAGA-exendin-4 PET/CT showed an increase in myocardial GLP-1R expression after MI in rats. The degree of ^{68}Ga-NODAGA-exendin-4 uptake correlated with the amount of CD68-positive macrophages in the infarcted area and α-SMA-positive myofibroblasts in the remote myocardium, which may be associated with the activation of repair mechanisms after ischemic injury.

3. ^{68}Ga-NODAGA-exendin-4 detected GLP-1R expression in inflamed atherosclerotic lesions in both non-diabetic LDLR$^{-/-}$ApoB$^{100/100}$ and diabetic IGF-II/LDLR$^{-/-}$ApoB$^{100/100}$ mice. The GLP-1R expression in atherosclerotic lesions may reflect M2 macrophage responses.

These findings provide proof-of-concept that a therapeutic antibody targeting PC may represent an approach to inhibit the atherogenic impact of OxPLs, and that the cardiovascular expression of GLP-1R is associated with inflammatory response and repair process. In contrast to MI, atherosclerotic lesions appear to exhibit GLP-1R densities that are too low for *in vivo* imaging.

Acknowledgments

This study was carried out at the Turku PET Centre, University of Turku, Turku, Finland, during the years 2014-2020. It was conducted within the Finnish Centre of Excellence in Cardiovascular and Metabolic Diseases supported by the Academy of Finland, University of Turku, Turku University Hospital, and Åbo Akademi University. I wish to express my warmest thanks to Professor Juhani Knuuti, Director of Turku PET Centre, Professor Emeritus Jaakko Hartiala and Adjunct Professor Jukka Kemppainen from the Department of Clinical Physiology and Nuclear Medicine for providing the excellent facilities to conduct research.

I express my heartfelt gratitude to my supervisors, Professor Antti Saraste and Professor Anne Roivainen. Antti, your enthusiasm, endless knowledge, ambition, and encouragement have guided me through this journey. I owe you a lot. The independence you gave me to carry out these projects, yet being always available as a backup, allowed me to grow and mature as researcher. Your keen interest in teaching me the clinical aspects, especially those that fall outside of my work, has been a true motivator. Moreover, you introduced me to the academic life and provided guidance for future post-doc life. Anne, your discretion, determination, trust, and elegance have kept me on the right track. Your expertise in preclinical imaging and your creative mindset have been of great value for my projects. I admire your attitude to see the positive side in every obstacle. I wish to extend my special thanks to Professor Juhani Knuuti for mentoring me during these years. Your passion for science is exceptional. The positive way you challenged and encouraged me in our group meetings has been crucial for me, especially in terms of conference presentations. Altogether, great coaches will make their player see what she can achieve.

The Cardiac team is warmly thanked for peer support and fruitful brainstorming. A heartfelt thank you to, my dearest friend, Iida Stenström for sharing all ups and downs in research and in life, you rock! Special thanks to "my boys", Teemu Maaniitty, Luis Eduardo Juarez-Orozco, and Valtteri Uusitalo (+Antti & Juhani), for scientific discussions, friendship, and terrific conference company.

I wish to thank my dear research fellows and friends within CoE and PET Centre: Simona, Minna, Sanna, Eleni, Miikka, Prince, Milena, Mueez, and Kerttu. The peer support, afterwork dinners & Italian wine have been essential for this thesis. Simona Malaspina, Minna Lahesmaa, Sanna Laurila, and Eleni Rebelos, I am fortunate to be surrounded by inspiring ladies like you. Your optimism, rationality, and energy have helped me through many challenges.

I wish to thank my amazing friends in my life. The "Terbio girls", Sofia, Norma, Riikka, and Mari deserve special thanks for sharing this journey from the first university lectures until today. You made everything a bit easier and lighter. I want to thank Heidi and Hanna, originally from the Department of Physiology, for long-lasting friendship. Heini and Aino, thank you for being friends of a lifetime. You have truly broadened my perspective in life and pushed me to reach this goal. An energetic thank you belongs to the running club Vauhtisammakko, especially to friends and coaches in the ultrarunning group. You kept my cholesterols low, mind clear, and made me always smile – "Ylämäki on ystävä".

I owe my deepest gratitude to my family for bringing happiness and balance to my life. Your smile and joy, especially during our hilarious family dinners and sailing trips have put all the worries aside. I wish to express my heartfelt thanks to my parents Taina and Ralf & Sirpa for your endless support and love throughout my studies and life. I am grateful to my bright twin brothers Matias and Otto & his partner Susanna, you mean a lot to me. The same sense of humor, lively ideas, and ambition we share have kept our parents busy. I also wish to acknowledge my stepbrothers Marcus and Alex & his partner Elvira. You all have always believed in me – Sydämellinen kiitos.

Turku, November 2020

Mia Ståhle

References

Adamo, L., Rocha-Resende, C., Prabhu, S. D., & Mann, D. L. (2020). Reappraising the role of inflammation in heart failure. *Nature Reviews Cardiology*, *17*, 269–285.

Adingupu, D. D., Göpel, S. O., Grönros, J., Behrendt, M., Sotak, M., Miliotis, T., Dahlqvist, U., Gan, L. M., & Jönsson-Rylander, A. C. (2019). SGLT2 inhibition with empagliflozin improves coronary microvascular function and cardiac contractility in prediabetic ob/ob$^{-/-}$ mice. *Cardiovascular Diabetology*, *18*(1), 1–15.

Allahverdian, S., Chehroudi, A. C., Mcmanus, B. M., Abraham, T., & Francis, G. A. (2014). Contribution of Intimal Smooth Muscle Cells to Cholesterol Accumulation and Macrophage-Like Cells in Human Atherosclerosis. *Circulation*, *129*, 1551–1559.

Andersen, A., Lund, A., Knop, F. K., & Vilsbøll, T. (2018). Glucagon-like peptide 1 in health and disease. *Nature Reviews Endocrinology*, *14*(7), 390–403.

Anitschkow, N., & Chalatow, S. (1983). On experimental cholesterin steatosis and its significance in the origin of some pathological processes. *Arteriosclerosis*, *3*(2), 178–182.

Antwi, K., Fani, M., Nicolas, G., Rottenburger, C., Heye, T., Reubi, J. C., Gloor, B., Christ, E., & Wild, D. (2015). Localization of Hidden Insulinomas with ^{68}Ga-DOTA-Exendin-4 PET/CT: A Pilot Study. *Journal of Nuclear Medicine*, *56*(7), 1075–1078.

Arakawa, M., Mita, T., Azuma, K., Ebato, C., Goto, H., Nomiyama, T., Fujitani, Y., Hirose, T., Kawamori, R., & Watada, H. (2010). Inhibition of monocyte adhesion to endothelial cells and attenuation of atherosclerotic lesion by a glucagon-like peptide-1 receptor agonist, exendin-4. *Diabetes*, *59*(4), 1030–1037.

Aravindhan, K., Bao, W., Harpel, M. R., Willette, R. N., Lepore, J. J., & Jucker, B. M. (2015). Cardioprotection resulting from glucagon-like peptide-1 administration involves shifting metabolic substrate utilization to increase energy efficiency in the rat heart. *PLoS ONE*, *10*(6), 1–18.

Bäck, M., Yurdagul, A., Tabas, I., Öörni, K., & Kovanen, P. T. (2019). Inflammation and its resolution in atherosclerosis: mediators and therapeutic opportunities. *Nature Reviews Cardiology*, *16*, 389–406.

Baggio, L. L., Yusta, B., Mulvihill, E. E., Cao, X., Streutker, C. J., Butany, J., Cappola, T. P., Margulies, K. B., & Drucker, D. J. (2018). GLP-1 receptor expression within the human heart. *Endocrinology*, *159*, 1570–1584.

Bajpai, G., Schneider, C., Wong, N., Bredemeyer, A., Hulsmans, M., Nahrendorf, M., Epelman, S., Kreisel, D., Liu, Y., Itoh, A., Shankar, T. S., Selzman, C. H., Drakos, S. G., & Lavine, K. J. (2018). The human heart contains distinct macrophage subsets with divergent origins and functions. *Nature Medicine*, *24*, 1234–45.

Balestrieri, M. L., Rizzo, M. R., Barbieri, M., Paolisso, P., D'Onofrio, N., Giovane, A., Siniscalchi, M., Minicucci, F., Sardu, C., D'Andrea, D., Mauro, C., Ferraraccio, F., Servillo, L., Chirico, F., Caiazzo, P., Paolisso, G., & Marfella, R. (2015). Sirtuin 6 expression and inflammatory activity in diabetic atherosclerotic plaques: Effects of incretin treatment. *Diabetes*, *64*(4), 1395–1406.

Ban, K., Kim, K. H., Cho, C. K., Sauve, M., Diamandis, E. P., Backx, P. H., Drucker, D. J., & Husain, M. (2010). Glucagon-Like Peptide (GLP)-1(9-36)amide-mediated cytoprotection is blocked by exendin(9-39) yet does not require the known GLP-1 receptor. *Endocrinology*, *151*(4), 1520–1531.

Ban, K., Noyan-Ashraf, M. H., Hoefer, J., Bolz, S.-S., Drucker, D. J., & Husain, M. (2008). Cardioprotective and vasodilatory actions of glucagon-like peptide 1 receptor are mediated through both glucagon-like peptide 1 receptor-dependent and -independent pathways. *Circulation*, *117*(18), 2340–2350.

Bax, J. J., Di Carli, M., Narula, J., & Delgado, V. (2019). Multimodality imaging in ischaemic heart failure. *The Lancet*, *393*(10175), 1056–1070.

Beanlands, R. S. B., Nichol, G., Huszti, E., Humen, D., Racine, N., Freeman, M., Gulenchyn, K. Y., Garrard, L., deKemp, R., Guo, A., Ruddy, T. D., Benard, F., Lamy, A., & Iwanochko, R. M. (2007). F-18-Fluorodeoxyglucose Positron Emission Tomography Imaging-Assisted Management of Patients With Severe Left Ventricular Dysfunction and Suspected Coronary Disease. A Randomized, Controlled Trial (PARR-2). *Journal of the American College of Cardiology*, *50*(20), 2002–2012.

Beer, A. J., Pelisek, J., Heider, P., Saraste, A., Reeps, C., Metz, S., Seidl, S., Kessler, H., Wester, H. J., Eckstein, H. H., & Schwaiger, M. (2014). PET/CT imaging of integrin αvβ3 expression in human carotid atherosclerosis. *JACC: Cardiovascular Imaging*, *7*(2), 178–187.

Bergmark, C., Dewan, A., Orsoni, A., Merki, E., Miller, E. R., Shin, M. J., Binder, C. J., Hörkkö, S., Krauss, R. M., Chapman, M. J., Witztum, J. L., & Tsimikas, S. (2008). A novel function of lipoprotein [a] as a preferential carrier of oxidized phospholipids in human plasma. *Journal of Lipid Research*, *49*(10), 2230–2239.

Bigalke, B., Phinikaridou, A., Andia, M. E., Cooper, M. S., Schuster, A., Wurster, T., Onthank, D., Münch, G., Blower, P., Gawaz, M., Nagel, E., & Botnar, R. M. (2014). PET/CT and MR imaging biomarker of lipid-rich plaques using [^{64}Cu]-labeled scavenger receptor (CD68-Fc). *International Journal of Cardiology*, *177*(1), 287–291.

Binder, C. J., Hörkkö, S., Dewan, A., Chang, M.-K., Kieu, E. P., Goodyear, C. S., Shaw, P. X., Palinski, W., Witztum, J. L., & Silverman, G. J. (2003). Pneumococcal vaccination decreases atherosclerotic lesion formation: molecular mimicry between Streptococcus pneumoniae and oxidized LDL. *Nature Medicine*, *9*(6), 736–743.

Binder, C. J., Papac-Milicevic, N., & Witztum, J. L. (2016). Innate sensing of oxidation-specific epitopes in health and disease. *Nature Reviews Immunology*, *16*(8), 485–497.

Boren, J., Chapman, M. J., Krauss, R. M., Packard, C. J., Bentzon, J. F., Binder, C. J., Daemen, M. J., Demer, L. L., Hegele, R. A., Nicholls, S. J., Nordestgaard, B. G., Watts, G. F., Bruckert, E., Fazio, S., Ference, B. A., Graham, I., Horton, J. D., & Landmesser, U. (2020). Low-density lipoproteins cause atherosclerotic cardiovascular disease: pathophysiological, genetic, and therapeutic insights: a consensus statement from the European Atherosclerosis Society Consensus panel. *European Heart Journal*, *41*(24), 2313–2330

Bose, A. K., Mocanu, M. M., Carr, R. D., Brand, C. L., Yellon, D. M., & Glp-, G. (2005). Glucagon-like Peptide 1 Can Directly protect the Heart Against Ischemia/Reperfusion Injury. *Diabetes*, *54*, 146–151.

Bose, A. K., Mocanu, M. M., Carr, R. D., & Yellon, D. M. (2007). Myocardial ischaemia-reperfusion injury is attenuated by intact glucagon like peptide-1 (GLP-1) in the in vitro rat heart and may involve the p70s6K pathway. *Cardiovascular Drugs and Therapy*, *21*(4), 253–256.

Boullier, A., Gillotte, K. L., Hörkkö, S., Green, S. R., Friedman, P., Dennis, E. a., Witztum, J. L., Steinberg, D., & Quehenberger, O. (2000). The binding of oxidized low density lipoprotein to mouse CD36 is mediated in part by oxidized phospholipids that are associated with both the lipid and protein moieties of the lipoprotein. *Journal of Biological Chemistry*, *275*(13), 9163–9169.

Braunwald, E. (1971). Control of myocardial oxygen consumption. Physiologic and clinical considerations. *The American Journal of Cardiology*, *27*(4), 416–432.

Braunwald, E. (2013). Heart Failure. *JACC: Heart Failure*, *1*(1), 1–20.

Briles, D., Forman, C., & Hudak, S. (1982). Anti-phosphorylcholine antibodies of the T15 idiotype are optimally protective against *Streptococcus Pneumoniae*. *J Exp Med, 156*, 1177–1185.

Bruen, R., Curley, S., Kajani, S., Crean, D., O'Reilly, M. E., Lucitt, M. B., Godson, C. G., McGillicuddy, F. C., & Belton, O. (2017). Liraglutide dictates macrophage phenotype in apolipoprotein E null mice during early atherosclerosis. *Cardiovascular Diabetology*, *16*(1), 1–13.

Bruen, R., Curley, S., Kajani, S., Lynch, G., O'Reilly, M. E., Dillon, E. T., Brennan, E. P., Barry, M., Sheehan, S., McGillicuddy, F. C., & Belton, O. (2019). Liraglutide attenuates preestablished atherosclerosis in apolipoprotein E-deficient mice via regulation of immune cell phenotypes and proinflammatory mediators. *Journal of Pharmacology and Experimental Therapeutics*, *370*(3), 447–458.

Buja, L. M., & Vander Heide, R. S. (2016). Pathobiology of Ischemic Heart Disease: Past, Present and Future. *Cardiovascular Pathology*, *25*(3), 214–220.

Burgmaier, M., Liberman, A., Möllmann, J., Kahles, F., Reith, S., Lebherz, C., Marx, N., & Lehrke, M. (2013). Glucagon-like peptide-1 (GLP-1) and its split products GLP-1(9-37) and GLP-1(28-37) stabilize atherosclerotic lesions in apoe$^{-/-}$ mice. *Atherosclerosis*, *231*(2), 427–435.

Caidahl, K., Hartford, M., Karlsson, T., Herlitz, J., Pettersson, K., De, F. U., & Frostegård, J. (2012). IgM-phosphorylcholine autoantibodies and outcome in acute coronary syndromes. *International Journal of Cardiology*, *167*(2), 464–469.

Caligiuri, G., Khallou-Laschet, J., Vandaele, M., Gaston, A. T., Delignat, S., Mandet, C., Kohler, H. V., Kaveri, S. V., & Nicoletti, A. (2007). Phosphorylcholine-Targeting Immunization Reduces Atherosclerosis. *Journal of the American College of Cardiology*, *50*(6), 540–546.

Camici, P. G., D'Amati, G., & Rimoldi, O. (2015). Coronary microvascular dysfunction: mechanisms and functional assessment. *Nature Reviews. Cardiology*, *12*(1), 48–62.

Centa, M., Gruber, S., Nilsson, D., Polyzos, K. A., Johansson, D. K., Hansson, G. K., … Malin, S. (2019). Atherosclerosis Susceptibility in Mice Is Independent of the V1 Immunoglobulin Heavy Chain Gene. *Arteriosclerosis, Thrombosis, and Vascular Biology*, *36*(1), 25–36.

Cesari, M., Penninx, B. W. J. H., Newman, A. B., Kritchevsky, S. B., Nicklas, B. J., Sutton-Tyrrell, K., Rubin, S. M., Ding, J., Simonsick, E. M., Harris, T. B., & Pahor, M. (2003). Inflammatory Markers and Onset of Cardiovascular Events: Results from the Health ABC Study. *Circulation*, *108*(19), 2317–2322.

Chang, M. I. K., Bergmark, C., Laurila, A., Hörkkö, S., Han, K. H., Friedman, P., Dennis, E. A., & Witztum, J. L. (1999). Monoclonal antibodies against oxidized low-density lipoprotein bind to apoptotic cells and inhibit their phagocytosis by elicited macrophages: Evidence that oxidation-specific epitopes mediate macrophage recognition. *Proceedings of the National Academy of Sciences of the United States of America*, *96*(11), 6353–6358.

Chang, M. K., Binder, C. J., Miller, Y. I., Subbanagounder, G., Silverman, G. J., Berliner, J. A., & Witztum, J. L. (2004). Apoptotic cells with oxidation-specific epitopes are immunogenic and proinflammatory. *Journal of Experimental Medicine*, *200*(11), 1359–1370.

Chang, M. K., Binder, C. J., Torzewski, M., & Witztum, J. L. (2002). C-reactive protein binds to both oxidized LDL and apoptotic cells through recognition of a common ligand: Phosphorylcholine of oxidized phospholipids. *Proceedings of the National Academy of Sciences of the United States of America*, *99*(20), 13043–13048.

Chareonthaitawee, P., Christian, T. F., Hirose, K., Gibbons, R. J., & Rumberger, J. A. (1995). Relation of initial infarct size to extent of left ventricular remodeling in the year after acute myocardial infarction. *Journal of the American College of Cardiology*, *25*(3), 567–573.

Chen, J., Wang, D., Wang, F., Shi, S., Chen, Y., Yang, B., Tang, Y., & Huang, C. (2017). Exendin-4 inhibits structural remodeling and improves Ca2+ homeostasis in rats with heart failure via the GLP-1 receptor through the eNOS/cGMP/PKG pathway. *Peptides*, *90*, 69–77.

Chen, W. R., Chen, Y. D., Tian, F., Yang, N., Cheng, L. Q., Hu, S. Y., Wang, J., Yang, J. J., Wang, S. F., & Gu, X. F. (2016). Effects of liraglutide on reperfusion injury in patients with ST-segment-elevation myocardial infarction. *Circulation: Cardiovascular Imaging*, *9*(12), 1–8.

Chen, W. R., Hu, S. Y., Chen, Y. D., Zhang, Y., Qian, G., Wang, J., Yang, J. J., Wang, Z. F., Tian, F., & Ning, Q. X. (2015). Effects of liraglutide on left ventricular function in patients with ST-segment elevation myocardial infarction undergoing primary percutaneous coronary intervention. *American Heart Journal*, *170*(5), 845–854.

Chen, W., Saxena, A., Li, N., Sun, J., Gupta, A., Lee, D. W., Tian, Q., Dobaczewski, M., & Frangogiannis, N. G. (2012). Endogenous IRAK-M attenuates postinfarction remodeling through effects on macrophages and fibroblasts. *Arteriosclerosis, Thrombosis, and Vascular Biology*, *32*(11), 2598–2608.

Chou, M. Y., Fogelstrand, L., Hartvigsen, K., Hansen, L. F., Woelkers, D., Shaw, P. X., Choi, J., Perkmann, T., Bäckhed, F., Miller, Y. I., Hörkkö, S., Corr, M., Witztum, J. L., & Binder, C. J. (2009). Oxidation-specific epitopes are dominant targets of innate natural antibodies in mice and humans. *Journal of Clinical Investigation*, *119*(5), 1335–1349.

Christ, E., Wild, D., Ederer, S., Béhé, M., Nicolas, G., Caplin, M. E., Brändle, M., Clerici, T., Fischli, S., Stettler, C., Ell, P. J., Seufert, J., Gloor, B., Perren, A., Reubi, J. C., & Forrer, F. (2013). Glucagon-like peptide-1 receptor imaging for the localisation of insulinomas: a prospective multicentre imaging study. *The Lancet. Diabetes & Endocrinology*, *1*(2), 115–122.

Cochain, C., Vafadarnejad, E., Arampatzi, P., Pelisek, J., Winkels, H., Ley, K., Wolf, D., Saliba, A. E., & Zernecke, A. (2018). Single-cell RNA-seq reveals the transcriptional landscape and heterogeneity of aortic macrophages in murine atherosclerosis. *Circulation Research*, *122*(12), 1661–1674.

Cohn, J. N., Levine, T. B., Olivari, M. T., Garberg, V., Lura, D., Francis, G. S., Simon, A. B., & Rector, T. (1984). Plasma Norepinephrine as a Guide to Prognosis in Patients with Chronic Congestive Heart Failure. *New England Journal of Medicine*, *311*, 819–823.

Cowie, M. R., Struthers, A. D., Wood, D. A., Coats, A. J. S., Thompson, S. G., Poole-Wilson, P. A., & Sutton, G. C. (1997). Value of natriuretic peptides in assessment of patients with possible new heart failure in primary care. *Lancet*, *350*(9088), 1349–1353.

Damås, J. K., Eiken, H. G., Øie, E., Bjerkeli, V., Yndestad, A., Ueland, T., Tønnessen, T., Geiran, O. R., Aass, H., Simonsen, S., Christensen, G., Frøland, S. S., Attramadal, H., Gullestad, L., & Aukrust, P. (2000). Myocardial expression of CC- and CXC-chemokines and their receptors in human end-stage heart failure. *Cardiovascular Research*, *47*(4), 778–787.

Danad, I., Raijmakers, P. G., Driessen, R. S., Leipsic, J., Raju, R., Naoum, C., Knuuti, J., Mäki, M., Underwood, R. S., Min, J. K., Elmore, K., Stuijfzand, W. J., Van Royen, N., Tulevski, I. I., Somsen, A. G., Huisman, M. C., Van Lingen, A. A., Heymans, M. W., Van De Ven, P. M., … Knaapen, P. (2017). Comparison of coronary CT angiography, SPECT, PET, and hybrid imaging for diagnosis of ischemic heart disease determined by fractional flow reserve. *JAMA Cardiology*, *2*(10), 1100–1107.

Daugherty, A., Tall, A. R., Daemen, M. J. A. P., Falk, E., Fisher, E. A., García-Cardeña, G., … Virmani, R. (2017). Recommendation on design, execution, and reporting of animal atherosclerosis studies: A scientific statement from the American Heart Association. *Circulation Research*, *121*(6), e53–e79.

Davies, M. J., D'Alessio, D. A., Fradkin, J., Kernan, W. N., Mathieu, C., Mingrone, G., Rossing, P., Tsapas, A., Wexler, D. J., & Buse, J. B. (2019). Management of hyperglycaemia in type 2 diabetes, 2018. A consensus report by the American Diabetes Association (ADA) and the European Association for the Study of Diabetes (EASD). *Diabetologia*, 221–228.

de Lemos, J. A., Morrow, D. A., Blazing, M. A., Jarolim, P., Wiviott, S. D., Sabatine, M. S., Califf, R. M., & Braunwald, E. (2007). Serial Measurement of Monocyte Chemoattractant Protein-1 After Acute Coronary Syndromes. Results From the A to Z Trial. *Journal of the American College of Cardiology*, *50*(22), 2117–2124.

DeNicola, M., Du, J., Wang, Z., Yano, N., Zhang, L., Wang, Y., Qin, G., Zhuang, S., & Zhao, T. C. (2014). Stimulation of glucagon-like peptide-1 receptor through exendin-4 preserves myocardial

performance and prevents cardiac remodeling in infarcted myocardium. *AJP: Endocrinology and Metabolism*, *307*(8), E630–E643.

Derlin, T., Sedding, D. G., Dutzmann, J., Haghikia, A., König, T., Napp, L. C., Schütze, C., Owsianski-Hille, N., Wester, H. J., Kropf, S., Thackeray, J. T., Bankstahl, J. P., Geworski, L., Ross, T. L., Bauersachs, J., & Bengel, F. M. (2018). Imaging of chemokine receptor CXCR4 expression in culprit and nonculprit coronary atherosclerotic plaque using motion-corrected [68Ga]pentixafor PET/CT. *European Journal of Nuclear Medicine and Molecular Imaging*, *45*(11), 1934–1944.

Dewey, M., Siebes, M., Kachelrieß, M., Kofoed, K. F., Maurovich-Horvat, P., Nikolaou, K., Bai, W., Kofler, A., Manka, R., Kozerke, S., Chiribiri, 1Amedeo, Schaeffter, T., Michallek, F., Bengel, F., Nekolla, S., Knaapen, P., Lubberink, M., Senior, R., Tang, M.-X., … Schreiber, L. (2020). Clinical quantitative cardiac imaging for the assessment of myocardial ischaemia. *Nature Reviews Cardiology*. *17*(7), 427–450.

Diebold, S., Moellmann, J., Kahles, F., Haj-Yehia, E., Liehn, E. A., Nickel, A., Lebherz, C., Maack, C., Marx, N., & Lehrke, M. (2018). Myocardial infarction is sufficient to increase GLP-1 secretion, leading to improved left ventricular contractility and mitochondrial respiratory capacity. *Diabetes, Obesity and Metabolism*, *20*(12), 2911–2918.

Dobaczewski, M., Chen, W., & Frangogiannis, N. G. (2011). Transforming growth factor (TGF)-β signaling in cardiac remodeling. *Journal of Molecular and Cellular Cardiology*, *51*(4), 600–606.

Drucker, D. J., Mojsov, S., & Habener, F. (1986). Cell-specific Post-translational Processing of Preproglucagon Expressed from a Metallothionein-glucagon Fusion gene. *The Journal of Biological Chemistry*, *261*(21), 9637–9643.

Drucker, D. J. (2015). Deciphering Metabolic Messages From the Gut Drives Therapeutic Innovation : The 2014 Banting Lecture, *64*, 317–326.

Duewell, P., Kono, H., Rayner, K. J., Sirois, C. M., Vladimer, G., Bauernfeind, F. G., Abela, G. S., Franchi, L., Nũez, G., Schnurr, M., Espevik, T., Lien, E., Fitzgerald, K. A., Rock, K. L., Moore, K. J., Wright, S. D., Hornung, V., & Latz, E. (2010). NLRP3 inflammasomes are required for atherogenesis and activated by cholesterol crystals. *Nature*, *464*(7293), 1357–1361.

Dweck, M. R., Aikawa, E., Newby, D. E., Tarkin, J. M., Rudd, J. H. F., Narula, J., & Fayad, Z. A. (2016). Noninvasive Molecular Imaging of Disease Activity in Atherosclerosis. *Circulation Research*, *119*(2), 330–340.

Dzau, V. J., Colucci, W. S., Hollenberg, N. K., & Williams, G. H. (1981). Relation of the renin-angiotensin-aldosterone system to clinical state in congestive heart failure. *Circulation*, *63*(3), 645–651.

Eng, J., Kleinman, W. A., Singh, L., Singh, G., & Raufman, J. P. (1992). Isolation and characterization of exendin-4, an exendin-3 analogue, from Heloderma suspectum venom: Further evidence for an exendin receptor on dispersed acini from guinea pig pancreas. *Journal of Biological Chemistry*, *267*(11), 7402–7405.

Epelman, S., Lavine, K. J., Beaudin, A. E., Sojka, D. K., Carrero, J. A., Calderon, B., Brija, T., Gautier, E. L., Ivanov, S., Satpathy, A. T., Schilling, J. D., Schwendener, R., Sergin, I., Razani, B., Forsberg, E. C., Yokoyama, W. M., Unanue, E. R., Colonna, M., Randolph, G. J., & Mann, D. L. (2014). Embryonic and adult-derived resident cardiac macrophages are maintained through distinct mechanisms at steady state and during inflammation. *Immunity*, *40*(1), 91–104.

Erdogdu, Ö., Nathanson, D., Sjöholm, Å., Nyström, T., & Zhang, Q. (2010). Exendin-4 stimulates proliferation of human coronary artery endothelial cells through eNOS-, PKA- and PI3K/Akt-dependent pathways and requires GLP-1 receptor. *Molecular and Cellular Endocrinology*, *325*(1–2), 26–35.

Eriksson, O., Velikyan, I., Selvaraju, R. K., Kandeel, F., Johansson, L., Antoni, G., Eriksson, B., Sörensen, J., & Korsgren, O. (2014). Detection of metastatic insulinoma by positron emission tomography with [68Ga]exendin-4-A case report. *Journal of Clinical Endocrinology and Metabolism*, *99*(5), 1519–1524.

Everett, B. M., Cornel, J. H., Lainscak, M., Anker, S. D., Abbate, A., Thuren, T., Libby, P., Glynn, R. J., & Ridker, P. M. (2019). Anti-inflammatory therapy with canakinumab for the prevention of hospitalization for heart failure. *Circulation*, *139*(10), 1289–1299.

Ewing, M., Karper, J., Nordzell, M., Karabina, S., Atout, D., Lettesjö, H., de Vries, M., Dahlbom, I., Camber, O., Frostegård, J., Kuiper, J., Ninio, E., Jukema, W., Pettersson, K., & Quax, P. (2013) Chapter 6: Optimizing natural occurring IgM antibodies for therapeutic use: inflammatory vascular disease treatment with anti-phosphorylcholine IgG. Available at: https://openaccess.leidenuniv.nl/bitstream/handle/1887/21063/06.pdf?sequence¼414. Accessed May 21, 2019.

Faber, R., Zander, M., Pena, A., Michelsen, M. M., Mygind, N. D., & Prescott, E. (2015). Effect of the glucagon-like peptide-1 analogue liraglutide on coronary microvascular function in patients with type 2 diabetes - a randomized, single-blinded, cross-over pilot study. *Cardiovascular Diabetology*, *14*(1), 1–11.

Falk, E., Nakano, M., Bentzon, J. F., Finn, A. V., & Virmani, R. (2013). Update on acute coronary syndromes: the pathologists' view. *European Heart Journal*, *34*(10), 719–728.

Fayad, Z. A., Mani, V., Woodward, M., Kallend, D., Abt, M., Burgess, T., Fuster, V., Ballantyne, C. M., Stein, E. A., Tardif, J.-C., Rudd, J. H. F., Farkouh, M. E., & Tawakol, A. (2011). Safety and efficacy of dalcetrapib on atherosclerotic disease using novel non-invasive multimodality imaging (dal-PLAQUE): a randomised clinical trial. *Lancet*, *378*(9802), 1547–1559.

Félétou, M., & Vanhoutte, P. M. (2006). Endothelial dysfunction: A multifaceted disorder. *American Journal of Physiology - Heart and Circulatory Physiology*, *291*(3), H985–H1002.

Figueroa, A. L., Abdelbaky, A., Truong, Q. A., Corsini, E., MacNabb, M. H., Lavender, Z. R., Lawler, M. A., Grinspoon, S. K., Brady, T. J., Nasir, K., Hoffmann, U., & Tawakol, A. (2013). Measurement of arterial activity on routine FDG PET/CT images improves prediction of risk of future CV events. *JACC: Cardiovascular Imaging*, *6*(12), 1250–1259.

Fiskesund, R., Stegmayr, B., Hallmans, G., Vikström, M., Weinehall, L., De Faire, U., & Frostegård, J. (2010). Low levels of antibodies against phosphorylcholine predict development of stroke in a population-based study from Northern Sweden. *Stroke*, *41*(4), 607–612.

Fiskesund, R., Su, J., Bulatovic, I., Vikström, M., de Faire, U., & Frostegård, J. (2012). IgM phosphorylcholine antibodies inhibit cell death and constitute a strong protection marker for atherosclerosis development, particularly in combination with other auto-antibodies against modified LDL. *Results in Immunology*, *2*, 13–18.

Folco, E. J., Sheikine, Y., Rocha, V. Z., Christen, T., Shvartz, E., Sukhova, G. K., Di Carli, M. F., & Libby, P. (2011). Hypoxia but not inflammation augments glucose uptake in human macrophages: Implications for imaging atherosclerosis with 18fluorine-labeled 2-deoxy-D-glucose positron emission tomography. *Journal of the American College of Cardiology*, *58*(6), 603–614.

Frangogiannis, N. G. (2014). The inflammatory response in myocardial injury, repair, and remodelling. *Nature Reviews. Cardiology*, *11*(5), 255–265.

Fukushima, K., Bravo, P. E., Higuchi, T., Schuleri, K. H., Lin, X., Abraham, M. R., Xia, J., Mathews, W. B., Dannals, R. F., Lardo, A. C., Szabo, Z., & Bengel, F. M. (2012). Molecular hybrid positron emission tomography/computed tomography imaging of cardiac angiotensin ii type 1 receptors. *Journal of the American College of Cardiology*, *60*(24), 2527–2534.

Furchgott, R. F., & Zawadzki, J. V. (1980). The Obligatory Role of Endothelial Cells in the Relaxation of Arterial Smooth Muscle by Acetylcholine. *Nature*, *288*, 373–376.

Gaemperli, O., Shalhoub, J., Owen, D. R. J., Lamare, F., Johansson, S., Fouladi, N., Davies, A. H., Rimoldi, O. E., & Camici, P. G. (2012). Imaging intraplaque inflammation in carotid atherosclerosis with ^{11}C-PK11195 positron emission tomography/computed tomography. *European Heart Journal*, *33*(15), 1902–1910.

Gan, L., Wikström, J., Bergström, G., & Wandt, B. (2004). Non-invasive imaging of coronary arteries in living mice using high-resolution echocardiography. *Scandinavian Cardiovascular Journal*, *38*, 121–126.

Gao, H., Kiesewetter, D. O., Zhang, X., Huang, X., Guo, N., Lang, L., Hida, N., Wang, H., Wang, H., Cao, F., Niu, G., & Chen, X. (2012). PET of glucagonlike peptide receptor upregulation after myocardial ischemia or reperfusion injury. *Journal of Nuclear Medicine : Official Publication, Society of Nuclear Medicine*, *53*(12), 1960–1968.

Garczorz, W., Gallego-Colon, E., Kosowska, A., Kłych-Ratuszny, A., Woźniak, M., Marcol, W., Niesner, K. J., & Francuz, T. (2018). Exenatide exhibits anti-inflammatory properties and modulates endothelial response to tumor necrosis factor α-mediated activation. *Cardiovascular Therapeutics*, *36*(2), 1–8.

Gaspari, T., Liu, H. Bin, Welungoda, I., Hu, Y., Widdop, R. E., Knudsen, L. B., Simpson, R. W., & Dear, A. E. (2011). A GLP-1 receptor agonist liraglutide inhibits endothelial cell dysfunction and vascular adhesion molecule expression in an ApoE$^{-/-}$ mouse model. *Diabetes and Vascular Disease Research*, *8*(2), 117–124.

Gerstein, H. C., Colhoun, H. M., Dagenais, G. R., Diaz, R., Lakshmanan, M., Pais, P., Probstfield, J., Riesmeyer, J. S., Riddle, M. C., Rydén, L., Xavier, D., Atisso, C. M., Dyal, L., Hall, S., Rao-Melacini, P., Wong, G., Avezum, A., Basile, J., Chung, N., … Zigrang, W. (2019). Dulaglutide and cardiovascular outcomes in type 2 diabetes (REWIND): a double-blind, randomised placebo-controlled trial. *The Lancet*, *394*(10193), 121–130.

Gigante, B., Leander, K., Vikström, M., Baldassarre, D., Veglia, F., Strawbridge, R. J., McLeod, O., Gertow, K., Sennblad, B., Shah, S., Zabaneh, D., Humphries, S. E., Kauhanen, J., Rauramaa, R., Smit, A. J., Mannarino, E., Giral, P., Tremoli, E., Hamsten, A., … de Faire, U. (2014). Low levels of IgM antibodies against phosphorylcholine are associated with fast carotid intima media thickness progression and cardiovascular risk in men. *Atherosclerosis*, *236*(2), 394–399.

Gimbrone, M. A., & García-Cardeña, G. (2016). Endothelial Cell Dysfunction and the Pathobiology of Atherosclerosis. *Circulation Research*, *118*(4), 620–636.

Goke, R., Fehmann, H. C., Linn, T., Schmidt, H., Krause, M., Eng, J., & Goke, B. (1993). Exendin-4 is a high potency agonist and truncated exendin-(9-39)-amide an antagonist at the glucagon-like peptide 1-(7-36)-amide receptor of insulin- secreting β-cells. *Journal of Biological Chemistry*, *268*(26), 19650–19655.

Goldstein, J. L., & Brown, M. S. (2015). A century of cholesterol and coronaries: From plaques to genes to statins. *Cell*, *161*(1), 161–172.

Goodwill, A. G., Tune, J. D., Noblet, J. N., Conteh, A. M., Sassoon, D., Casalini, E. D., & Mather, K. J. (2014). Glucagon-like peptide-1 (7–36) but not (9–36) augments cardiac output during myocardial ischemia via a Frank–Starling mechanism. *Basic Research in Cardiology*, *109*(5).

Gould, K. L., Johnson, N. P., Bateman, T. M., Beanlands, R. S., Bengel, F. M., Bober, R., … Narula, J. (2013). Anatomic versus physiologic assessment of coronary artery disease: Role of coronary flow reserve, fractional flow reserve, and positron emission tomography imaging in revascularization decision-making. *Journal of the American College of Cardiology*, *62*(18), 1639–1653.

Graziano, M. P., Hey, P. J., Borkowski, D., Chicci, G. G., & Strader, C. D. (1993). Cloning and functional expression of a human glucagon-like peptide-1 receptor. *Biochemical and Biophysical Research Communications, 196,* 141–146.

Gross, L., Paintmayer, L., Lehner, S., Brandl, L., Brenner, C., Grabmaier, U., … Brunner, S. (2016). FDG-PET reveals improved cardiac regeneration and attenuated adverse remodelling following Sitagliptin + G-CSF therapy after acute myocardial infarction. *European Heart Journal Cardiovascular Imaging*, *17*(2), 136–145.

Grönman, M., Tarkia, M., Kiviniemi, T., Halonen, P., Kuivanen, A., Savunen, T., … Saraste, A. (2017). Imaging of αvβ3integrin expression in experimental myocardial ischemia with [^{68}Ga]NODAGA-RGD positron emission tomography. *Journal of Translational Medicine*, *15*(1), 1–11.

Grönros, J., Wikström, J., Brandt-Eliasson, U., Forsberg, G. B., Behrendt, M., Hansson, G. I., & Gan, L. M. (2008). Effects of rosuvastatin on cardiovascular morphology and function in an ApoE-

knockout mouse model of atherosclerosis. *AJP. Heart and Circulatory Physiology*, *295*(5), H2046–H2053.

Grönros, J., Jung, C., Lundberg, J. O., Cerrato, R., Östenson, C. G., & Pernow, J. (2011). Arginase inhibition restores in vivo coronary microvascular function in type 2 diabetic rats. *American Journal of Physiology - Heart and Circulatory Physiology*, *300*(4), 1174–1181.

Gupta, A., Taqueti, V. R., van de Hoef, T. P., Bajaj, N. S., Bravo, P. E., Murthy, V. L., Osborne, M. T., Seidelmann, S. B., Vita, T., Bibbo, C. F., Harrington, M., Hainer, J., Rimoldi, O., Dorbala, S., Bhatt, D. L., Blankstein, R., Camici, P. G., & Di Carli, M. F. (2017). Integrated Noninvasive Physiological Assessment of Coronary Circulatory Function and Impact on Cardiovascular Mortality in Patients With Stable Coronary Artery Disease. *Circulation*, *136*(24), 2325–2336.

Hahn, C., & Schwartz, M. A. (2008). The role of cellular adaptation to mechanical forces in atherosclerosis. *Arteriosclerosis, Thrombosis, and Vascular Biology*, *28*(12), 2101–2107.

Hamada, M., Nakamura, M., Tran, M. T. N., Moriguchi, T., Hong, C., Ohsumi, T., … Takahashi, S. (2014). MafB promotes atherosclerosis by inhibiting foam-cell apoptosis. *Nature Communications*, *5*, 3147.

Hartupee, J., & Mann, D. L. (2016). Neurohormonal activation in heart failure with reduced ejection fraction. *Nature Reviews Cardiology*, *14*(1), 30–38.

Haukkala, J., Laitinen, I., Luoto, P., Iveson, P., Wilson I., Karlsen, H., … Roivainen, A. (2009). ^{68}Ga-DOTA-RGD peptide: biodistribution and binding into atherosclerotic plaques in mice. *European Journal of Nuclear Medicine and Molecular Imaging*, *36*(12), 2058–2067.

Heinonen, S. E., Leppänen, P., Kholová, I., Lumivuori, H., Häkkinen, S.-K., Bosch, F., … Ylä-Herttuala, S. (2007). Increased atherosclerotic lesion calcification in a novel mouse model combining insulin resistance, hyperglycemia, and hypercholesterolemia. *Circulation Research*, *101*(10), 1058–1067.

Hellberg, S., Liljenbäck, H., Eskola, O., Morisson-Iveson, V., Morrison, M., Trigg, W., … Roivainen, A. (2018). Positron Emission Tomography Imaging of Macrophages in Atherosclerosis with ^{18}F-GE-180, a Radiotracer for Translocator Protein (TSPO). *Contrast Media and Molecular Imaging*, *2018*.

Hellberg, S., Silvola, J. M. U., Kiugel, M., Liljenbäck, H., Metsälä, O., Viljanen, T., … Saraste, A. (2016). Type 2 diabetes enhances arterial uptake of choline in atherosclerotic mice: an imaging study with positron emission tomography tracer ^{18}F-fluoromethylcholine. *Cardiovascular Diabetology*, *15*(1), 26.

Hellberg, S., Silvola, J. M. U., Kiugel, M., Liljenbäck, H., Savisto, N., Li, X. G., … Saraste, A. (2017). 18-kDa translocator protein ligand ^{18}F-FEMPA: Biodistribution and uptake into atherosclerotic plaques in mice. *Journal of Nuclear Cardiology*, *24*(3), 862–871.

Heo, G. S., Kopecky, B., Sultan, D., Ou, M., Feng, G., Bajpai, G., Zhang, X., Luehmann, H., Detering, L., Su, Y., Leuschner, F., Combadière, C., Kreisel, D., Gropler, R. J., Brody, S. L., Liu, Y., & Lavine, K. J. (2019). Molecular Imaging Visualizes Recruitment of Inflammatory Monocytes and Macrophages to the Injured Heart. *Circulation Research*, *124*(6), 881–890.

Hernandez, A. F., Green, J. B., Janmohamed, S., D'Agostino, R. B., Granger, C. B., Jones, N. P., Leiter, L. A., Rosenberg, A. E., Sigmon, K. N., Somerville, M. C., Thorpe, K. M., McMurray, J. J. V., Del Prato, S., Del Prato, S., McMurray, J. J. V., D'Agostino, R. B., Granger, C. B., Hernandez, A. F., Janmohamed, S., … Mandal, T. (2018). Albiglutide and cardiovascular outcomes in patients with type 2 diabetes and cardiovascular disease (Harmony Outcomes): a double-blind, randomised placebo-controlled trial. *The Lancet*, *392*(10157), 1519–1529.

Herzog, B. A., Husmann, L., Valenta, I., Gaemperli, O., Siegrist, P. T., Tay, F. M., Burkhard, N., Wyss, C. A., & Kaufmann, P. A. (2009). Long-Term Prognostic Value of ^{13}N-Ammonia Myocardial Perfusion Positron Emission Tomography. Added Value of Coronary Flow Reserve. *Journal of the American College of Cardiology*, *54*(2), 150–156.

Hess A., Thackeray J., Wollert K., Bengel F. Radionuclide Image-Guded Repair of the Heart. (2019). *JACC: Cardiovascular Imaging,* [Online ahead of print].

Hess, A., Derlin, T., Koenig, T., Diekmann, J., Wittneben, A., Wang, Y., … Thackeray, J. T. (2020). Molecular imaging-guided repair after acute myocardial infarction by targeting the chemokine receptor CXCR4, *European Heart Journal*, [Online ahead of print].

Heuvelman, V., Van Raalte, D., & Smits M. (2020). Cardiovascular effects of GLP-1 receptor agonists: from mechanistic studies in humans to clinical outcomes. *Cardiovascular Research*, *116*, 916–930.

Higuchi, T., Bengel, F. M., Seidl, S., Watzlowik, P., Kessler, H., Hegenloh, R., … Schwaiger, M. (2008). Assessment of αvβ3 integrin expression after myocardial infarction by positron emission tomography. *Cardiovascular Research*, *78*(2), 395–403.

Higuchi, T., Rischpler, C., Fukushima, K., Isoda, T., Xia, J., Javadi, M. S., … Bengel, F. M. (2013). Targeting of endothelin receptors in the healthy and infarcted rat heart using the PET tracer ^{18}F-FBzBMS. *Journal of Nuclear Medicine*, *54*(2), 277–282.

Hilgendorf, I., Gerhardt, L. M. S., Tan, T. C., Winter, C., Holderried, T. A. W., Chousterman, B. G., Iwamoto, Y., Liao, R., Zirlik, A., Scherer-Crosbie, M., Hedrick, C. C., Libby, P., Nahrendorf, M., Weissleder, R., & Swirski, F. K. (2014). Ly-6 chigh monocytes depend on nr4a1 to balance both inflammatory and reparative phases in the infarcted myocardium. *Circulation Research*, *114*(10), 1611–1622.

Hogan, A. E., Gaoatswe, G., Lynch, L., Corrigan, M. A., Woods, C., Connell, J. O., & Shea, D. O. (2014). Glucagon-like peptide 1 analogue therapy directly modulates innate immune-mediated inflammation in individuals with type 2 diabetes mellitus. *Diabetologia*, 781–784.

Horckmans, M., Ring, L., Duchene, J., Santovito, D., Schloss, M. J., Drechsler, M., Weber, C., Soehnlein, O., & Steffens, S. (2016). Neutrophils orchestrate post-myocardial infarction healing by polarizing macrophages towards a reparative phenotype. *European Heart Journal*, *38*(3), 187–197

Hörkkö, S., Bird, D. a., Miller, E., Itabe, H., Leitinger, N., Subbanagounder, G., Berliner, J. a., Friedman, P., Dennis, E. a., Curtiss, L. K., Palinski, W., & Witztum, J. L. (1999). Monoclonal autoantibodies specific for oxidized phospholipids or oxidized phospholipid-protein adducts inhibit macrophage uptake of oxidized low-density lipoproteins. *Journal of Clinical Investigation*, *103*(1), 117–128.

Hulsmans, M., Clauss, S., Xiao, L., Aguirre, A. D., King, K. R., Hanley, A., Hucker, W. J., Wülfers, E. M., Seemann, G., Courties, G., Iwamoto, Y., Sun, Y., Savol, A. J., Sager, H. B., Lavine, K. J., Fishbein, G. A., Capen, D. E., Da Silva, N., Miquerol, L., … Nahrendorf, M. (2017). Macrophages Facilitate Electrical Conduction in the Heart. *Cell*, *169*(3), 510-522.e20.

Hyafil, F., Cornily, J. C., Rudd, J. H. F., Machac, J., Feldman, L. J., & Fayad, Z. A. (2009). Quantification of inflammation within rabbit atherosclerotic plaques using the macrophage-specific CT contrast agent N1177: A comparison with ^{18}F-FDG PET/CT and histology. *Journal of Nuclear Medicine*, *50*(6), 959–965.

Hyafil, F., Pelisek, J., Laitinen, I., Schottelius, M., Mohring, M., Döring, Y., … Markus, S. (2017). Imaging the Cytokine Receptor CXCR4 in atherosclerotic plaques with the radiotracer ^{68}Ga-Pentixafor for PET. *Journal of Nuclear Medicine*, *58*(3), 499–506.

Hyafil, F., & Vigne, J. (2019). Nuclear Imaging Focus on Vascular Probes. *Arteriosclerosis, Thrombosis, and Vascular Biology*, 1–10.

Imai, Y., Kuba, K., Neely, G. G., Yaghubian-Malhami, R., Perkmann, T., van Loo, G., Ermolaeva, M., Veldhuizen, R., Leung, Y. H. C., Wang, H., Liu, H., Sun, Y., Pasparakis, M., Kopf, M., Mech, C., Bavari, S., Peiris, J. S. M., Slutsky, A. S., Akira, S., … Penninger, J. M. (2008). Identification of Oxidative Stress and Toll-like Receptor 4 Signaling as a Key Pathway of Acute Lung Injury. *Cell*, *133*(2), 235–249.

Imhof, A., Koenig, W., Jaensch, A., Mons, U., Brenner, H., & Rothenbacher, D. (2015). Long-term prognostic value of IgM antibodies against phosphorylcholine for adverse cardiovascular events in patients with stable coronary heart disease. *Atherosclerosis*, *243*(2), 414–420.

Irace, C., De Luca, S., Shehaj, E., Carallo, C., Loprete, A., Scavelli, F., & Gnasso, A. (2013). Exenatide improves endothelial function assessed by flow mediated dilation technique in subjects with type 2 diabetes: Results from an observational research. *Diabetes and Vascular Disease Research*, *10*(1), 72–77.

Ishii, H., Nishio, M., Takahashi, H., Aoyama, T., Tanaka, M., Toriyama, T., Tamaki, T., Yoshikawa, D., Hayashi, M., Amano, T., Matsubara, T., & Murohara, T. (2010). Comparison of Atorvastatin 5 and 20 mg/d for Reducing F-18 Fluorodeoxyglucose Uptake in Atherosclerotic Plaques on Positron Emission Tomography/Computed Tomography: A Randomized, Investigator-Blinded, Open-Label, 6-Month Study in Japanese Adults Scheduled. *Clinical Therapeutics*, *32*(14), 2337–2347.

Ismahil, M. A., Hamid, T., Bansal, S. S., Patel, B., Kingery, J. R., & Prabhu, S. D. (2014). Remodeling of the mononuclear phagocyte network underlies chronic inflammation and disease progression in heart failure critical importance of the cardiosplenic axis. *Circulation Research*, *114*(2), 266–282.

Jenkins, W. S. A., Vesey, A. T., Stirrat, C., Connell, M., Lucatelli, C., Neale, A., Moles, C., Vickers, A., Fletcher, A., Pawade, T., Wilson, I., Rudd, J. H. F., van Beek, E. J. R., Mirsadraee, S., Dweck, M. R., & Newby, D. E. (2017). Cardiac αvβ3 integrin expression following acute myocardial infarction in humans. *Heart*, *103*(8), 607–615.

Jenkins, W. S., Vesey, A. T., Vickers, A., Neale, A., Moles, C., Connell, M., Joshi, N. V., Lucatelli, C., Fletcher, A. M., Spratt, J. C., Mirsadraee, S., Van Beek, E. J. R., Rudd, J. H. F., Newby, D. E., & Dweck, M. R. (2019). In vivo alpha-V beta-3 integrin expression in human aortic atherosclerosis. *Heart*, 1868–1875.

Jensen, R. V., Hjortbak, M. V., & Bøtker, H. E. (2020). Ischemic Heart Disease: An Update. *Seminars in Nuclear Medicine*, *50*(3), 195–207.

Jodal, A., Lankat-Buttgereit, B., Brom, M., Schibli, R., & Béhé, M. (2014). A comparison of three (67/68)Ga-labelled exendin-4 derivatives for β-cell imaging on the GLP-1 receptor: the influence of the conjugation site of NODAGA as chelator. *EJNMMI Research*, *4*(1), 31.

Jojima, T., Uchida, K., Akimoto, K., Tomotsune, T., Yanagi, K., Iijima, T., Suzuki, K., Kasai, K., & Aso, Y. (2017). Liraglutide, a GLP-1 receptor agonist, inhibits vascular smooth muscle cell proliferation by enhancing AMP-activated protein kinase and cell cycle regulation, and delays atherosclerosis in ApoE deficient mice. *Atherosclerosis*, *261*, 44–51.

Jorsal, A., Kistorp, C., Holmager, P., Tougaard, R. S., Nielsen, R., Hänselmann, A., Nilsson, B., Møller, J. E., Hjort, J., Rasmussen, J., Boesgaard, T. W., Schou, M., Videbæk, L., Gustafsson, I., Flyvbjerg, A., Wiggers, H., & Tarnow, L. (2017). Effect of liraglutide, a glucagon-like peptide-1 analogue, on left ventricular function in stable chronic heart failure patients with and without diabetes (LIVE)—a multicentre, double-blind, randomised, placebo-controlled trial. *European Journal of Heart Failure*, *19*(1), 69–77.

Joshi, N. V., Vesey, A. T., Williams, M. C., Shah, A. S. V., Calvert, P. A., Craighead, F. H. M., Yeoh, S. E., Wallace, W., Salter, D., Fletcher, A. M., Van Beek, E. J. R., Flapan, A. D., Uren, N. G., Behan, M. W. H., Cruden, N. L. M., Mills, N. L., Fox, K. A. A., Rudd, J. H. F., Dweck, M. R., & Newby, D. E. (2014). ^{18}F-fluoride positron emission tomography for identification of ruptured and high-risk coronary atherosclerotic plaques: A prospective clinical trial. *The Lancet*, *383*(9918), 705–713.

Kahles, F., Meyer, C., Möllmann, J., Diebold, S., Findeisen, H. M., Lebherz, C., Trautwein, C., Koch, A., Tacke, F., Marx, N., & Lehrke, M. (2014). GLP-1 Secretion Is Increased by Inflammatory Stimuli in an IL-6-Dependent Manner, Leading to Hyperinsulinemia and Blood Glucose Lowering. *Diabetes*, *63*(10), 3221–3229.

Kahles, F., Rückbeil, M. V, Mertens, R. W., Foldenauer, A. C., Arrivas, M. C., Moellmann, J., Lebherz, C., Biener, M., Giannitsis, E., Katus, H. A., Marx, N., & Lehrke, M. (2019). Glucagon-like peptide 1 levels predict cardiovascular risk in patients with acute myocardial infarction. *European Heart Journal*, *41*(7), 882–889.

Katz, A. M., & Rolett, E. L. (2015). Heart failure: when form fails to follow function. *European Heart Journal*, *37*, 449–454.

Kiesewetter, D. O., Gao, H., Ma, Y., Niu, G., Quan, Q., Guo, N., & Chen, X. (2012). 18F-radiolabeled analogs of exendin-4 for PET imaging of GLP-1 in insulinoma. *European Journal of Nuclear Medicine and Molecular Imaging*, *39*(3), 463–473.

Kim, E. J., Kim, S., Seo, H. S., Lee, Y. J., Eo, J. S., Jeong, J. M., Lee, B., Kim, J. Y., Park, Y. M., & Jeong, M. (2016). Novel PET imaging of atherosclerosis with ^{68}Ga-Labeled NOTA-Neomannosylated human serum albumin. *Journal of Nuclear Medicine*, *57*(11), 1792–1797.

Kim, M., Platt, M. J., Shibasaki, T., Quaggin, S. E., Backx, P. H., Seino, S., Simpson, J. A., & Drucker, D. J. (2013). GLP-1 receptor activation and Epac2 link atrial natriuretic peptide secretion to control of blood pressure. *Nature Medicine*, *19*(5), 567–575.

Kiugel, Max, Dijkgraaf, I., Kytö, V., Helin, S., Liljenbäck, H., Saanijoki, T., … Saraste, A. (2014). Dimeric [(68)Ga]DOTA-RGD Peptide Targeting αvβ3 Integrin Reveals Extracellular Matrix Alterations after Myocardial Infarction. *Molecular Imaging and Biology, 16*(6), 793–801.

Kiugel, M., Kytö, V., Saanijoki, T., Liljenbäck, H., Metsälä, O., Ståhle, M., … Saraste, A. (2016). Evaluation of ^{68}Ga-labeled peptide tracer for detection of gelatinase expression after myocardial infarction in rat. *Journal of Nuclear Cardiology, 25*(4):1114–1123.

Kiugel, M., Hellberg, S., Käkelä, M., Liljenbäck, H., Saanijoki, T., Li, X. G., Tuomela, J., Knuuti, J., Saraste, A., & Roivainen, A. (2018). Evaluation of [^{68}Ga]Ga-DOTA-TCTP-1 for the detection of metalloproteinase 2/9 expression in mouse atherosclerotic plaques. *Molecules*, *23*(12), 1–11.

Klein, R., Celiker-Guler, E., Rotstein, B. H., & deKemp, R. A. (2020). PET and SPECT Tracers for Myocardial Perfusion Imaging. *Seminars in Nuclear Medicine*, *50*(3), 208–218.

Knaapen, P., Germans, T., Knuuti, J., Paulus, W. J., Dijkmans, P. A., Allaart, C. P., Lammertsma, A. A., & Visser, F. C. (2007). Myocardial energetics and efficiency: Current status of the noninvasive approach. *Circulation*, *115*(7), 918–927.

Knudsen, L. B., & Lau, J. (2019). The Discovery and Development of Liraglutide and Semaglutide. *Frontiers in Endocrinology*, *10*.

Knuuti, J., Wijns, W., Achenbach, S., Agewall, S., Barbato, E., Bax, J. J., Capodanno, D., Cuisset, T., Deaton, C., Dickstein, K., Edvardsen, T., Escaned, J., Funck-Brentano, C., Gersh, B. J., Gilard, M., Hasdai, D., Hatala, R., Mahfoud, F., Masip, J., … Clapp, B. (2020). 2019 ESC guidelines for the diagnosis and management of chronic coronary syndromes. *European Heart Journal*, *41*(3), 407–477.

Krishnamurthy, P., Rajasingh, J., Lambers, E., Qin, G., Losordo, D. W., & Kishore, R. (2009). IL-10 inhibits inflammation and attenuates left ventricular remodeling after myocardial infarction via activation of STAT3 and suppression of HuR. *Circulation Research*, *104*(2), 9–18.

Kristensen, J., Mortensen, U. M., Schmidt, M., Nielsen, P. H., Nielsen, T. T., & Maeng, M. (2009). Lack of cardioprotection from subcutaneously and preischemic administered Liraglutide in a closed chest porcine ischemia reperfusion model. *BMC Cardiovascular Disorders*, *9*, 1–8.

Kugiyama, K., Kerns, S. A., Morrisett, J. D., Roberts, R., & Henry, P. D. (1990). Impairment of endothelium-dependent arterial relaxation by lysolecithin in modified low-density lipoproteins. *Nature*, *344*(6262), 160-2.

Kyhl, K., Lønborg, J., Hartmann, B., Kissow, H., Poulsen, S. S., Ali, H. El, Kjær, A., Dela, F., Engstrøm, T., & Treiman, M. (2017). Lack of effect of prolonged treatment with liraglutide on cardiac remodeling in rats after acute myocardial infarction. *Peptides*, *93*(March), 1–12.

Laitinen, I. E. K., Luoto, P., Någren, K., Marjamäki, P. M., Silvola, J. M. U., Hellberg, S., … Roivainen, A. (2010). Uptake of ^{11}C-choline in mouse atherosclerotic plaques. *Journal of Nuclear Medicine*, *51*(5), 798–802.

Laitinen, I., Notni, J., Pohle, K., Rudelius, M., Farrell, E., Nekolla, S. G., … Schwaiger, M. (2013). Comparison of cyclic RGD peptides for αvβ3 integrin detection in a rat model of myocardial infarction. *EJNMMI Research*, *3*(1), 1–9.

Laitinen, I., Saraste, A., Weidl, E., Poethko, T., Weber, A. W., Nekolla, S. G., … Schwaiger, M. (2009). Evaluation of alphavbeta3 integrin-targeted positron emission tomography tracer ^{18}F-galacto-RGD for imaging of vascular inflammation in atherosclerotic mice. *Circulation. Cardiovascular Imaging*, *2*(4), 331–338.

Lapa, C., Reiter, T., Werner, R. A., Ertl, G., Wester, H. J., Buck, A. K., Bauer, W. R., & Herrmann, K. (2015a). [^{68}Ga]Pentixafor-PET/CT for Imaging of Chemokine Receptor 4 Expression after Myocardial Infarction. *JACC: Cardiovascular Imaging*, *8*(12), 1466–1468.

Lapa, C., Reiter, T., Li, X., Werner, R. A., Samnick, S., Jahns, R., Buck, A. K., Ertl, G., & Bauer, W. R. (2015b). Imaging of myocardial inflammation with somatostatin receptor based PET/CT - A comparison to cardiac MRI. *International Journal of Cardiology*, *194*, 44–49.

Lavine, K. J., Epelman, S., Uchida, K., Weber, K. J., Nichols, C. G., Schilling, J. D., Ornitz, D. M., Randolph, G. J., & Mann, D. L. (2014). Distinct macrophage lineages contribute to disparate patterns of cardiac recovery and remodeling in the neonatal and adult heart. *Proceedings of the National Academy of Sciences of the United States of America*, *111*(45), 16029–16034.

Lawler, P. R., Bhatt, D. L., Godoy, L. C., Lüscher, T. F., Bonow, R. O., Verma, S., & Ridker, P. M. (2020). Targeting cardiovascular inflammation: next steps in clinical translation. *European Heart Journal*, *1*, 1–24.

Lee, S. J., Hoa, C., Quach, T., Jung, K., Paik, J., Lee, J. H., Park, J. W., & Lee, K. (2016). Oxidized Low-Density Lipoprotein Stimulates Macrophage ^{18}F-FDG Uptake via Hypoxia-Inducible Factor-1 a Activation Through Nox2-Dependent Reactive Oxygen Species Generation. *Journal of Nuclear Medicine*, 1699–1706.

Lee, W. W., Marinelli, B., Van Der Laan, A. M., Sena, B. F., Gorbatov, R., Leuschner, F., Dutta, P., Iwamoto, Y., Ueno, T., Begieneman, M. P. V., Niessen, H. W. M., Piek, J. J., Vinegoni, C., Pittet, M. J., Swirski, F. K., Tawakol, A., Di Carli, M., Weissleder, R., & Nahrendorf, M. (2012). PET/MRI of inflammation in myocardial infarction. *Journal of the American College of Cardiology*, *59*(2), 153–163.

Lehrer-Graiwer, J., Parmanand, S., Amr, A., Esad, V., Magnus, K., Amos, B., Jill, F., Van Bruggen, N., Tang, M. T., Frendeus, B., Rudd, J. H. F., Hsieh, F., Ballantyne, C. M., Ghoshhajra, B., Rosenson, R. S., Koren, M., Roth, E. M., Duprez, D. A., Fayad, Z. A., & Tawakol, A. A. (2015). FDG-PET imaging for oxidized LDL in stable atherosclerotic disease: A phase II study of safety, tolerability, and anti-inflammatory activity. *JACC: Cardiovascular Imaging*, *8*(4), 493–494.

Leitinger, N., Tyner, T. R., Oslund, L., Rizza, C., Subbanagounder, G., Lee, H., Shih, P. T., Mackman, N., Tigyi, G., Territo, M. C., Berliner, J. A., & Vora, D. K. (1999). Structurally similar oxidized phospholipids differentially regulate endothelial binding of monocytes and neutrophils. *Proceedings of the National Academy of Sciences of the United States of America*, *96*(21), 12010–12015.

Lepore, J. J., Olson, E., Demopoulos, L., Haws, T., Fang, Z., Barbour, A. M., Fossler, M., Davila-Roman, V. G., Russell, S. D., & Gropler, R. J. (2016). Effects of the Novel Long-Acting GLP-1 Agonist, Albiglutide, on Cardiac Function, Cardiac Metabolism, and Exercise Capacity in Patients With Chronic Heart Failure and Reduced Ejection Fraction. *JACC: Heart Failure*, *4*(7), 559–566.

Levy, B. I., Heusch, G., & Camici, P. G. (2019). The many faces of myocardial ischemia and angina. *Cardiovascular Research*, 1460–1470.

Lewis, M. J., Malik, T. H., Ehrenstein, M. R., Boyle, J. J., Botto, M., & Haskard, D. O. (2009). Immunoglobulin M is required for protection against atherosclerosis in low-density lipoprotein receptor-deficient mice. *Circulation*, *120*(5), 417–426.

Li, X., Bauer, W., Israel, I., Kreissl, M. C., Weirather, J., Richter, D., … Samnick, S. (2014). Targeting p-selectin by gallium-68-labeled fucoidan positron emission tomography for noninvasive characterization of vulnerable plaques: Correlation with in vivo 17.6t mri. *Arteriosclerosis, Thrombosis, and Vascular Biology*, *34*(8), 1661–1667.

Li, X., Bauer, W., Kreissl, M. C., Weirather, J., Bauer, E., Israel, I., … Samnick, S. (2013). Specific somatostatin receptor II expression in arterial plaque: ^{68}Ga-DOTATATE autoradiographic,

immunohistochemical and flow cytometric studies in apoE-deficient mice. *Atherosclerosis*, *230*(1), 33–39.

Li, X., Heber, D., Leike, T., Beitzke, D., Lu, X., Zhang, X., Wei, Y., Mitterhauser, M., Wadsak, W., Kropf, S., Wester, H. J., Loewe, C., Hacker, M., & Haug, A. R. (2018). [^{68}Ga]Pentixafor-PET/MRI for the detection of Chemokine receptor 4 expression in atherosclerotic plaques. *European Journal of Nuclear Medicine and Molecular Imaging*, *45*(4), 558–566.

Libby, P. (2002). Inflammation in atherosclerosis. *Nature*, *420*, 868–874.

Libby, P., & Hansson, G. K. (2019). From Focal Lipid Storage to Systemic Inflammation. *Journal of the American College of Cardiology*, *74*(12), 1594–1607.

Liu, J., Kerwin, W. S., Caldwell, J. H., Ferguson, M. S., Hippe, D. S., Alessio, A. M., Martinez-Malo, V., Pimentel, K., Miyaoka, R. S., Kohler, T. R., Hatsukami, T. S., & Yuan, C. (2016). High resolution FDG-microPET of carotid atherosclerosis: plaque components underlying enhanced FDG uptake. *International Journal of Cardiovascular Imaging*, *32*(1), 145–152.

Liu, Q., Anderson, C., Broyde, A., Polizzi, C., Fernandez, R., Baron, A., & Parkes, D. G. (2010). Glucagon-like peptide-1 and the exenatide analogue AC3174 improve cardiac function, cardiac remodeling, and survival in rats with chronic heart failure. *Cardiovascular Diabetology*, *9*, 76.

Lønborg, J., Vejlstrup, N., Kelbæk, H., Bøtker, H. E., Kim, W. Y., Mathiasen, A. B., Jørgensen, E., Helqvist, S., Saunamki, K., Clemmensen, P., Holmvang, L., Thuesen, L., Krusell, L. R., Jensen, J. S., Køber, L., Treiman, M., Holst, J. J., & Engstrøm, T. (2012). Exenatide reduces reperfusion injury in patients with ST-segment elevation myocardial infarction. *European Heart Journal*, *33*(12), 1491–1499.

Ludmer, P. L., Selwyn, A. P., Shook, T. L., Wayne, R. R., Mudge, G. H., Alexander, R. W., & Ganz, P. (1986). Paradoxical Vasoconstriction Induced by Acetylcholine in Atherosclerotic Coronary Arteries. *New England Journal of Medicine*, *315*, 1046–1051.

Luo, Y., Pan, Q., Shao, Y., Yu, M., Wu, W., Xue, H., Kiesewetter, D. O., Zhu, Z., Li, F., Zhao, Y., & Chen, X. (2016). Glucagon-like Peptide-1 Receptor PET/CT with ^{68}Ga-NOTA-exendin-4 for Detecting Localized Insulinoma: a Prospective Cohort Study. *Journal of Nuclear Medicine*, 715–721.

Mach, F., Baigent, C., Catapano, A. L., Koskinas, K. C., Casula, M., Badimon, L., Chapman, M. J., De Backer, G. G., Delgado, V., Ference, B. A., Graham, I. M., Halliday, A., Landmesser, U., Mihaylova, B., Pedersen, T. R., Riccardi, G., Richter, D. J., Sabatine, M. S., Taskinen, M. R., … Patel, R. S. (2020). 2019 ESC/EAS Guidelines for the management of dyslipidaemias: Lipid modification to reduce cardiovascular risk. *European Heart Journal*, *41*(1), 111–188.

Majmudar, M. D., Keliher, E. J., Heidt, T., Leuschner, F., Truelove, J., Sena, B. F., … Nahrendorf, M. (2013). Monocyte-directed RNAi targeting CCR2 improves infarct healing in atherosclerosis-prone mice. *Circulation*, *127*(20), 2038–2046.

Makowski, M. R., Ebersberger, U., Nekolla, S., & Schwaiger, M. (2008). In vivo molecular imaging of angiogenesis, targeting αvβ3 integrin expression, in a patient after acute myocardial infarction. *European Heart Journal*, *29*(18), 2201.

Malek, A. M., & Alper, S. L. (1999). Hemodynamic Shear Stress and Its Role in Atherosclerosis. *Stress: The International Journal on the Biology of Stress*, *282*(21), 2035–2042.

Mankoff, D. A. (2007). A definition of molecular imaging. *Journal of Nuclear Medicine*, *48*(6).

Margulies, K. B., Hernandez, A. F., Redfield, M. M., Givertz, M. M., Oliveira, G. H., Cole, R., Mann, D. L., Whellan, D. J., Kiernan, M. S., Felker, G. M., McNulty, S. E., Anstrom, K. J., Shah, M. R., Braunwald, E., & Cappola, T. P. (2016). Effects of liraglutide on clinical stability among patients with advanced heart failure and reduced ejection fraction: A randomized clinical trial. *JAMA - Journal of the American Medical Association*, *316*(5), 500–508.

Marinescu, M. A., Löffler, A. I., Ouellette, M., Smith, L., Kramer, C. M., & Bourque, J. M. (2015). Coronary microvascular dysfunction, microvascular angina, and treatment strategies. *JACC: Cardiovascular Imaging*, *8*(2), 210–220.

Marso, S. P., Daniels, G. H., Brown-Frandsen, K., Kristensen, P., Mann, J. F. E., Nauck, M. A., Nissen, S. E., Pocock, S., Poulter, N. R., Ravn, L. S., Steinberg, W. M., Stockner, M., Zinman, B., Bergenstal, R. M., & Buse, J. B. (2016a). Liraglutide and Cardiovascular Outcomes in Type 2 Diabetes. *New England Journal of Medicine*, *375*(4), 311–322.

Marso, S. P., Bain, S. C., Consoli, A., Eliaschewitz, F. G., Jódar, E., Leiter, L. A., Lingvay, I., Rosenstock, J., Seufert, J., Warren, M. L., Woo, V., Hansen, O., Holst, A. G., Pettersson, J., & Vilsbøll, T. (2016b). Semaglutide and Cardiovascular Outcomes in Patients with Type 2 Diabetes. *New England Journal of Medicine*, *375*(19), 1834–1844.

Mathew, R. C., Bourque, J. M., Salerno, M., & Kramer, C. M. (2019). Cardiovascular Imaging Techniques to Assess Microvascular Dysfunction. *JACC: Cardiovascular Imaging*, 1–14.

Maurovich-Horvat, P., Ferencik, M., Voros, S., Merkely, B., & Hoffmann, U. (2014). Comprehensive plaque assessment by coronary CT angiography. *Nature Reviews Cardiology*, *11*(7), 390–402.

McKay, R. G., Pfeffer, M. A., Pasternak, R. C., Markis, J. E., Come, P. C., Nakao, S., Alderman, J. D., Ferguson, J. J., Safian, R. D., & Grossman, W. (1986). Left ventricular remodeling after myocardial infarction: A corollary to infarct expansion. *Circulation*, *74*(4), 693–702.

McMurray, J. J. V., Packer, M., Desai, A. S., Gong, J., Lefkowitz, M. P., Rizkala, A. R., Rouleau, J. L., Shi, V. C., Solomon, S. D., Swedberg, K., & Zile, M. R. (2014). Angiotensin-neprilysin inhibition versus enalapril in heart failure. *New England Journal of Medicine*, *371*(11), 993–1004.

Meester, E. J., Krenning, B. J., de Swart, J., Segbers, M., Barrett, H. E., Bernsen, M. R., … de Jong, M. (2019). Perspectives on Small Animal Radionuclide Imaging; Considerations and Advances in Atherosclerosis. *Frontiers in Medicine*, *6*, 1–11.

Meletta, R., Slavik, R., Mu, L., Rancic, Z., Borel, N., Schibli, R., Ametamey, S. M., Krämer, S. D., & Müller Herde, A. (2017). Cannabinoid receptor type 2 (CB2) as one of the candidate genes in human carotid plaque imaging: Evalu1ation of the novel radiotracer [^{11}C]RS-016 targeting CB2 in atherosclerosis. *Nuclear Medicine and Biology*, *47*, 31–43.

Menichetti, L., Kusmic, C., Panetta, D., Arosio, D., Petroni, D., Matteucci, M., … Manzoni, L. (2013). MicroPET/CT imaging of αvβ3 integrin via a novel ^{68}Ga-NOTA-RGD peptidomimetic conjugate in rat myocardial infarction. *European Journal of Nuclear Medicine and Molecular Imaging*, *40*(8), 1265–1274.

MERIT-HF, I. (1999). Effect of metoprolol CR/XL in chronic heart failure: Metoprolol CR/XL randomised intervention trial in congestive heart failure (MERIT-HF). *Lancet*, *353*, 2001–2007.

Mikkola, K., Yim, C.-B., Fagerholm, V., Ishizu, T., Elomaa, V.-V., Rajander, J., Jurttila, J., Saanijoki, T., Tolvanen, T., Tirri, M., Gourni, E., Béhé, M., Gotthardt, M., Reubi, J. C., Mäcke, H., Roivainen, A., Solin, O., & Nuutila, P. (2013). ^{64}Cu- and ^{68}Ga-Labelled [Nle^{14},Lys^{40}(Ahx-NODAGA)NH$_2$]-Exendin-4 for Pancreatic Beta Cell Imaging in Rats. *Molecular Imaging and Biology*, *16*(2), 293–293.

Miller, Y. I., Choi, S. H., Wiesner, P., Fang, L., Harkewicz, R., Hartvigsen, K., Boullier, A., Gonen, A., Diehl, C. J., Que, X., Montano, E., Shaw, P. X., Tsimikas, S., Binder, C. J., & Witztum, J. L. (2011). Oxidation-specific epitopes are danger-associated molecular patterns recognized by pattern recognition receptors of innate immunity. *Circulation Research*, *108*(2), 235–248.

Monazzam, A., Lau, J., Velikyan, I., Li, S. C., Razmara, M., Rosenström, U., Eriksson, O., & Skogseid, B. (2018). Increased Expression of GLP-1R in Proliferating Islets of Men1 Mice is Detectable by [^{68}Ga]Ga-DO3A-VS-Cys40-Exendin-4 /PET. *Scientific Reports*, *8*(1), 1–9.

Moore, K. J., Koplev, S., Fisher, E. A., Tabas, I., Björkegren, J. L. M., Doran, A. C., & Kovacic, J. C. (2018). Macrophage Trafficking, Inflammatory Resolution, and Genomics in Atherosclerosis: JACC Macrophage in CVD Series (Part 2). *Journal of the American College of Cardiology*, *72*(18), 2181–2197.

Morooka, M., Kubota, K., Kadowaki, H., Ito, K., Okazaki, O., Kashida, M., Mitsumoto, T., Iwata, R., Ohtomo, K., & Hiroe, M. (2009). ^{11}C-methionine PET of acute myocardial infarction. *Journal of Nuclear Medicine*, *50*(8), 1283–1287.

Murthy, V. L., Naya, M., Foster, C. R., Hainer, J., Gaber, M., Di Carli, G., Blankstein, R., Dorbala, S., Sitek, A., Pencina, M. J., & Di Carli, M. F. (2011). Improved cardiac risk assessment with noninvasive measures of coronary flow reserve. *Circulation*, *124*(20), 2215–2224.

Nagashima, M., Watanabe, T., Terasaki, M., Tomoyasu, M., Nohtomi, K., Kim-Kaneyama, J., Miyazaki, a, & Hirano, T. (2011). Native incretins prevent the development of atherosclerotic lesions in apolipoprotein E knockout mice. *Diabetologia*, *54*(10), 2649–2659.

Nahrendorf, M., Keliher, E., Panizzi, P., Zhang, H., Hembrador, S., Figueiredo, J. L., Aikawa, E., Kelly, K., Libby, P., & Weissleder, R. (2009). [18]F-4V for PET-CT Imaging of VCAM-1 Expression in Atherosclerosis. *JACC: Cardiovascular Imaging*, *2*(10), 1213–1222.

Nahrendorf, M., & Swirski, F. K. (2013). Monocyte and macrophage heterogeneity in the heart. *Circulation Research*, *112*(12), 1624–1633.

Nahrendorf, M., Swirski, F. K., Aikawa, E., Stangenberg, L., Wurdinger, T., Figueiredo, J. L., Libby, P., Weissleder, R., & Pittet, M. J. (2007). The healing myocardium sequentially mobilizes two monocyte subsets with divergent and complementary functions. *Journal of Experimental Medicine*, *204*(12), 3037–3047.

Nakamura, I., Hasegawa, K., Wada, Y., Hirase, T., Node, K., & Watanabe, Y. (2013). Detection of early stage atherosclerotic plaques using PET and CT fusion imaging targeting P-selectin in low density lipoprotein receptor-deficient mice. *Biochemical and Biophysical Research Communications*, *433*(1), 47–51.

Nalin, L., Selvaraju, R. K., Velikyan, I., Berglund, M., Andréasson, S., Wikstrand, A., Rydén, A., Lubberink, M., Kandeel, F., Nyman, G., Korsgren, O., Eriksson, O., & Jensen-Waern, M. (2014). Positron emission tomography imaging of the glucagon-like peptide-1 receptor in healthy and streptozotocin-induced diabetic pigs. *European Journal of Nuclear Medicine and Molecular Imaging*, *41*(9), 1800–1810.

Nathan, C., & Cunningham-Bussel, A. (2013). Beyond oxidative stress: An immunologist's guide to reactive oxygen species. *Nature Reviews Immunology*, *13*(5), 349–361.

Nauck, M. A., Meier, J. J., Cavender, M. A., Abd El Aziz, M., & Drucker, D. J. (2017). Cardiovascular Actions and Clinical Outcomes With Glucagon-Like Peptide-1 Receptor Agonists and Dipeptidyl Peptidase-4 Inhibitors. *Circulation*, 849–870.

Newby, D. E., Adamson, P. D., Berry, C., Boon, N. A., Dweck, M. R., Flather, M., Forbes, J., Hunter, A., Lewis, S., MacLean, S., Mills, N. L., Norrie, J., Roditi, G., Shah, A. S. V., Timmis, A. D., Van Beek, E. J. R., & Williams, M. C. (2018). Coronary CT angiography and 5-year risk of myocardial infarction. *New England Journal of Medicine*, *379*(10), 924–933.

Nidorf, S. M., Fiolet, A. T. L., Mosterd, A., Eikelboom, J. W., Schut, A., Opstal, T. S. J., … Thompson, P. L. (2020). Colchicine in Patients with Chronic Coronary Disease. *New England Journal of Medicine*, 1–10.

Nielsen, R., Jorsal, A., Iversen, P., Tolbod, L. P., Bouchelouche, K., Sørensen, J., Harms, J., Flyvbjerg, A., Tarnow, L., Kistorp, C., & Gustafsson, I. (2017). Effect of liraglutide on myocardial glucose uptake and blood flow in stable chronic heart failure patients : A double-blind , randomized , placebo-controlled LIVE sub-study. *Journal of Nuclear Cardiology*, *26*(2):585–597.

Nikolaidis, L. A., Mankad, S., Sokos, G. G., Miske, G., Shah, A., Elahi, D., & Shannon, R. P. (2004). Effects of Glucagon-Like Peptide-1 in Patients with Acute Myocardial Infarction and Left Ventricular Dysfunction after Successful Reperfusion. *Circulation*, *109*(8), 962–965.

Nordestgaard, B. G., & Langsted, A. (2016). Lipoprotein (a) as a cause of cardiovascular disease: Insights from epidemiology, genetics, and biology. *Journal of Lipid Research*, *57*(11), 1953–1975.

Noyan-Ashraf, M. H., Abdul Momen, M., Ban, K., Sadi, A. M., Zhou, Y. Q., Riazi, A. M., Baggio, L. L., Henkelman, R. M., Husain, M., & Drucker, D. J. (2009). GLP-1R agonist liraglutide activates cytoprotective pathways and improves outcomes after experimental myocardial infarction in mice. *Diabetes*, *58*(4), 975–983.

Nyström, T., Gutniak, M. K., Zhang, Q., Zhang, F., Holst, J. J., Ahren, B., & Sjöholm, Å. (2004). Effects of glucagon-like peptide-1 on endothelial function in type 2 diabetes patients with stable coronary artery disease. *Am J Physiol Endocrinol Metab 287:*, *287*, E1209–E1215.

Ogawa, M, Nakamura, S., Saito, Y., Kosugi, M., & Magata, Y. (2012). What Can Be Seen by F-18-FDG PET in Atherosclerosis Imaging? The Effect of Foam Cell Formation on F-18-FDG Uptake to Macrophages In Vitro. *Journal of Nuclear Medicine*, *53*(1), 55–58.

Ogawa, Mikako, Ishino, S., Mukai, T., Asano, D., Teramoto, N., Watabe, H., Kudomi, N., Shiomi, M., Magata, Y., Iida, H., & Saji, H. (2004). 18F-FDG accumulation in atherosclerotic plaques: Immunohistochemical and PET imaging study. *Journal of Nuclear Medicine*, *45*(7), 1245–1250.

Paeng, J. C., Lee, Y. S., Lee, J. S., Jeong, J. M., Kim, K. B., Chung, J. K., & Lee, D. S. (2013). Feasibility and kinetic characteristics of ^{68}Ga-NOTA-RGD PET for in vivo atherosclerosis imaging. *Annals of Nuclear Medicine*, *27*(9), 847–854.

Palinski, W. (1996). Cloning of monoclonal autoantibodies to epitopes of oxidized lipoproteins from apolipoprotein E-deficient mice. *J Clin Invest*, *98*, 800–814.

Palmer, R. M., Ferrige, A. G., & Moncada, S. (1987). Nitric Oxide Release Accounts for the Biological Activity of Endothelium-Derived Relaxing Factor. *Nature*, *327*, 524–526.

Panjwani, N., Mulvihill, E. E., Longuet, C., Yusta, B., Campbell, J. E., Brown, T. J., Streutker, C., Holland, D., Cao, X., Baggio, L. L., & Drucker, D. J. (2013). GLP-1 receptor activation indirectly reduces hepatic lipid accumulation but does not attenuate development of atherosclerosis in diabetic male ApoE^{-/-} mice. *Endocrinology*, *154*(1), 127–139.

Pasterkamp, G., Den Ruijter, H. M., & Libby, P. (2016). Temporal shifts in clinical presentation and underlying mechanisms of atherosclerotic disease. *Nature Reviews Cardiology*, *14*(1), 21–29.

Patlak, C. S., Blasberg, R. G., & Fenstermacher, J. D. (1983). Graphical evaluation of blood-to-brain transfer constants from multiple-time uptake data. *Journal of Cerebral Blood Flow and Metabolism*, *3*(1), 1–7.

Paulmier, B., Duet, M., Khayat, R., Pierquet-Ghazzar, N., Laissy, J. P., Maunoury, C., Hugonnet, F., Sauvaget, E., Trinquart, L., & Faraggi, M. (2008). Arterial wall uptake of fluorodeoxyglucose on PET imaging in stable cancer disease patients indicates higher risk for cardiovascular events. *Journal of Nuclear Cardiology*, *15*(2), 209–217.

Pfeffer, M. A., Pfeffer, J. M., Fishbein, M. C., Fletcher, P. J., Spadaro, J., Kloner, R. A., & Braunwald, E. (1979). Myocardial Infarct Size and Ventricular Function in Rats. *Circulation Research*, *44*, 503–512.

Pedersen, S. F., Sandholt, B. V., Keller, S. H., Hansen, A. E., Clemmensen, A. E., Sillesen, H., … Kjær, A. (2015). ^{64}Cu-DOTATATE PET/MRI for detection of activated macrophages in carotid atherosclerotic plaques: Studies in patients undergoing endarterectomy. *Arteriosclerosis, Thrombosis, and Vascular Biology*, *35*(7), 1696–1703.

Pellikka, P. A., Arruda-Olson, A., Chaudhry, F. A., Chen, M. H., Marshall, J. E., Porter, T. R., & Sawada, S. G. (2020). Guidelines for Performance, Interpretation, and Application of Stress Echocardiography in Ischemic Heart Disease: From the American Society of Echocardiography. *Journal of the American Society of Echocardiography*, *33*(1), 1-41.e8.

Penny, W. F., Ben-Yehuda, O., Kuroe, K., Long, J., Bond, A., Bhargava, V., … Peterson, K. L. (2001). Improvement of coronary artery endothelial dysfunction with lipid-lowering therapy: Heterogeneity of segmental response and correlation with plasma-oxidized low density lipoprotein. *Journal of the American College of Cardiology*, *37*(3), 766–774.

Piotrowski, K., Becker, M., Zugwurst, J., Biller-Friedmann, I., Spoettl, G., Greif, M., Leber, A. W., Becker, A., Laubender, R. P., Lebherz, C., Goeke, B., Marx, N., Parhofer, K. G., & Lehrke, M. (2013). Circulating concentrations of GLP-1 are associated with coronary atherosclerosis in humans. *Cardiovascular Diabetology*, *12*, 117.

Ponikowski, P., Voors, A. A., Anker, S. D., Bueno, H., Cleland, J. G. F., Coats, A. J. S., Falk, V., González-Juanatey, J. R., Harjola, V. P., Jankowska, E. A., Jessup, M., Linde, C., Nihoyannopoulos, P., Parissis, J. T., Pieske, B., Riley, J. P., Rosano, G. M. C., Ruilope, L. M.,

Ruschitzka, F., … Davies, C. (2016). 2016 ESC Guidelines for the diagnosis and treatment of acute and chronic heart failure. *European Heart Journal*, *37*(27), 2129-2200.

Poulsen, C. B., Al-Mashhadi, A. L., Von Wachenfeldt, K., Bentzon, J. F., Nielsen, L. B., Al-Mashhadi, R. H., Thygesen, J., Tolbod, L., Larsen, J. R., Frøkiær, J., Tawakol, A., Vucic, E., Fredrickson, J., Baruch, A., Frendéus, B., Robertson, A. K. L., Moestrup, S. K., Drouet, L., & Falk, E. (2016). Treatment with a human recombinant monoclonal IgG antibody against oxidized LDL in atherosclerosis-prone pigs reduces cathepsin S in coronary lesions. *International Journal of Cardiology*, *215*, 506–515.

Powell-Braxton, L.,, Véniant, M., Latvala, R., Hirano, K., Won, W., Ross, J., Dybdal, N., Zlot, C., Young, S., & Davidson, N. (1998) A mouse model of human familial hypercholesterolemia: Markedly elevated low density lipoprotein cholesterol levels and severe atherosclerosis on a low-fat chow diet. *Nature Medicine, 4,* 934–938.

Prabhu, S. D., & Frangogiannis, N. G. (2016). The biological basis for cardiac repair after myocardial infarction. *Circulation Research*, *119*(1), 91–112.

Pyke, C., Heller, R. S., Kirk, R. K., Ørskov, C., Reedtz-Runge, S., Kaastrup, P., Hvelplund, A., Bardram, L., Calatayud, D., & Knudsen, L. B. (2014). GLP-1 receptor localization in monkey and human tissue: novel distribution revealed with extensively validated monoclonal antibody. *Endocrinology*, *155*(4), 1280–1290.

Pyke, C., & Knudsen, L. B. (2013). The Glucagon-Like Peptide-1 Receptor—or Not? *Endocrinology*, *154*(1), 4–8.

Que, X., Hung, M.-Y., Yeang, C., Gonen, A., Prohaska, T. A., Sun, X., Diehl, C., Määttä, A., Gaddis, D. E., Bowden, K., Pattison, J., Macdonald, J. G., Ylä-Herttuala, S., Mellon, P. L., Hedrick, C. C., Ley, K., Miller, Y. I., Glass, C. K., Peterson, K. L., … Witztum, J. L. (2018). Oxidized phospholipids are proinflammatory and proatherogenic in hypercholesterolaemic mice. *Nature*, *558*, 301–6.

Rahman, M., Sing, S., Golabkesh, Z., Fiskesund, R., Gustafsson, T., Jogestrand, T., Frostegård, A. G., Hafström, I., Liu, A., & Frostegård, J. (2016). IgM antibodies against malondialdehyde and phosphorylcholine are together strong protection markers for atherosclerosis in systemic lupus erythematosus: Regulation and underlying mechanisms. *Clinical Immunology*, *166–167*, 27–37.

Raitakari, O. T., Pitkänen, O. P., Lehtimäki, T., Lahdenperä, S., Iida, H., Ylä-Herttuala, S., … Knuuti, J. (1997). In vivo low density lipoprotein oxidation relates to coronary reactivity in young men. *Journal of the American College of Cardiology*, *30*(1), 97–102.

Rakipovski, G., Rolin, B., Nøhr, J., Klewe, I., Frederiksen, K. S., Augustin, R., Hecksher-Sørensen, J., Ingvorsen, C., Polex-Wolf, J., & Knudsen, L. B. (2018). The GLP-1 Analogs Liraglutide and Semaglutide Reduce Atherosclerosis in ApoE$^{-/-}$ and LDLr$^{-/-}$ Mice by a Mechanism That Includes Inflammatory Pathways. *JACC: Basic to Translational Science*, *3*(6), 844–857.

Ravassa, S., Zudaire, A., Carr, R. D., & Díez, J. (2011). Antiapoptotic effects of GLP-1 in murine HL-1 cardiomyocytes. *American Journal of Physiology - Heart and Circulatory Physiology*, *300*(4), 1361–1372.

Reimer, K. A., & Jennings, R. B. (1979). The "Wavefront Phenomenon" of Myocardial Ischemic Cell Death. II. Transmural Progression of Necrosis Within the Framework of Ischemic Bed Size (Myocardium at Risk) and Collateral Flow. *Lab Investig*, *40*(6), 633–644.

Reimer, K. A., Lowe, J. E., Rasmussen, M. M., & Jennings, R. B. (1977). The wavefront phenomenon of ischemic cell death. 1. Myocardial infarct size vs duration of coronary occlusion in dogs. *Circulation*, *56*(5), 786–794.

Reiter, T., Kircher, M., Schirbel, A., Werner, R. A., Kropf, S., Ertl, G., Buck, A. K., Wester, H. J., Bauer, W. R., & Lapa, C. (2018). Imaging of C-X-C Motif Chemokine Receptor CXCR4 Expression After Myocardial Infarction With [^{68}Ga]Pentixafor-PET/CT in Correlation With Cardiac MRI. *JACC: Cardiovascular Imaging*, *11*(10), 1541–1543.

Richards, P., Parker, H. E., Adriaenssens, A. E., Hodgson, J. M., Cork, S. C., Trapp, S., Gribble, F. M., & Reimann, F. (2014). Identification and characterization of GLP-1 receptor-expressing cells using a new transgenic mouse model. *Diabetes*, *63*(4), 1224–1233.

Ridker, P. M., Hennekens, C. H., Buring, J. E., & Rifai, N. (2000). C-reactive protein and other markers of inflammation in the prediction of cardiovascular disease in diabetes. *New England Journal of Medicine*, *324*, 836–843.

Ridker, P. M., Everett, B. M., Thuren, T., MacFadyen, J. G., Chang, W. H., Ballantyne, C., Fonseca, F., Nicolau, J., Koenig, W., Anker, S. D., Kastelein, J. J. P., Cornel, J. H., Pais, P., Pella, D., Genest, J., Cifkova, R., Lorenzatti, A., Forster, T., Kobalava, Z., … Glynn, R. J. (2017). Antiinflammatory Therapy with Canakinumab for Atherosclerotic Disease. *New England Journal of Medicine*, *377*(12), 1119–1131.

Ridker, P. M., & Lüscher, T. F. (2014). Anti-inflammatory therapies for cardiovascular disease. *European Heart Journal*, *35*(27), 1782–1791.

Riehle, C., & Bauersachs, J. (2019). Small animal models of heart failure. *Cardiovascular Research*, *115*(13), 1838–1849.

Rikitake, Y., Hirata, K., Kawashima, S., & Inoue, N. (2000). Inhibition of endothelium-dependent arterial relaxation by oxidized phosphatidylcholine. *Atherosclerosis*, *152*, 79–87.

Rinne, P., Silvola, J. M. U., Hellberg, S., Ståhle, M., Liljenbäck, H., Salomäki, H., … Savontaus, E. (2014). Pharmacological activation of the melanocortin system limits plaque inflammation and ameliorates vascular dysfunction in atherosclerotic mice. *Arteriosclerosis, Thrombosis, and Vascular Biology*, *34*(7), 1346–54.

Rinne, Petteri, Hellberg, S., Kiugel, M., Virta, J., Li, X.-G., Käkelä, M., … Roivainen, A. (2015). Comparison of Somatostatin Receptor 2-Targeting PET Tracers in the Detection of Mouse Atherosclerotic Plaques. *Molecular Imaging and Biology*, *18*(1), 99–108.

Rischpler, C., Dirschinger, R. J., Nekolla, S. G., Kossmann, H., Nicolosi, S., Hanus, F., van Marwick, S., Kunze, K. P., Meinicke, A., Götze, K., Kastrati, A., Langwieser, N., Ibrahim, T., Nahrendorf, M., Schwaiger, M., & Laugwitz, K.-L. (2016). Prospective Evaluation of ^{18}F-Fluorodeoxyglucose Uptake in Postischemic Myocardium by Simultaneous Positron Emission Tomography/Magnetic Resonance Imaging as a Prognostic Marker of Functional Outcome. *Circulation. Cardiovascular Imaging*, *9*(4), e004316.

Rizzo, M., Chandalia, M., Patti, A. M., Di Bartolo, V., Rizvi, A. A., Montalto, G., & Abate, N. (2014). Liraglutide decreases carotid intima-media thickness in patients with type 2 diabetes: 8-month prospective pilot study. *Cardiovascular Diabetology*, *13*(1), 2–6.

Robinson, J. G., Farnier, M., Krempf, M., Bergeron, J., Luc, G., Averna, M., Stroes, E. S., Langslet, G., Raal, F. J., El Shahawy, M., Koren, M. J., Lepor, N. E., Lorenzato, C., Pordy, R., Chaudhari, U., & Kastelein, J. J. P. (2015a). Efficacy and safety of alirocumab in reducing lipids and cardiovascular events. *New England Journal of Medicine*, *372*(16), 1489–1499.

Robinson, E., Cassidy, R. S., Tate, M., Zhao, Y., Lockhart, S., Calderwood, D., Church, R., McGahon, M. K., Brazil, D. P., McDermott, B. J., Green, B. D., & Grieve, D. J. (2015b). Exendin-4 protects against post-myocardial infarction remodelling via specific actions on inflammation and the extracellular matrix. *Basic Research in Cardiology*, *110*(2), 20.

Rodriguez-Porcel, M., Cai, W., Gheysens, O., Willmann, J. K., Chen, K., Wang, H., Chen, I. Y., He, L., Wu, J. C., Li, Z. B., Mohamedali, K. A., Kim, S., Rosenblum, M. G., Chen, X., & Gambhir, S. S. (2008). Imaging of VEGF receptor in a rat myocardial infarction model using PET. *Journal of Nuclear Medicine*, *49*(4), 667–673.

Rominger, A., Saam, T., Wolpers, S., Cyran, C. C., Schmidt, M., Foerster, S., Nikolaou, K., Reiser, M. F., Bartenstein, P., & Hacker, M. (2009). ^{18}F-FDG PET/CT identifies patients at risk for future vascular events in an otherwise asymptomatic cohort with neoplastic disease. *Journal of Nuclear Medicine*, *50*(10), 1611–1620.

Roos, S. T., Timmers, L., Biesbroek, P. S., Nijveldt, R., Kamp, O., van Rossum, A. C., van Hout, G. P. J., Stella, P. R., Doevendans, P. A., Knaapen, P., Velthuis, B. K., van Royen, N., Voskuil, M., Nap,

A., & Appelman, Y. (2016). No benefit of additional treatment with exenatide in patients with an acute myocardial infarction. *International Journal of Cardiology*, *220*, 809–814.

Ross, R. (1993). The pathogenesis of atherosclerosis: a perspective for the 1990s. *Nature*, *362*, 801–809.

Rudd, J. H. F., Warburton, T. D., Fryer, H. A., Jones, J. C., Clark, N., Antoun, P., Johnström, A. P., Davenport, P. J., Kirkpatrick, B. N., Arch, J. D. P., & Weissberg, P. L. (2002). Imaging Atherosclerotic Plaque Inflammation With [^{18}F]-Fluorodeoxyglucose Positron Emission Tomography. *Circulation*, *105*(23), 2708–2711.

Rudd, J. H. F., Myers, K. S., Bansilal, S., Machac, J., Woodward, M., Fuster, V., … Fayad, Z. a. (2009). Relationships among regional arterial inflammation, calcification, risk factors, and biomarkers: A prospective fluorodeoxyglucose positron-emission tomography/computed tomography imaging study. *Circulation: Cardiovascular Imaging*, *2*(2), 107–115.

Sager, H. B., Hulsmans, M., Lavine, K. J., Moreira, M. B., Heidt, T., Courties, G., Sun, Y., Iwamoto, Y., Tricot, B., Khan, O. F., Dahlman, J. E., Borodovsky, A., Fitzgerald, K., Anderson, D. G., Weissleder, R., Libby, P., Swirski, F. K., & Nahrendorf, M. (2016). Proliferation and Recruitment Contribute to Myocardial Macrophage Expansion in Chronic Heart Failure. *Circulation Research*, *119*(7), 853–864.

Saraste, A., Kytö, V., Saraste, M., Vuorinen, T., Hartiala, J., & Saukko, P. (2006). Coronary flow reserve and heart failure in experimental coxsackievirus myocarditis. A transthoracic Doppler echocardiography study. *American Journal of Physiology. Heart and Circulatory Physiology*, *291*(2), H871-5.

Saraste, A., Kytö, V., Laitinen, I., Saraste, M., Leppänen, P., Ylä-Herttuala, S., Saukko, P., Hartiala, J., & Knuuti, J. (2008). Severe coronary artery stenoses and reduced coronary flow velocity reserve in atherosclerotic mouse model. Doppler echocardiography validation study. *Atherosclerosis*, *200*(1), 89–94.

Sassoon, D. J., Tune, J. D., Mather, K. J., Noblet, J. N., Eagleson, M. A., Conteh, A. M., Sturek, J. T., & Goodwill, A. G. (2017). Glucagon-like peptide 1 receptor activation augments cardiac output and improves cardiac efficiency in obese swine after myocardial infarction. *Diabetes*, *66*(8), 2230–2240.

Schiopu, A., Frendéus, B., Jansson, B., Söderberg, I., Ljungcrantz, I., Araya, Z., Shah, P. K., Carlsson, R., Nilsson, J., & Fredrikson, G. N. (2007). Recombinant Antibodies to an Oxidized Low-Density Lipoprotein Epitope Induce Rapid Regression of Atherosclerosis in Apobec-1$^{-/-}$/Low-Density Lipoprotein Receptor$^{-/-}$ Mice. *Journal of the American College of Cardiology*, *50*(24), 2313–2318.

Schnitzler, J. G., Hoogeveen, R. M., Ali, L., Prange, K. H. M., Waissi, F., Van Weeghel, M., Bachmann, J. C., Versloot, M., Borrelli, M. J., Yeang, C., De Kleijn, D. P. V., Houtkooper, R. H., Koschinsky, M. L., De Winther, M. P. J., Groen, A. K., Witztum, J. L., Tsimikas, S., Stroes, E. S. G., & Kroon, J. (2020). Atherogenic Lipoprotein(a) Increases Vascular Glycolysis, Thereby Facilitating Inflammation and Leukocyte Extravasation. *Circulation Research*, 1346–1359.

Schnitzler, J. G., Moens, S. J. B., Tiessens, F., Bakker, G. J., Dallinga-Thie, G. M., Groen, A. K., … Kroon, J. (2017). Nile Red Quantifier: A novel and quantitative tool to study lipid accumulation in patient-derived circulating monocytes using confocal microscopy. *Journal of Lipid Research*, *58*(11), 2210–2219.

Scholz, K. H., Maier, S. K. G., Maier, L. S., Lengenfelder, B., Jacobshagen, C., Jung, J., Fleischmann, C., Werner, G. S., Olbrich, H. G., Ott, R., Mudra, H., Seidl, K., Schulze, P. C., Weiss, C., Haimerl, J., Friede, T., & Meyer, T. (2018). Impact of treatment delay on mortality in ST-segment elevation myocardial infarction (STEMI) patients presenting with and without haemodynamic instability: Results from the German prospective, multicentre FITT-STEMI trial. *European Heart Journal*, *39*(13), 1065–1074.

Schwitter, J., & Arai, A. E. (2011). Assessment of cardiac ischaemia and viability: Role of cardiovascular magnetic resonance. *European Heart Journal*, *32*(7), 799–809.

Seferović, P. M., Coats, A. J. S., Ponikowski, P., Filippatos, G., Huelsmann, M., Jhund, P. S., Polovina, M. M., Komajda, M., Seferović, J., Sari, I., Cosentino, F., Ambrosio, G., Metra, M., Piepoli, M., Chioncel, O., Lund, L. H., Thum, T., De Boer, R. A., Mullens, W., … Rosano, G. M. C. (2020). European Society of Cardiology/Heart Failure Association position paper on the role and safety of new glucose-lowering drugs in patients with heart failure. *European Journal of Heart Failure*, *22*(2), 196–213.

Sherif, H. M., Saraste, A., Nekolla, S. G., Weidl, E., Reder, S., Tapfer, A., … Schwaiger, M. (2012). Molecular imaging of early αvβ3 integrin expression predicts long-term left-ventricle remodeling after myocardial infarction in rats. *Journal of Nuclear Medicine*, *53*(2), 318–323.

Selvaraju, R. K., Velikyan, I., Johansson, L., Wu, Z., Todorov, I., Shively, J., Kandeel, F., Korsgren, O., & Eriksson, O. (2013). In Vivo Imaging of the Glucagonlike Peptide 1 Receptor in the Pancreas with ^{68}Ga-Labeled DO3A-Exendin-4. *Journal of Nuclear Medicine*, *54*(8), 1458–1463.

Shah, S. J., Lam, C. S. P., Svedlund, S., Saraste, A., Hage, C., Tan, R. S., Beussink-Nelson, L., Faxén, U. L., Fermer, M. L., Broberg, M. A., Gan, L. M., & Lund, L. H. (2018). Prevalence and correlates of coronary microvascular dysfunction in heart failure with preserved ejection fraction: PROMIS-HFpEF. *European Heart Journal*, *39*(37), 3439–3450.

Shaw, L. J., Hausleiter, J., Achenbach, S., Al-Mallah, M., Berman, D. S., Budoff, M. J., Cademartiri, F., Callister, T. Q., Chang, H. J., Kim, Y. J., Cheng, V. Y., Chow, B. J. W., Cury, R. C., Delago, A. J., Dunning, A. L., Feuchtner, G. M., Hadamitzky, M., Karlsberg, R. P., Kaufmann, P. A., … Min, J. K. (2012). Coronary computed tomographic angiography as a gatekeeper to invasive diagnostic and surgical procedures: Results from the multicenter confirm (coronary ct angiography evaluation for clinical outcomes: An international multicenter) registry. *Journal of the American College of Cardiology*, *60*(20), 2103–2114.

Shaw, P. X., Hörkkö, S., Chang, M. K., Curtiss, L. K., Palinski, W., Silverman, G. J., & Witztum, J. L. (2000). Natural antibodies with the T15 idiotype may act in atherosclerosis, apoptotic clearance, and protective immunity. *Journal of Clinical Investigation*, *105*(12), 1731–1740.

Shiraishi, D., Fujiwara, Y., Komohara, Y., Mizuta, H., & Takeya, M. (2012). Glucagon-like peptide-1 (GLP-1) induces M2 polarization of human macrophages via STAT3 activation. *Biochemical and Biophysical Research Communications*, *425*(2), 304–308.

Sicari, R., Rigo, F., Cortigiani, L., Gherardi, S., Galderisi, M., & Picano, E. (2009). Additive Prognostic Value of Coronary Flow Reserve in Patients With Chest Pain Syndrome and Normal or Near-Normal Coronary Arteries. *American Journal of Cardiology*, *103*(5), 626–631.

Silvestre, J. S., Heymes, C., Oubénaïssa, A., Robert, V., Aupetit-Faisant, B., Carayon, A., Swynghedauw, B., & Delcayre, C. (1999). Activation of cardiac aldosterone production in rat myocardial infarction. Effect of angiotensin II receptor blockade and role in cardiac fibrosis. *Circulation*, *99*(20), 2694–2701.

Silvola, J. M. U., Saraste, A., Laitinen, I., Savisto, N., Laine, V. J. O., Heinonen, S. E., … Knuuti, J. (2011). Effects of age, diet, and type 2 diabetes on the development and FDG uptake of atherosclerotic plaques. *JACC. Cardiovascular Imaging*, *4*(12), 1294–1301.

Silvola, J.M.U., Virtanen, H., Siitonen, R., Hellberg, S., Liljenbäck, H., Metsälä, O., Ståhle, M., Saanijoki, T., Käkelä, M., Hakovirta, H., Ylä-Herttuala, S., Saukko, P., Jauhiainen, M., Veres, T. Z., Jalkanen, S., Knuuti, J., Saraste, A., & Roivainen, A. (2016). Leukocyte trafficking-associated vascular adhesion protein 1 is expressed and functionally active in atherosclerotic plaques. *Scientific Reports*, *6*, 35089.

Silvola, Johanna M. U., Li, X.-G., Virta, J., Marjamäki, P., Liljenbäck, H., Hytönen, J. P., Tarkia, M., Saunavaara, V., Hurme, S., Palani, S., Hakovirta, H., Ylä-Herttuala, S., Saukko, P., Chen, Q., Low, P. S., Knuuti, J., Saraste, A., & Roivainen, A. (2018). Aluminum fluoride-18 labeled folate enables in vivo detection of atherosclerotic plaque inflammation by positron emission tomography. *Scientific Reports*, *8*(1), 9720.

Sokos, G. G., Nikolaidis, L. A., Mankad, S., Elahi, D., & Shannon, R. P. (2006). Glucagon-Like Peptide-1 Infusion Improves Left Ventricular Ejection Fraction and Functional Status in Patients With Chronic Heart Failure. *Journal of Cardiac Failure*, *12*(9), 694–699.

Stanley, W. C., Recchia, F. A., & Lopaschuk, G. D. (2005). Myocardial substrate metabolism in the normal and failing heart. *Physiological Reviews*, *85*(3), 1093–1129.

Su, H., Gorodny, N., Gomez, L. F., Gangadharmath, U. B., Mu, F., Chen, G., … Tamarappoo, B. K. (2014). Atherosclerotic plaque uptake of a novel integrin tracer ^{18}F-Flotegatide in a mouse model of atherosclerosis. *Journal of Nuclear Cardiology*, *21*(3), 553–562.

Stary, H. C. (2000). Lipid and macrophage accumulations in arteries of children and the development of atherosclerosis. *The American Journal of Clinical Nutrition*, *72*, 1297S-306S.

Stone, P. H., Saito, S., Takahashi, S., Makita, Y., Nakamura, S., Kawasaki, T., Takahashi, A., Katsuki, T., Nakamura, S., Namiki, A., Hirohata, A., Matsumura, T., Yamazaki, S., Yokoi, H., Tanaka, S., Otsuji, S., Yoshimachi, F., Honye, J., Harwood, D., … Feldman, C. L. (2012). Prediction of progression of coronary artery disease and clinical outcomes using vascular profiling of endothelial shear stress and arterial plaque characteristics: The PREDICTION study. *Circulation*, *126*(2), 172–181.

Su, J., Georgiades, A., Wu, R., Thulin, T., de Faire, U., & Frostegård, J. (2006). Antibodies of IgM subclass to phosphorylcholine and oxidized LDL are protective factors for atherosclerosis in patients with hypertension. *Atherosclerosis*, *188*(1), 160–166.

Sun, Y., Zeng, Y., Zhu, Y., Feng, F., Xu, W., Wu, C., Xing, B., Zhang, W., Wu, P., Cui, L., Wang, R., Li, F., Chen, X., & Zhu, Z. (2014). Application of ^{68}Ga-PRGD2 PET/CT for $\alpha_v\beta_3$-integrin Imaging of Myocardial Infarction and Stroke. *Theranostics, 4,* 778–786.

Sudo, M., Li, Y., Hiro, T., Takayama, T., Mitsumata, M., Shiomi, M., Sugitani, M., Matsumoto, T., Hao, H., & Hirayama, A. (2017). Inhibition of plaque progression and promotion of plaque stability by glucagon-like peptide-1 receptor agonist: Serial in vivo findings from iMap-IVUS in Watanabe heritable hyperlipidemic rabbits. *Atherosclerosis*, *265*, 283–291.

Sun, F., Wu, S., Wang, J., Guo, S., Chai, S., Yang, Z., Li, S., Zhang, Y., Ji, L., & Zhan, S. (2015a). Effect of glucagon-like peptide-1 receptor agonists on lipid profiles among type 2 diabetes: A systematic review and network meta-analysis. *Clinical Therapeutics*, *37*(1), 225-241.

Sun, F., Wu, S., Guo, S., Yu, K., Yang, Z., Li, L., Zhang, Y., Quan, X., Ji, L., & Zhan, S. (2015b). Impact of GLP-1 receptor agonists on blood pressure, heart rate and hypertension among patients with type 2 diabetes: A systematic review and network meta-analysis. *Diabetes Research and Clinical Practice*, *110*(1), 26–37.

Sun, Y., Cleutjens, J. P. M., Djaz-Arias, A. A., & Weber, K. T. (1994). Cardiac angiotensin converting enzyme and myocardial fibrosis in the rat. *Cardiovascular Research*, *9*, 1423–1432.

Sutton, M. G. S. J., & Sharpe, N. (2000). Left Ventricular Remodeling After Myocardial Infarction : Pathophysiology and Therapy. *Circulation*, *101*(25), 2981–2988.

Swirski, F. K., & Nahrendorf, M. (2018). Cardioimmunology: the immune system in cardiac homeostasis and disease. *Nature Reviews Immunology*, *18*(12), 733–744.

Tabas, I. (2010). Macrophage death and defective inflammation resolution in atherosclerosis. *Nature Reviews Immunology*, *10*(1), 36–46.

Tabas, I., & Bornfeldt, K. E. (2016). Macrophage Phenotype and Function in Different Stages of Atherosclerosis. *Circulation Research*, *118*(4), 653–667.

Tahara, N., Kai, H., Ishibashi, M., Nakaura, H., Kaida, H., Baba, K., Hayabuchi, N., & Imaizumi, T. (2006). Simvastatin attenuates plaque inflammation: evaluation by fluorodeoxyglucose positron emission tomography. *Journal of the American College of Cardiology*, *48*(9), 1825–1831.

Tahara, N., Mukherjee, J., De Haas, H. J., Petrov, A. D., Tawakol, A., Haider, N., Tahara, A., Constantinescu, C. C., Zhou, J., Boersma, H. H., Imaizumi, T., Nakano, M., Finn, A., Fayad, Z., Virmani, R., Fuster, V., Bosca, L., & Narula, J. (2014). 2-deoxy-2-[18F]fluoro-d-mannose positron emission tomography imaging in atherosclerosis. *Nature Medicine*, *20*(2), 215–219.

Tait, S. W. G., Ichim, G., & Green, D. R. (2014). Die another way - non-apoptotic mechanisms of cell death. *Journal of Cell Science*, *127*(10), 2135–2144.

Taqueti, V. R., & Di Carli, M. F. (2018). Coronary Microvascular Disease Pathogenic Mechanisms and Therapeutic Options: JACC State-of-the-Art Review. *Journal of the American College of Cardiology*, *72*(21), 2625–2641.

Tardif, J. C., Kouz, S., Waters, D. D., Bertrand, O. F., Diaz, R., Maggioni, A. P., … Roubille, F. (2019). Efficacy and safety of low-dose colchicine after myocardial infarction. *New England Journal of Medicine*, *381*(26), 2497–2505.

Tarkin, J. M., Calcagno, C., Dweck, M. R., Evans, N. R., Chowdhury, M. M., Gopalan, D., Newby, D. E., Fayad, Z. A., Bennett, M. R., & Rudd, J. H. F. (2019). ^{68}Ga-DOTATATE PET Identifies Residual Myocardial Inflammation and Bone Marrow Activation After Myocardial Infarction. *Journal of the American College of Cardiology*, *73*(19), 2489–2491.

Tarkin, J. M., Joshi, F. R., Evans, N. R., Chowdhury, M. M., Figg, N. L., Shah, A. V., Starks, L. T., Martin-Garrido, A., Manavaki, R., Yu, E., Kuc, R. E., Grassi, L., Kreuzhuber, R., Kostadima, M. A., Frontini, M., Kirkpatrick, P. J., Coughlin, P. A., Gopalan, D., Fryer, T. D., … Rudd, J. H. F. (2017). Detection of Atherosclerotic Inflammation by ^{68}Ga-DOTATATE PET Compared to [^{18}F]FDG PET Imaging. *Journal of the American College of Cardiology*, *69*(14), 1774–1791.

Tarkin, J. M., Joshi, F. R., Rajani, N. K., & Rudd, J. H. F. (2015). PET imaging of atherosclerosis. *Future Cardiology*, *11*(1), 115–131.

Tate, M., Robinson, E., Green, B. D., McDermott, B. J., & Grieve, D. J. (2016). Exendin-4 attenuates adverse cardiac remodelling in streptozocin-induced diabetes via specific actions on infiltrating macrophages. *Basic Research in Cardiology*, *111*(1), 1.

Tawakol, A., Migrino, R. Q., Hoffmann, U., Abbara, S., Houser, S., Gewirz, H., … Fischman, A. J. (2005). Noninvasive in Vivo Measurement of Vascular Inflammation With F-18 Fluorodeoxyglucose Positron Emission Tomography. *Journal of Nuclear Cardiology*, *12*, 294–301.

Tawakol, A., Singh, P., Mojena, M., Pimentel-Santillana, M., Emami, H., MacNabb, M., Rudd, J. H. F., Narula, J., Enriquez, J. a., Traves, P. G., Fernandez-Velasco, M., Bartrons, R., Martin-Sanz, P., Fayad, Z. a., Tejedor, A., & Bosca, L. (2015). HIF-1 and PFKFB3 Mediate a Tight Relationship Between Proinflammatory Activation and Anerobic Metabolism in Atherosclerotic Macrophages. *Arteriosclerosis, Thrombosis, and Vascular Biology*, 1463–1471.

Tawakol, A, Singh, P., Rudd, J. H. F., Soffer, J., Cai, G., Vucic, E., Brannan, S. P., Tarka, E. A., Shaddinger, B. C., Sarov-Blat, L., Matthews, P., Subramanian, S., Farkouh, M., & Fayad, Z. A. (2014). Effect of treatment for 12 weeks with rilapladib, a lipoprotein-associated phospholipase A2 inhibitor, on arterial inflammation as assessed with ^{18}F-fluorodeoxyglucose-positron emission tomography imaging. *Journal of the American College of Cardiology*, *63*(1), 86–88.

Tawakol, Ahmed, Fayad, Z. a, Mogg, R., Alon, A., Klimas, M. T., Dansky, H., Subramanian, S. S., Abdelbaky, A., Rudd, J. H. F., Farkouh, M. E., Nunes, I. O., Beals, C. R., & Shankar, S. S. (2013). Intensification of statin therapy results in a rapid reduction in atherosclerotic inflammation: results of a multicenter fluorodeoxyglucose-positron emission tomography/computed tomography feasibility study. *Journal of the American College of Cardiology*, *62*(10), 909–917.

Tawakol, Ahmed, Migrino, R. Q., Bashian, G. G., Bedri, S., Vermylen, D., Cury, R. C., Yates, D., LaMuraglia, G. M., Furie, K., Houser, S., Gewirtz, H., Muller, J. E., Brady, T. J., & Fischman, A. J. (2006). In vivo ^{18}F-fluorodeoxyglucose positron emission tomography imaging provides a noninvasive measure of carotid plaque inflammation in patients. *Journal of the American College of Cardiology*, *48*(9), 1818–1824.

Thackeray, J. T., Derlin, T., Haghikia, A., Napp, L. C., Wang, Y., Ross, T. L., Schäfer, A., Tillmanns, J., Wester, H. J., Wollert, K. C., Bauersachs, J., & Bengel, F. M. (2015a). Molecular Imaging of the Chemokine Receptor CXCR4 after Acute Myocardial Infarction. *JACC: Cardiovascular Imaging*, *8*(12), 1417–1426.

Thackeray, J. T., Bankstahl, J. P., Wang, Y., Korf-Klingebiel, M., Walte, A., Wittneben, A., Wollert, K. C., & Bengel, F. M. (2015b). Targeting post-infarct inflammation by PET imaging: comparison of ^{68}Ga-citrate and ^{68}Ga-DOTATATE with ^{18}F-FDG in a mouse model. *European Journal of Nuclear Medicine and Molecular Imaging*, *42*(2), 317–327.

Thackeray, J. T., Bankstahl, J. P., Wang, Y., Wollert, K. C., & Bengel, F. M. (2016). Targeting amino acid metabolism for molecular imaging of inflammation early after myocardial infarction. *Theranostics*, *6*(11), 1768–1779.

Thackeray, J. T., Hupe, H. C., Wang, Y., Bankstahl, J. P., Berding, G., Ross, T. L., Bauersachs, J., Wollert, K. C., & Bengel, F. M. (2018a). Myocardial Inflammation Predicts Remodeling and Neuroinflammation After Myocardial Infarction. *Journal of the American College of Cardiology*, *71*(3), 263–275.

Thackeray, J. T., & Bengel, F. M. (2018b). Molecular Imaging of Myocardial Inflammation With Positron Emission Tomography Post-Ischemia: A Determinant of Subsequent Remodeling or Recovery. *JACC: Cardiovascular Imaging*, *11*(9), 1340–1355.

The SOLVD, I. (1991). Effect on Enalapril on Survival in Patients with Reduced left Ventricular Ejection Fractions and Congestive Heart failure. *The New England Journal of Medicine*, *325*, 293–302.

Thorens, B. (1992). Expression cloning of the pancreatic beta cell receptor for the gluco-incretin hormone glucagon-like peptide 1. *Proceedings of the National Academy of Sciences of the United States of America*, *89*(18), 8641–8645.

Thygesen, K., Alpert, J. S., Jaffe, A. S., Chaitman, B. R., Bax, J. J., Morrow, D. A., White, H. D., Mickley, H., Crea, F., Van De Werf, F., Bucciarelli-Ducci, C., Katus, H. A., Pinto, F. J., Antman, E. M., Hamm, C. W., De Caterina, R., Januzzi, J. L., Apple, F. S., Garcia, M. A. A., … Windecker, S. (2019). Fourth universal definition of myocardial infarction (2018). *European Heart Journal*, *40*(3), 237–269.

Timmers, L., Henriques, J. P. S., de Kleijn, D. P. V, DeVries, J. H., Kemperman, H., Steendijk, P., Verlaan, C. W. J., Kerver, M., Piek, J. J., Doevendans, P. a., Pasterkamp, G., & Hoefer, I. E. (2009). Exenatide Reduces Infarct Size and Improves Cardiac Function in a Porcine Model of Ischemia and Reperfusion Injury. *Journal of the American College of Cardiology*, *53*(6), 501–510.

Timmers, L., Pasterkamp, G., De Hoog, V. C., Arslan, F., Appelman, Y., & De Kleijn, D. P. V. (2012). The innate immune response in reperfused myocardium. *Cardiovascular Research*, *94*(2), 276–283.

Tomas, L., Edsfeldt, A., Mollet, I. G., Matic, L. P., Prehn, C., Adamski, J., Paulsson-Berne, G., Hedin, U., Nilsson, J., Bengtsson, E., Gonçalves, I., & Björkbacka, H. (2018). Altered metabolism distinguishes high-risk from stable carotid atherosclerotic plaques. *European Heart Journal*, *39*(24), 2301–2310.

Torre-Amione, G., Kapadia, S., Lee, J., Durand, J.-B., Bies, R. D., Young, J. B., & Mann, D. L. (1996). Tumor Necrosis Factor-α and Tumor Necrosis Factor Receptors in the Failing Human Heart. *Circulation*, *93*, 704–711.

Travers, J. G., Kamal, F. A., Robbins, J., Yutzey, K. E., & Blaxall, B. C. (2016). Cardiac fibrosis: The fibroblast awakens. *Circulation Research*, *118*(6), 1021–1040.

Tsiantoulas, D., Perkmann, T., Afonyushkin, T., Mangold, A., Prohaska, T. A., Papac-Milicevic, N., Millischer, V., Bartel, C., Hörkkö, S., Boulanger, C. M., Tsimikas, S., Fischer, M. B., Witztum, J. L., Lang, I. M., & Binder, C. J. (2015). Circulating microparticles carry oxidation-specific epitopes and are recognized by natural IgM antibodies. *Journal of Lipid Research*, *56*(2), 440–448.

Tsimikas, S., Bergmark, C., Beyer, R. W., Patel, R., Pattison, J., Miller, E., Juliano, J., & Witztum, J. L. (2003). Temporal increases in plasma markers of oxidized low-density lipoprotein strongly reflect the presence of acute coronary syndromes. *Journal of the American College of Cardiology*, *41*(3), 360–370.

Tsimikas, S., Brilakis, E. S., Miller, E. R., Mcconnell, J. P., Lennon, R. J., Kornman, K. S., Witztum, J. L., & Berger, P. B. (2005). Oxidized Phospholipids, Lp(a) Lipoprotein, and Coronary Artery Disease. *The New England Journal of Medicine*, 46–57.

Tsimikas, S., Miyanohara, A., Hartvigsen, K., Merki, E., Shaw, P. X., Chou, M. Y., Pattison, J., Torzewski, M., Sollors, J., Friedmann, T., Lai, N. C., Hammond, H. K., Getz, G. S., Reardon, C. A., Li, A. C., Banka, C. L., & Witztum, J. L. (2011). Human oxidation-specific antibodies reduce foam cell formation and atherosclerosis progression. *Journal of the American College of Cardiology*, *58*(16), 1715–1727.

Tsimikas, S., & Stroes, E. S. G. (2020). The dedicated "Lp(a) clinic": A concept whose time has arrived? *Atherosclerosis*, *300*, 1–9.

Tsimikas, S., Willeit, P., Willeit, J., Santer, P., Mayr, M., Xu, Q., Mayr, A., Witztum, J. L., & Kiechl, S. (2012). Oxidation-specific biomarkers, prospective 15-year cardiovascular and stroke outcomes, and net reclassification of cardiovascular events. *Journal of the American College of Cardiology*, *60*(21), 2218–2229.

Tsujioka, H., Imanishi, T., Ikejima, H., Kuroi, A., Takarada, S., Tanimoto, T., Kitabata, H., Okochi, K., Arita, Y., Ishibashi, K., Komukai, K., Kataiwa, H., Nakamura, N., Hirata, K., Tanaka, A., & Akasaka, T. (2009). Impact of Heterogeneity of Human Peripheral Blood Monocyte Subsets on Myocardial Salvage in Patients With Primary Acute Myocardial Infarction. *Journal of the American College of Cardiology*, *54*(2), 130–138.

Turkington, T.G. Introduction to PET Instrumentation. (2001). *J Nucl Med Technol*, *29*, 1–8.

Tuunanen, H., & Knuuti, J. (2011). Metabolic remodelling in human heart failure. *Cardiovascular Research*, *90*(2), 251–257.

Ussher, J. R., Baggio, L. L., Campbell, J. E., Mulvihill, E. E., Kim, M., Kabir, M. G., Cao, X., Baranek, B. M., Stoffers, D. A., Seeley, R. J., & Drucker, D. J. (2014). Inactivation of the cardiomyocyte glucagon-like peptide-1 receptor (GLP-1R) unmasks cardioprotection. *Molecular Metabolism*, *3*(5), 507–517.

van der Laan, A. M., Ter Horst, E. N., Delewi, R., Begieneman, M. P. V., Krijnen, P. A. J., Hirsch, A., Lavaei, M., Nahrendorf, M., Horrevoets, A. J., Niessen, H. W. M., & Piek, J. J. (2014). Monocyte subset accumulation in the human heart following acute myocardial infarction and the role of the spleen as monocyte reservoir. *European Heart Journal*, *35*(6), 376–385.

van der Valk, F. M., Verweij, S. L., Zwinderman, K. A. H., Strang, A. C., Kaiser, Y., Marquering, H. A., Nederveen, A. J., Stroes, E. S. G., Verberne, H. J., & Rudd, J. H. F. (2016a). Thresholds for Arterial Wall Inflammation Quantified by ^{18}F-FDG PET Imaging: Implications for Vascular Interventional Studies. *JACC: Cardiovascular Imaging*, *9*(10), 1198–1207.

van der Valk, F. M., Bekkering, S., Kroon, J., Yeang, C., Van Den Bossche, J., Van Buul, J. D., Ravandi, A., Nederveen, A. J., Verberne, H. J., Scipione, C., Nieuwdorp, M., Joosten, L. A. B., Netea, M. G., Koschinsky, M. L., Witztum, J. L., Tsimikas, S., Riksen, N. P., & Stroes, E. S. G. (2016b). Oxidized phospholipids on Lipoprotein(a) elicit arterial wall inflammation and an inflammatory monocyte response in humans. *Circulation*, *134*(8), 611–624.

van Dijk, R. a., Kolodgie, F., Ravandi, a., Leibundgut, G., Hu, P. P., Prasad, a., Mahmud, E., Dennis, E. a., Curtiss, L. K., Witztum, J. L., Wasserman, B., Otsuka, F., Virmani, R., & Tsimikas, S. (2012). Differential Expression of Oxidation-Specific Epitopes and Apolipoprotein(a) in Progressing and Ruptured Human Coronary and Carotid Atherosclerotic Lesions. *The Journal of Lipid Research*, *53*, 2773–2790.

Varasteh, Z., Mohanta, S., Robu, S., Braeuer, M., Li, Y., Omidvari, N., Topping, G., Sun, T., Nekolla, S., Richter, A., Weber, C., Habenicht, A., Haberkorn, U., & Weber, W. (2019) Molecular Imaging of Fibroblast Activity After Myocardial Infarction Using a ^{68}Ga-Labeled Fibroblast Activation Protein Inhibitor, FAPI-04. *Journal of Nuclear Medicine, 60,* 1743–1749.

Velikyan, I., & Eriksson, O. (2020). Advances in GLP-1 receptor targeting radiolabeled agent development and prospective of theranostics. *Theranostics*, *10*(1), 437–461.

Véniant, M. M., Herz, J., & Young, S. G. (1998). Lipoprotein clearance mechanisms in LDL B100-only " mice. *The Journal of Clinical Investigtion*, *102*(8), 1559–1568.

Verbeuren, T. J., Coene, M. C., Jordaens, F. H., Van Hove, C. E., Zonnekeyn, L. L., & Herman, A. G. (1986). Effect of hypercholesterolemia on vascular reactivity in the rabbit. II. Influence of treatment with dipyridamole on endothelium-dependent and endothelium-independent responses in isolated aortas of control and hypercholesterolemic rabbits. *Circulation Research*, *59*(5), 496–504.

Vinué, Á., Navarro, J., Herrero-Cervera, A., García-Cubas, M., Andrés-Blasco, I., Martínez-Hervás, S., Real, J. T., Ascaso, J. F., & González-Navarro, H. (2017). The GLP-1 analogue lixisenatide decreases atherosclerosis in insulin-resistant mice by modulating macrophage phenotype. *Diabetologia*, *60*(9), 1801–1812.

Virchow, R. (1858) Cellular Pathology. London: John Churchill.

Virmani, R., Kolodgie, F. D., Burke, a. P., Farb, a., & Schwartz, S. M. (2000). Lessons From Sudden Coronary Death : A Comprehensive Morphological Classification Scheme for Atherosclerotic Lesions. *Arteriosclerosis, Thrombosis, and Vascular Biology*, *20*(5), 1262–1275.

Volanakis, J. E., & Kaplan, M. H. (1971). Specificity of C-reactive Protein for Choline Phosphate Residues of Pneumococcal C-polysaccharide. *Proc Soc Exp Biol Med*, *136*, 612–614.

von Scheidt, M., Zhao, Y., Kurt, Z., Pan, C., Zeng, L., Yang, X., … Lusis, A. J. (2017). Applications and Limitations of Mouse Models for Understanding Human Atherosclerosis. *Cell Metabolism*, *25*(2), 248–261.

Vöö, S., Kwee, R. M., Sluimer, J. C., Schreuder, F. H. B. M., Wierts, R., Bauwens, M., Heeneman, S., Cleutjens, J. P. M., Van Oostenbrugge, R. J., Daemen, J. W. H., Daemen, M. J. A. P., Mottaghy, F. M., & Kooi, M. E. (2016). Imaging intraplaque inflammation in carotid atherosclerosis with ^{18}F-fluorocholine positron emission tomography-computed tomography. *Circulation: Cardiovascular Imaging*, *9*(5), 1–8.

Walton, K. A., Hsieh, X., Gharavi, N., Wang, S., Wang, G., Yeh, M., Cole, A. L., & Berliner, J. A. (2003). Receptors involved in the oxidized 1-palmitoyl-2-arachidonoyl-sn-glycero-3-phosphorylcholine-mediated synthesis of interleukin-8: A role for toll-like receptor 4 and a glycosylphosphatidylinositol-anchored protein. *Journal of Biological Chemistry*, *278*(32), 29661–29666.

Watson, A., Leitinger, N., & Navab, M. (1997). Structural identification by mass spectrometry of oxidized phospholipids in minimally oxidized low density lipoprotein that induce monocyte/endothelial interactions. *Journal of Biological*, *272*(21), 13597–13607.

Wei, R., Ma, S., Wang, C., Ke, J., Yang, J., Li, W., Liu, Y., Hou, W., Feng, X., Wang, G., & Hong, T. (2016). Exenatide exerts direct protective effects on endothelial cells through the AMPK/Akt/eNOS pathway in a GLP-1 receptor-dependent manner. *AJP: Endocrinology And Metabolism*, *310*(11), E947–E957.

Werner, R. A., Thackeray, J. T., Diekmann, J., Weiberg, D., Bauersachs, J., & Bengel, F. M. (2020). The Changing Face of Nuclear Cardiology : Guiding Cardiovascular Care towards Molecular Medicine, *61*(7), 951–961.

Wikström, J., Grönros, J., Bergström, G., & Gan, L. (2005). Functional and morphologic imaging of coronary atherosclerosis in living mice using high-resolution color Doppler echocardiography and ultrasound biomicroscopy. *Journal of the American College of Cardiology*, *46*(4), 720–727.

Wild, D., Wicki, A., Mansi, R., Béhé, M., Keil, B., Bernhardt, P., Christofori, G., Ell, P. J., & Mäcke, H. R. (2010). Exendin-4-based radiopharmaceuticals for glucagonlike peptide-1 receptor PET/CT and SPECT/CT. *Journal of Nuclear Medicine*, *51*(7), 1059–1067.

Willems, I. E., Havenith, M. G., De Mey, J. G., & Daemen, M. J. (1994). The alpha-smooth muscle actin-positive cells in healing human myocardial scars. *The American Journal of Pathology*, *145*(4), 868–875.

Winkels, H., Ehinger, E., Vassallo, M., Buscher, K., Dinh, H. Q., Kobiyama, K., Hamers, A. A. J., Cochain, C., Vafadarnejad, E., Saliba, A. E., Zernecke, A., Pramod, A. B., Ghosh, A. K., Michel,

N. A., Hoppe, N., Hilgendorf, I., Zirlik, A., Hedrick, C. C., Ley, K., & Wolf, D. (2018). Atlas of the immune cell repertoire in mouse atherosclerosis defined by single-cell RNA-sequencing and mass cytometry. *Circulation Research*, *122*(12), 1675–1688.

Wohlfart, P., Linz, W., Hübschle, T., Linz, D., Huber, J., Hess, S., Crowther, D., Werner, U., & Ruetten, H. (2013). Cardioprotective effects of lixisenatide in rat myocardial ischemia-reperfusion injury studies. *Journal of Translational Medicine*, *11*, 84.

Wollenweber, T., Roentgen, P., Schäfer, A., Schatka, I., Zwadlo, C., Brunkhorst, T., Berding, G., Bauersachs, J., & Bengel, F. M. (2014). Characterizing the inflammatory tissue response to acute myocardial infarction by clinical multimodality noninvasive imaging. *Circulation: Cardiovascular Imaging*, *7*(5), 811–818.

Woo, J. S., Kim, W., Ha, S. J., Kim, J. B., Kim, S. J., Kim, W. S., Seon, H. J., & Kim, K. S. (2013). Cardioprotective effects of exenatide in patients with ST-segment-elevation myocardial infarction undergoing primary percutaneous coronary intervention: Results of exenatide myocardial protection in revascularization study. *Arteriosclerosis, Thrombosis, and Vascular Biology*, *33*(9), 2252–2260.

Wu, J., Xu, X., Zhu, J., Ding, B., Du, T., Gao, G., Mao, X., Ye, L., Lee, K.-O., & Ma, J. (2011). Effect of Exenatide on Inflammatory and Oxidative Stress Markers in Patients with Type 2 Diabetes Mellitus. *Diabetes Technology & Therapeutics*, *13*(2), 143–148.

Yan, F. X., Li, H. M., Li, S. X., He, S. H., Dai, W. P., Li, Y., Wang, T. T., Shi, M. M., Yuan, H. X., Xu, Z., Zhou, J. G., Ning, D. S., Mo, Z. W., Ou, Z. J., & Ou, J. S. (2017). The oxidized phospholipid POVPC impairs endothelial function and vasodilation via uncoupling endothelial nitric oxide synthase. *Journal of Molecular and Cellular Cardiology*, *112*, 40–48.

Ye, Y. X., Calcagno, C., Binderup, T., Courties, G., Keliher, E. J., Wojtkiewicz, G. R., Iwamoto, Y., Tang, J., Pérez-Medina, C., Mani, V., Ishino, S., Johnbeck, C. B., Knigge, U., Fayad, Z. A., Libby, P., Weissleder, R., Tawakol, A., Dubey, S., Belanger, A. P., … Nahrendorf, M. (2015). Imaging Macrophage and Hematopoietic Progenitor Proliferation in Atherosclerosis. *Circulation Research*, *117*(10), 835–845.

Yellon, D. M., & Housenloy, D. J. (2007). Myocardial reperfusion injury. *New England Journal of Medicine*, *357*(11), 1121–1135.

Ylä-Herttuala, S., Palinski, W., Rosenfeld, M. E., Parthasarathy, S., Carew, T. E., Butler, S., Witztum, J. L., & Steinberg, D. (1989). Evidence for the presence of oxidatively modified low density lipoprotein in atherosclerotic lesions of rabbit and man. *Journal of Clinical Investigation*, *84*(4), 1086–1095.

Younce, C. W., Niu, J., Ayala, J., Burmeister, M. A., Smith, L. H., Kolattukudy, P., & Ayala, J. E. (2014). Exendin-4 improves cardiac function in mice overexpressing monocyte chemoattractant protein-1 in cardiomyocytes. *Journal of Molecular and Cellular Cardiology*, *76*, 172–176.

Yu, C. M., Tipoe, G. L., Wing-Hon Lai, K., & Lau, C. P. (2001). Effects of combination of angiotensin-converting enzyme inhibitor and angiotensin receptor antagonist on inflammatory cellular infiltration and myocardial interstitial fibrosis after acute myocardial infarction. *Journal of the American College of Cardiology*, *38*(4), 1207–1215.

Yun, M., Yeh, D., Araujo, L. I., Jang, S., Newberg, A., & Alavi, A. (2001). F-18 FDG Uptake in the Large Arteries. *Clin Nuclear Med*, *26*(4), 314–319.

Zernecke, A., Winkels, H., Cochain, C., Williams, J. W., Wolf, D., Soehnlein, O., … Ley, K. (2020). Meta-Analysis of Leukocyte Diversity in Atherosclerotic Mouse Aortas. *Circulation Research*, *127*(3), 402–426.

Zhang, L.-H., Pang, X.-F., Bai, F., Wang, N.-P., Shah, A. I., McKallip, R. J., Li, X.-W., Wang, X., & Zhao, Z.-Q. (2015a). Preservation of Glucagon-Like Peptide-1 Level Attenuates Angiotensin II-Induced Tissue Fibrosis by Altering AT1/AT 2 Receptor Expression and Angiotensin-Converting Enzyme 2 Activity in Rat Heart. *Cardiovascular Drugs and Therapy*, 243–255.

Zhan, J. K., Wang, Y. J., Wang, Y., Tang, Z. Y., Tan, P., Huang, W., & Liu, Y. S. (2015b). The protective effect of GLP-1 analogue in arterial calcification through attenuating osteoblastic differentiation of human VSMCs. *International Journal of Cardiology*, *189*(1), 188–193.

Zhang, Z., Machac, J., Helft, G., Worthley, S. G., Tang, C., Zaman, A. G., Rodriguez, O. J., Buchsbaum, M. S., Fuster, V., & Badimon, J. J. (2006). Non-invasive imaging of atherosclerotic plaque macrophage in a rabbit model with F-18 FDG PET: A histopathological correlation. *BMC Nuclear Medicine*, *6*, 1–7.

Zhao, T., Parikh, P., Bhashyam, S., Bolukoglu, H., Poornima, I., Shen, Y. T., & Shannon, R. P. (2006). Direct effects of glucagon-like peptide-1 on myocardial contractility and glucose uptake in normal and postischemic isolated rat hearts. *Journal of Pharmacology and Experimental Therapeutics*, *317*(3), 1106–1113.

Zheng, K. H., Tsimikas, S., Pawade, T., Kroon, J., Jenkins, W. S. A., Doris, M. K., White, A. C., Timmers, N. K. L. M., Hjortnaes, J., Rogers, M. A., Aikawa, E., Arsenault, B. J., Witztum, J. L., Newby, D. E., Koschinsky, M. L., Fayad, Z. A., Stroes, E. S. G., Boekholdt, S. M., & Dweck, M. R. (2019). Lipoprotein(a) and Oxidized Phospholipids Promote Valve Calcification in Patients With Aortic Stenosis. *Journal of the American College of Cardiology*, *73*(17), 2150–2162.

Ziadi, M. C., Dekemp, R. A., Williams, K. A., Guo, A., Chow, B. J. W., Renaud, J. M., Ruddy, T. D., Sarveswaran, N., Tee, R. E., & Beanlands, R. S. B. (2011). Impaired myocardial flow reserve on rubidium-82 positron emission tomography imaging predicts adverse outcomes in patients assessed for myocardial ischemia. *Journal of the American College of Cardiology*, *58*(7), 740–748.

UNIVERSITY
OF TURKU